Contact Angle

Young's Equation
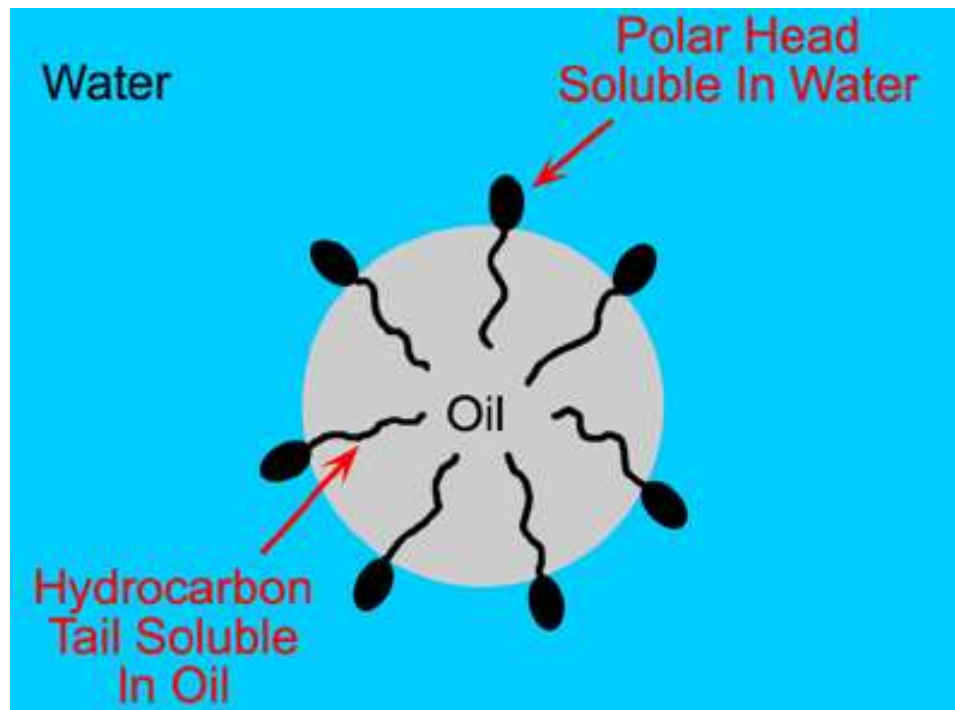
$$\gamma_{SL} + \gamma_{LV} \cos\theta_c = \gamma_{SV}$$

$\gamma_S = \gamma_L \cdot \cos\theta + \gamma_{SL}$ [Young equation]

where

θ : Contact angle
γ_S : Solid surface free energy
γ_L : Liquid surface free energy
γ_{SL} : Solid/Liquid interfacial free energy

Liquid droplet

Solid
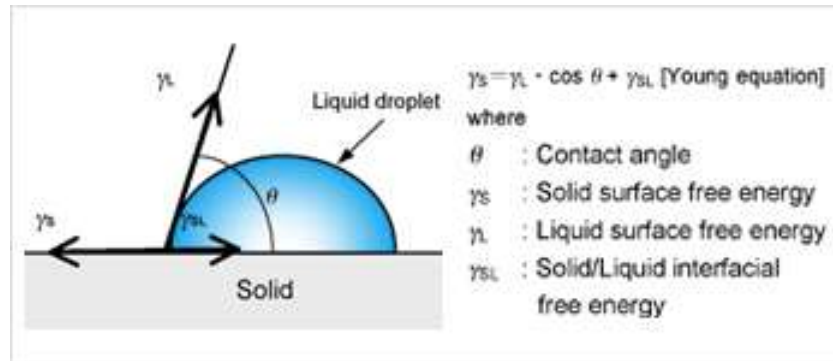
Surface Energy Minimization

- Surfactants
- DLVO
- Polymeric
- Nucleation
- Ostwald Ripening
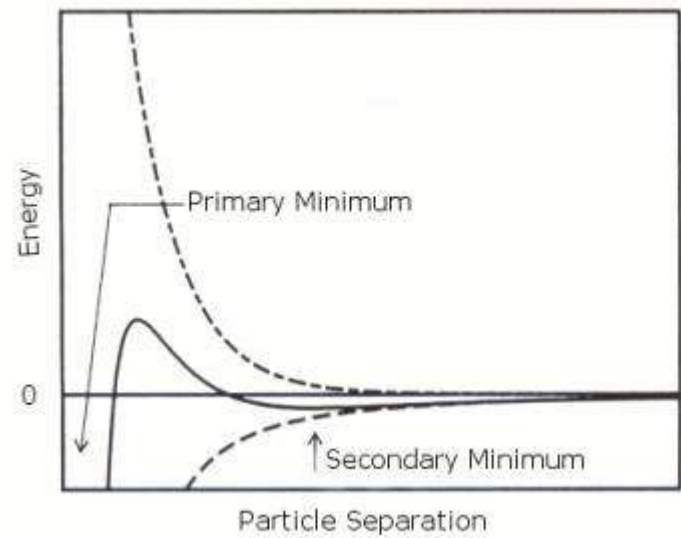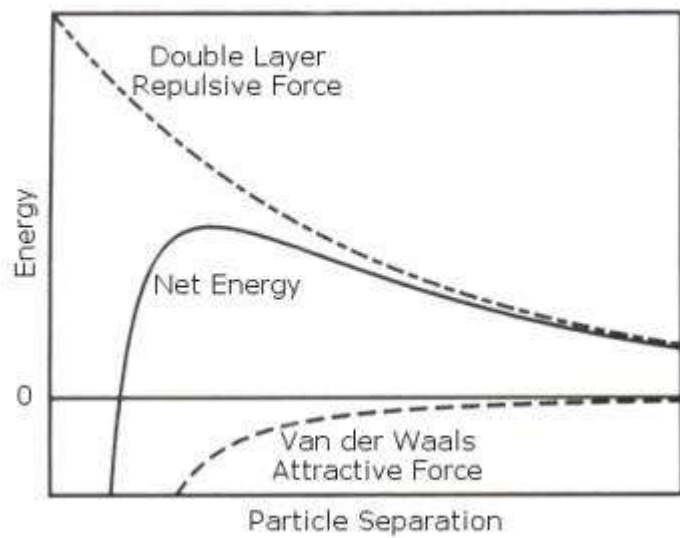- Sintering
- Restructure

Surfactant

DLVO Theory

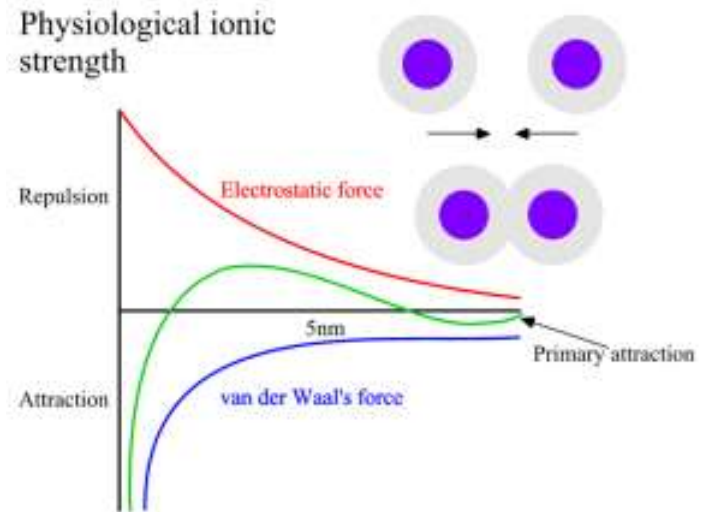$$V_T = V_A + V_R + V_S$$
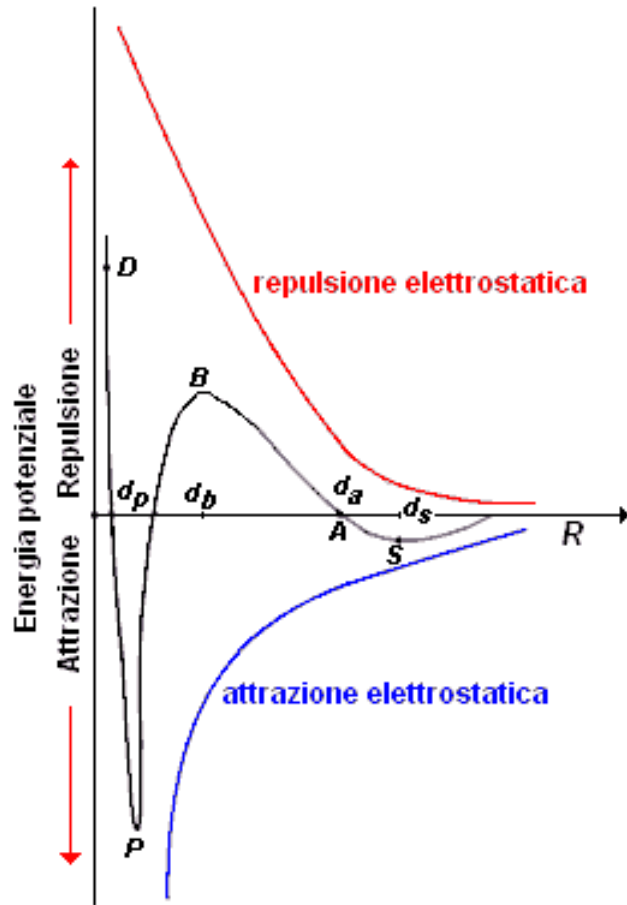
$$V_A = -A/(12 \pi D^2)$$

A is the Hamaker constant and D is the particle separation

$$V_R = 2 \pi \varepsilon a \xi^2 \exp(-\kappa D)$$

a is the particle radius, π is the solvent permeability,
κ is a function of the ionic composition and ξ is the zeta potential
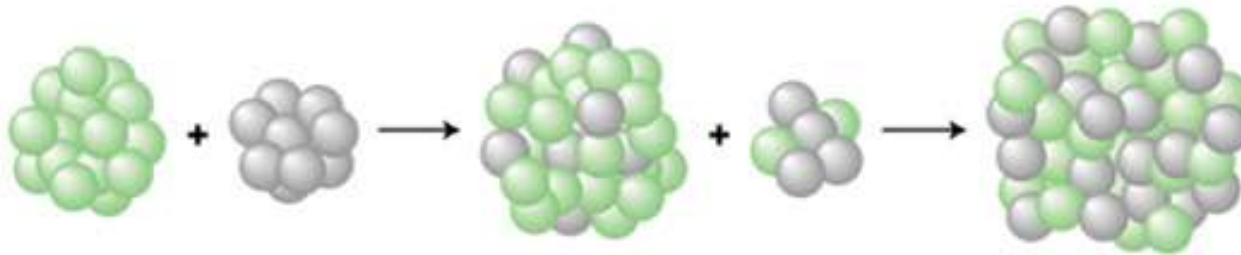
Left figure labels: Double Layer Repulsive Force, Net Energy, Van der Waals Attractive Force, Energy, 0, Particle Separation

Right figure labels: Primary Minimum, Secondary Minimum, Energy, 0, Particle Separation

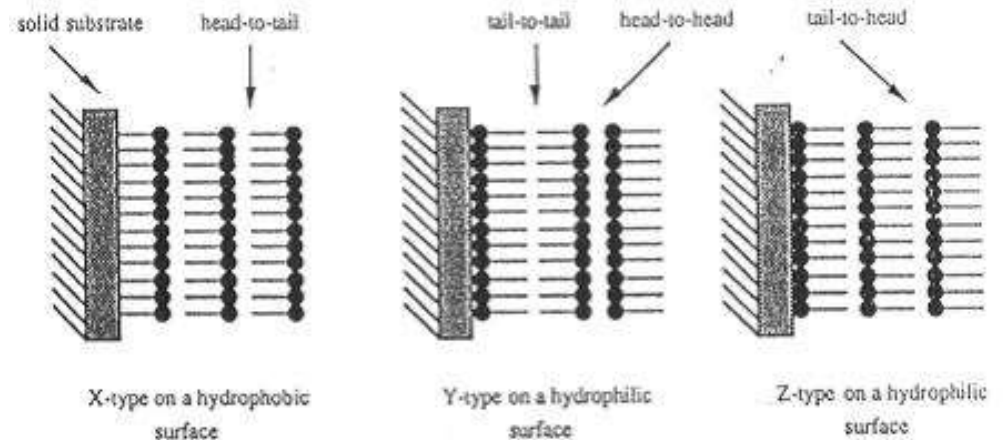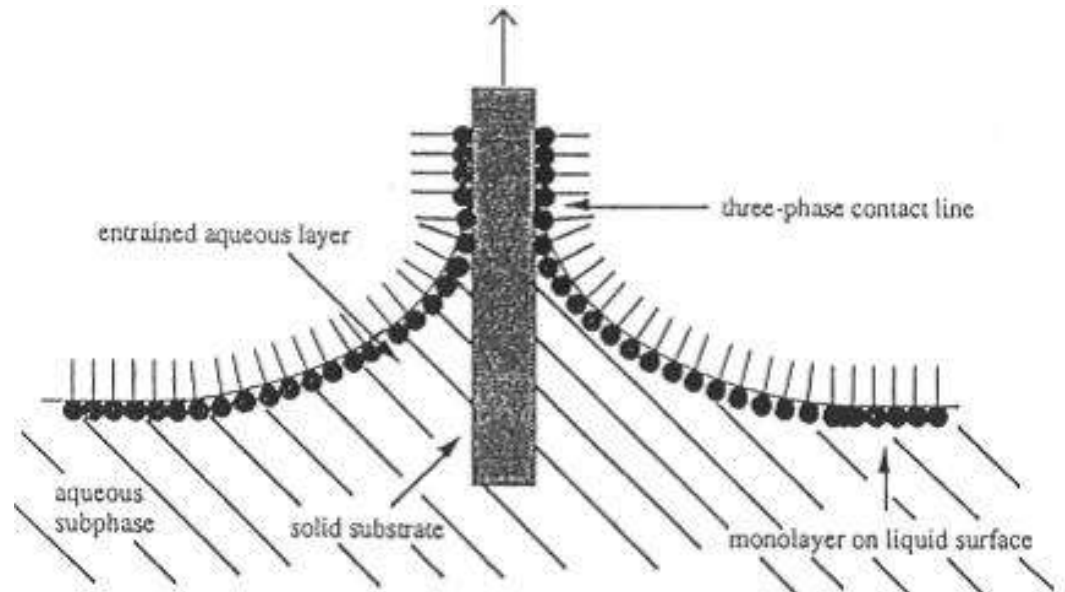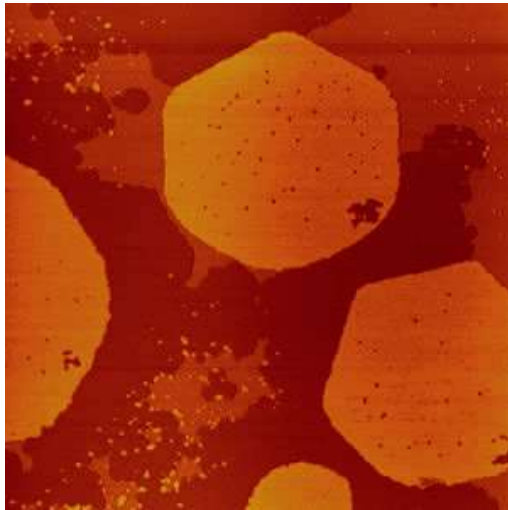# DLVO Theory

a Coalescence

b Ostwald ripening

Two main mechanisms are shown here: **a**, coalescence sintering, and **b**, Ostwald ripening sintering. Coalescence sintering occurs when two clusters touch or collide and merge to form one bigger cluster. In contrast, Ostwald ripening sintering occurs by evaporation of atoms from one cluster, which then transfer to another. This is a dynamic process — both clusters exchange atoms, but the rate of loss from the smaller cluster is higher, because of the lower average coordination of atoms at the surface and their relative ease of removal. Thus big clusters get bigger at the expense of smaller clusters, which shrink and eventually disappear. The latter process is the usual form of sintering for metal clusters on a supported surface that are well spaced apart, although coalescence can occur for a high density of clusters. In general, the presence of the surface results in SMORS (surface-mediated Ostwald ripening sintering) in which material is transferred from one cluster to another by diffusion across the surface, and not through the gas phase.

Synthesis of Nanoparticles and Surface Modifications
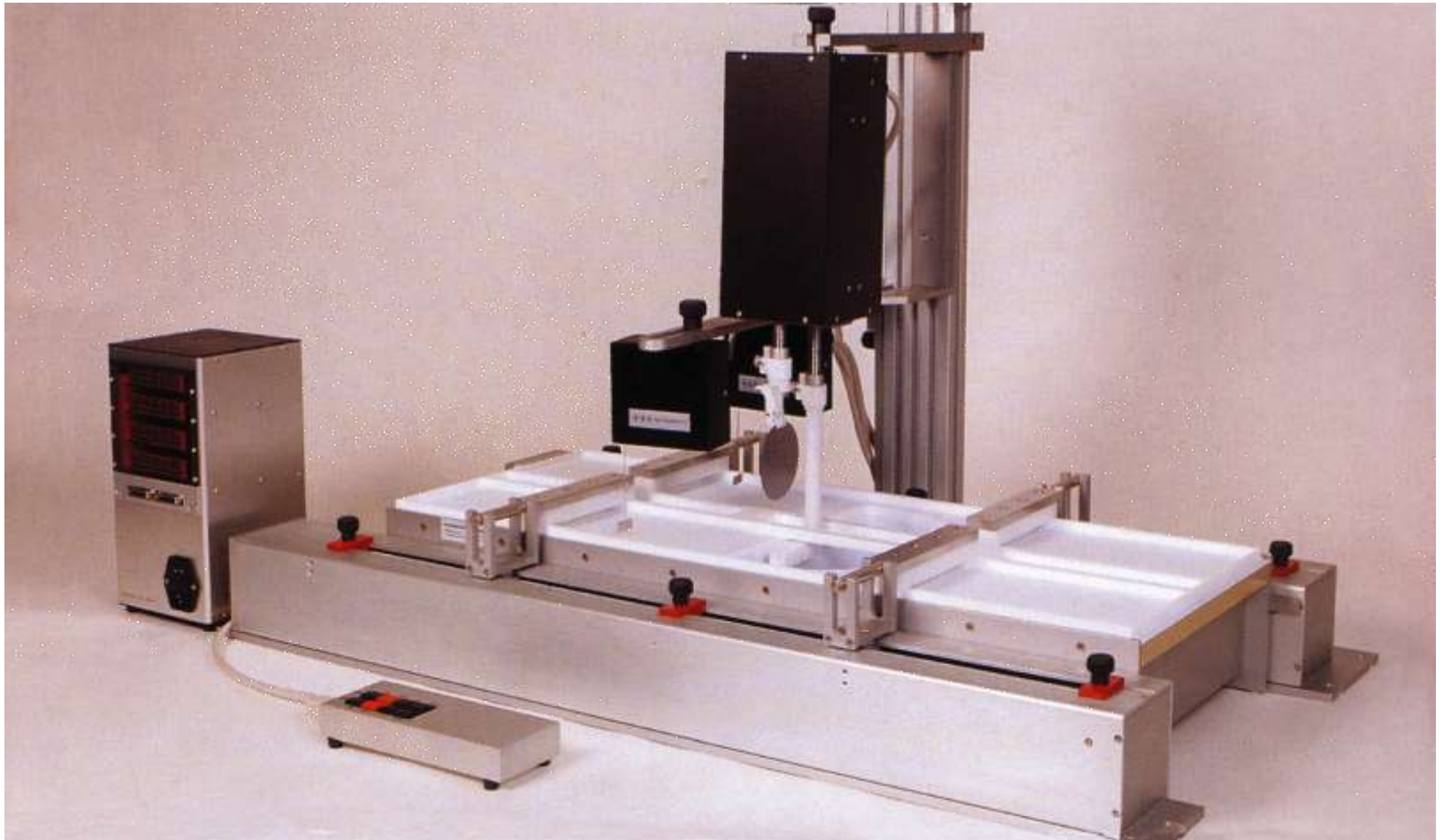
Self-Assembly

- Static assembly
- Dynamic assembly

    - RT = 8.314 J/mol x 300 = 2.4 kJ/mol
- Driving forces
    - Chemisorption
    - Surface effect
    - Hydrophobic-hydrophilic
    - Intermolecular forces
    - Capillary force
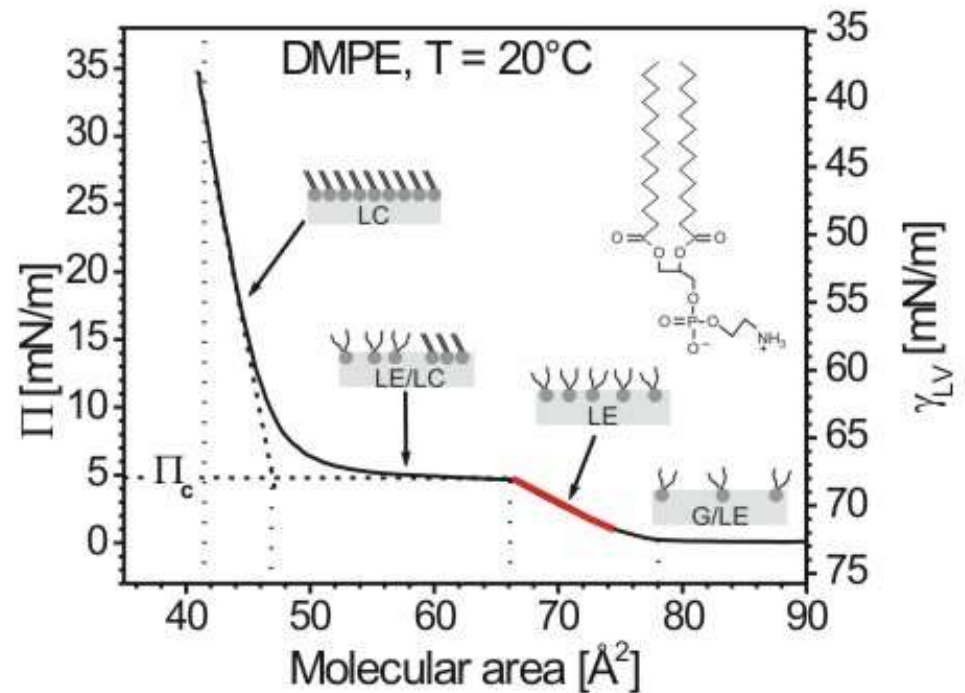
Langmuir-Blodgett Films

three-phase contact line

entrained aqueous layer

aqueous subphase

solid substrate

monolayer on liquid surface

solid substrate   head-to-tail

tail-to-tail   head-to-head

tail-to-head

X-type on a hydrophobic surface

Y-type on a hydrophilic surface

Z-type on a hydrophilic surface

Langmuir-Blodgett Films

Isotherm
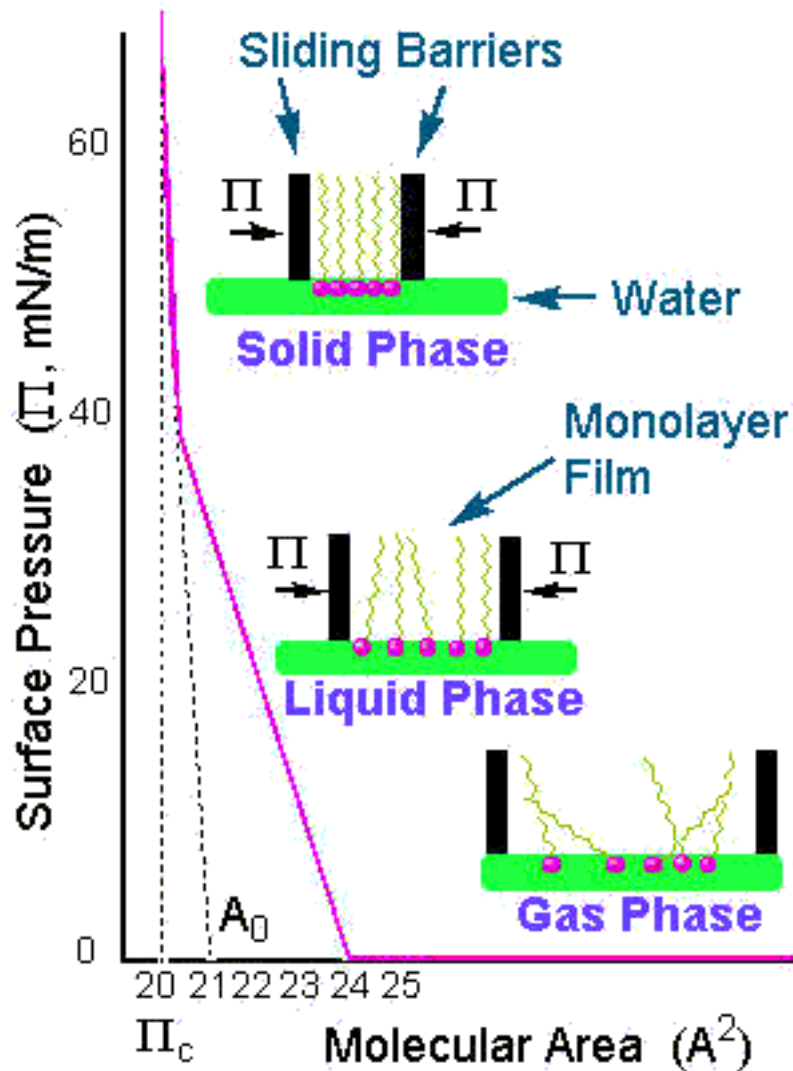
Self-Assemble Monolayer (SAM)

Chem. Rev. **2005**, *105*, 1103–1169

Organic Interface:
- Determines surface properties
- Presents chemical functional groups

Terminal Functional Group

Spacer (Alkane Chain)

Ligand or Head Group

Metal Substrate

Organic Interphase (1-3 nm):
- Provides well-defined thickness
- Acts as a physical barrier
- Alters electronic conductivity and local optical properties

Metal-Sulfur Interface:
- Stabilizes surface atoms
- Modifies electronic states

S-Au 25-30 Kcal/mole
Si-O 190 kcal/mole

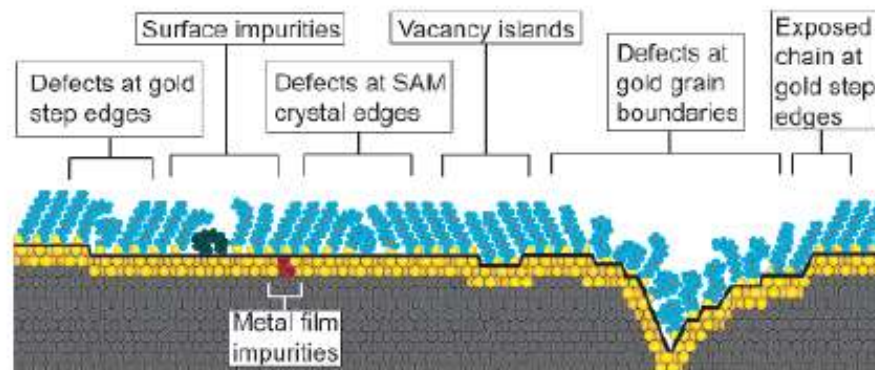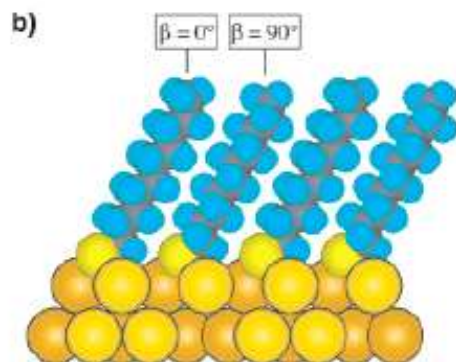| Ligand	Substrates	Thin Films or Bulk Material	Nanoparticles or Other Nanostructures	Ligand	Substrates	Thin Films or Bulk Material	Nanoparticles or Other Nanostructures
ROH	Fe₂O₃		55	RSSR'	Ag	89	90
	Si-H	36			Au	20	90-92
	Si	37			CdS		61
RCOO-/RCOOH	α-Al₂O₃	38,39			Pd	30	
	Fe₂O₃		40		Au	93	
	Ni		41,42				
	Ti/TiO₂	43					
RCOO-OOCR	Si(111):H	44		RCSSH	Au	94	
	Si(100):H				CdSe		95
Ene-diol	Fe₂O₃		45				
RNH₂	FeS₂	46		RS₂O₃Na⁺	Au	96	98
	Mica	47			Cu	97	
	Stainless Steel 316L	48		RSeH	Ag	99	
	YBa₂Cu₃O₇₋δ	49			Au	100,101	
	CdSe		50		CdS		60
RC≡N	Ag	51			CdSe		102
	Au			RSeSeR'	Au	101	
R-N≡N⁺(BF₄⁻)	GaAs(100)	52		R₃P	Au		103
	Pd	52			FeS₂	46	
	Si(111):H	52			CdS		104
RSH	Ag	26	53,54		CdSe		104
	Ag₅₀Ni₅₀	55			CdTe		104
	AgS		56	R₃P=O	Co		105,106
	Au	26	57		CdS		104
	AuAg		58		CdSe		104
	AuCu		58		CdTe		104
	AuₓPd₁₋ₓ		58	RPO₃²⁻/RP(O)(OH)₂	Al	107	
	CdTe		59		Al-OH	108	
	CdSe		60		Ca₁₀(PO₄)₆CO₃)₂(OH)₂	109	
	CdS		61,62		GaAs	110	
	Cu	26	58		GaN	110	
	FePt		63-66		Indium tin oxide (ITO)	111	
	GaAs	67			Mica	112	
	Ge	68			TiO₂	113,114	
	Hg	69-71			ZrO₂	114,115	
	HgTe		72		CdSe		116-118
	InP	73			CdTe		118,119
	Ir		74				
	Ni	75		RPO₄²⁻	Al₂O₃	120	
	PbS		76-78		Nb₂O₅	120	
	Pd	30	74,79		Ta₂O₅	121	
	PdAg		58		TiO₂	120,122	
	Pt	32	80	RN≡C	Pt	123	124
	Ru		81	RHC=CH₂	Si	37	
	Stainless Steel 316L	48		RC≡CH	Si(111):H	125	
	YBa₂Cu₃O₇₋δ	82					
	Zn	83		RSiX₃	HfO₂	126	
	ZnSe	84		X = H, Cl, OCH₂CH₃			
	ZnS		85		ITO	127	
RSAc	Au	86			PtO	128	
	Au		87		TiO₂	113,126,129	
RSR'	Au	88			ZrO₂	126,129	

Figure 7. Schematic illustration of some of the intrinsic and extrinsic defects found in SAMs formed on poly-crystalline substrates. The dark line at the metal–sulfur interface is a visual guide for the reader and indicates the changing topography of the substrate itself.
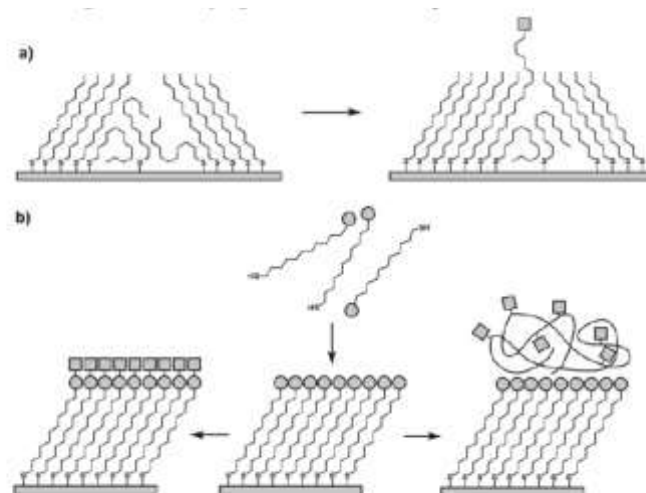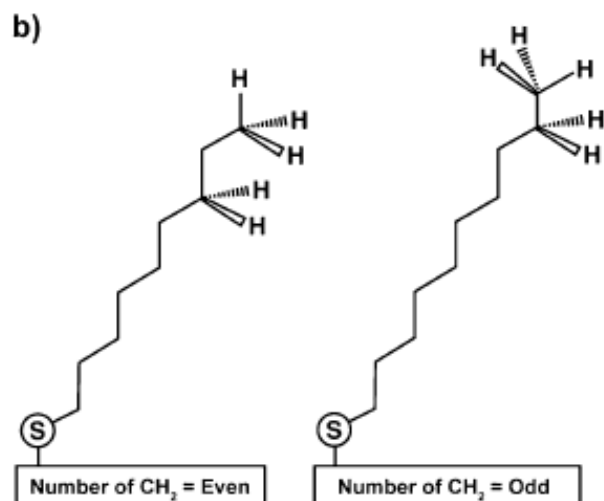
ᵃ (a) Insertion of a functional adsorbate at a defect site in a preformed SAM. (b) Transformation of a SAM with exposed functional groups (circles) by either chemical reaction or adsorption of another material.
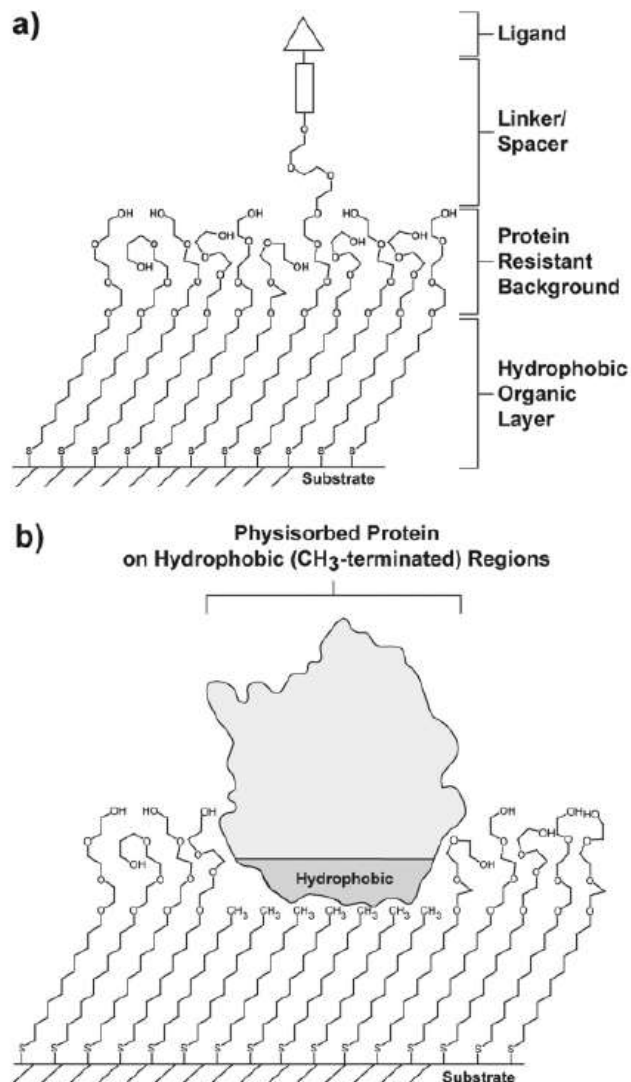
Figure 21. Schematic illustrations of (a) a mixed SAM and (b) a patterned SAM. Both types are used for applications in biology and biochemistry.
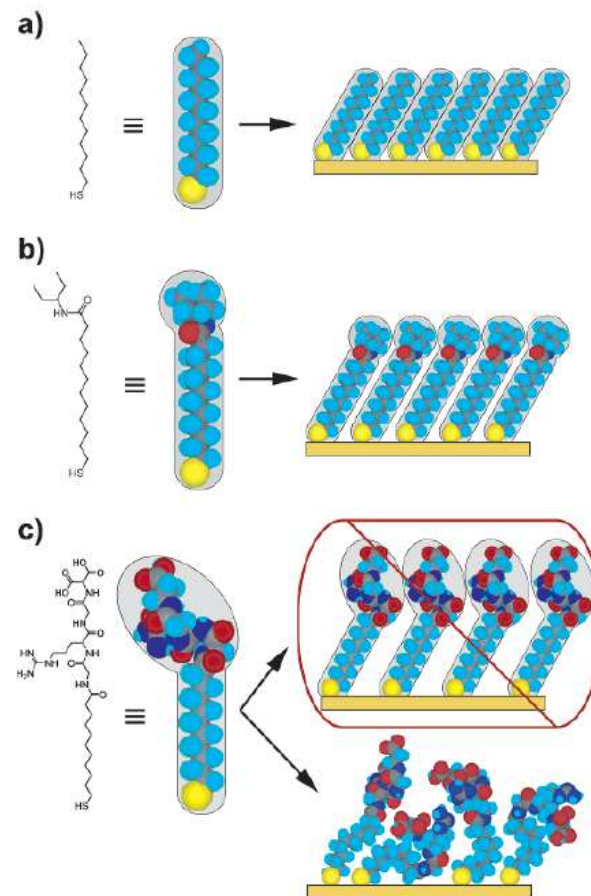
Figure 22. Schematic diagram illustrating the effects that large terminal groups have on the packing density and organization of SAMs. (a) Small terminal groups such as $-CH_3$, $-CN$, etc., do not distort the secondary organization of the organic layer and have no effect on the sulfur arrangement. (b) Slightly larger groups (like the branched amide shown here) begin to distort the organization of the organic layer, but the strongly favorable energetics of metal−sulfur binding drive a highly dense arrangement of adsorbates. (c) Large terminal groups (peptides, proteins, antibodies) sterically are unable to adopt a secondary organization similar to that for alkanethiols with small terminal groups. The resulting structures probably are more disordered and less dense than those formed with the types of molecules in a and b.

Quasi-crystalline
helical structure
adopted by OEG
in air and vacuum

Amorphous structure
adopted by OEG in water
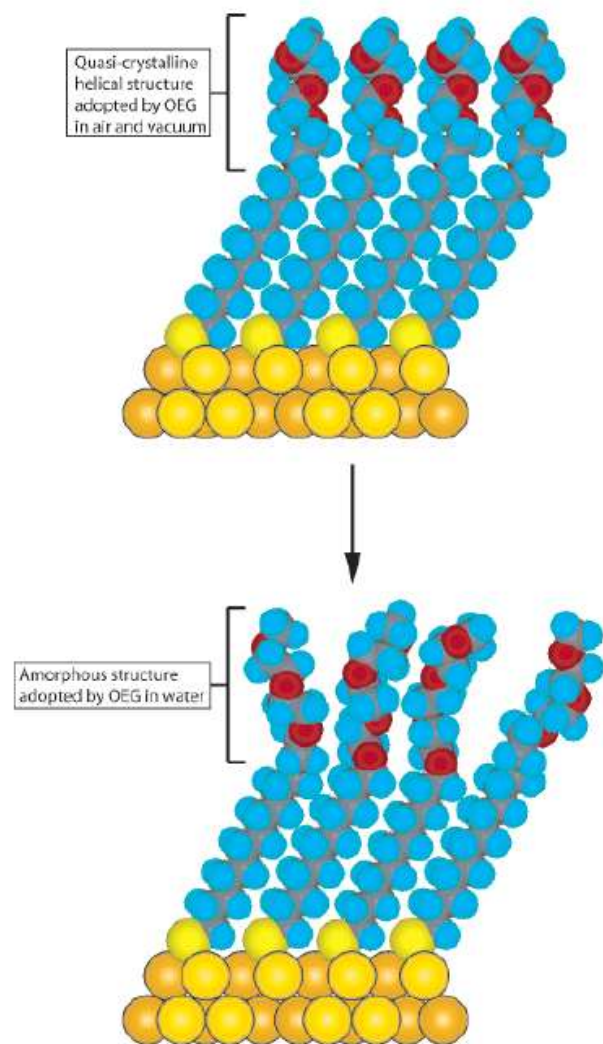
Figure 23. Schematic illustration of the order−disorder transition evidenced by SAMs of alkanethiolates terminated with triethylene glycol. The EG_3 group loses conformational ordering upon solvation in water.
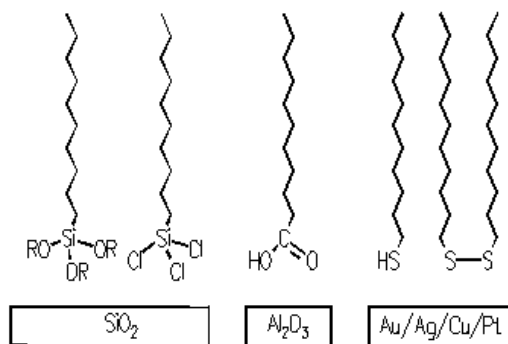
Temperature Programmed Desorption
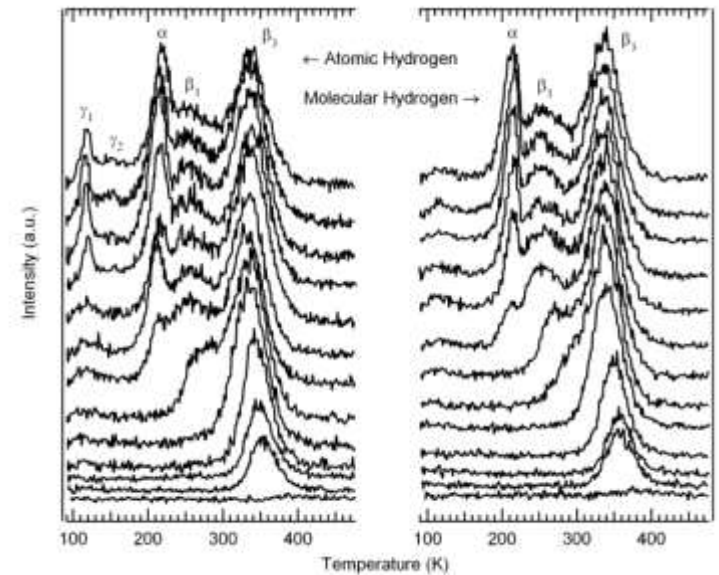
Self-Assembly

- Substrates
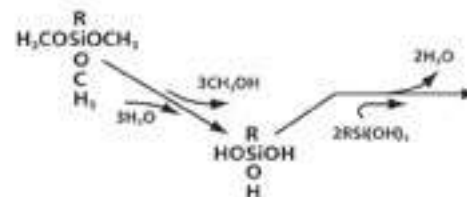- Interstitial adhesion layer
- Noble metal layer
- Organo-sulfur

Organosilanes

Self-assembled monolayers

- Surface
- silicon oxide: silanisation
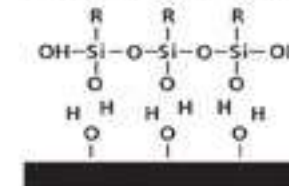- aluminum oxide: fatty acids
- metals: thiols and sulfides

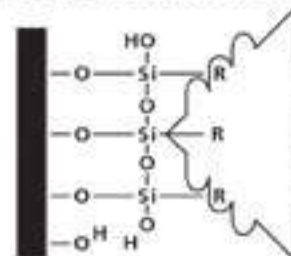Immersion of substrate in a solution containing the adequate molecules for 12 - 24 hours yields an ordered monolayer

Hydrolysis (1)

Condensation of Oligomers (2)
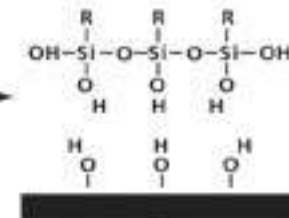
**Bond Formation (4)**
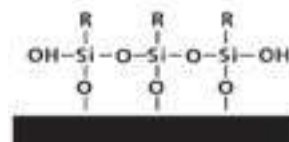
Hydrogen Bonding (3)
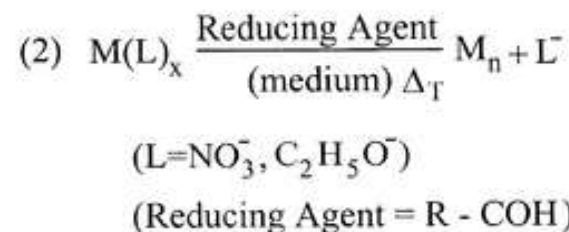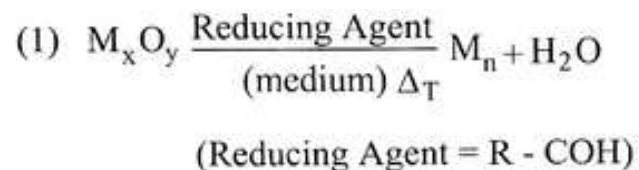
Reaction and bond formation of the R group (5)

Synthesis of Silver Nanoparticles

1. *A solution of AgNO$_3$ (1.0 x 10^{-3} M) in deionized water was heated until it began to boil.*
2. *Sodium citrate solution was added dropwise to the silver nitrate solution as soon as the boiling commenced. The color of the solution slowly turned into grayish yellow, indicating the reduction of the Ag+ ions.*
3. *Heating was continued for an additional 15 min, and then the solution was cooled to room temperature before employing for further experimentation.*
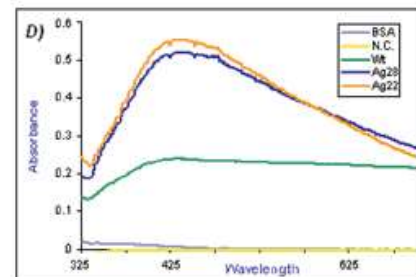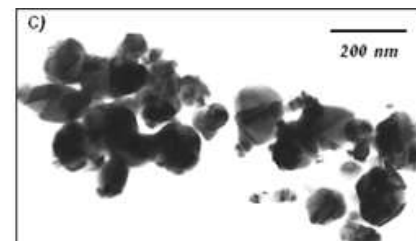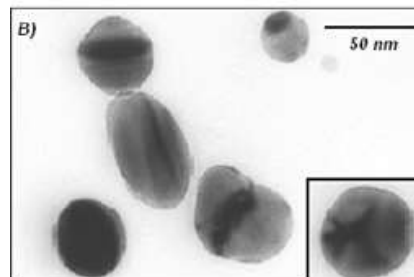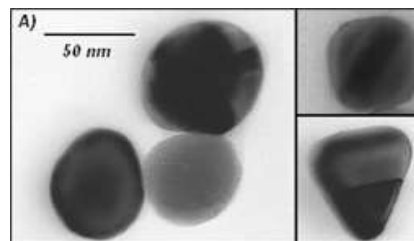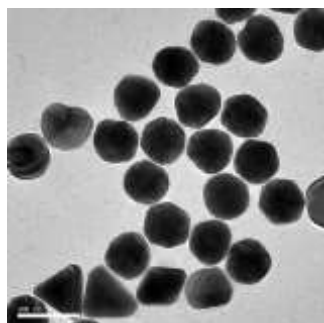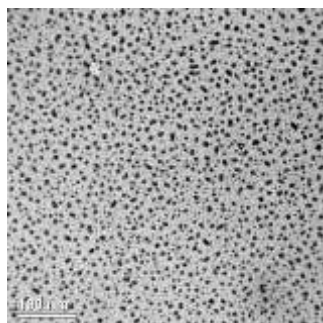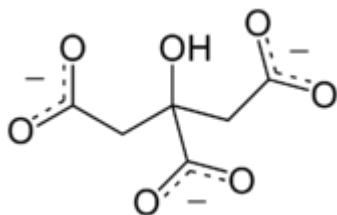
Synthesis of Gold Nanoparticles

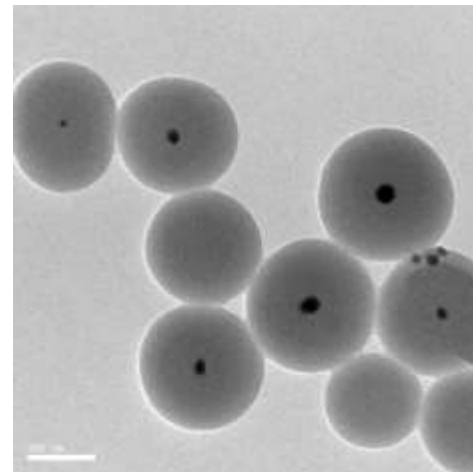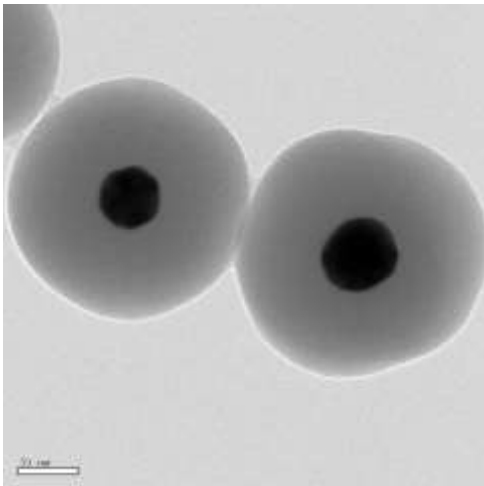1. Add 20 mL of 1.0 mM $HAuCl_4$ to a 50 mL round bottom flask on a stirring hot plate.
2. Add a magnetic stir bar and bring the solution to a boil.
3. To the boiling solution, add 2 mL of a 1% solution of trisodium citrate dihydrate
4. The gold sol gradually forms as the citrate reduces the gold(III). Stop heating when a deep red color is obtained.

$$(1) \quad M_xO_y \xrightarrow[\text{(medium)} \ \Delta_T]{\text{Reducing Agent}} M_n + H_2O$$

$$(\text{Reducing Agent} = R - COH)$$

$$(2) \quad M(L)_x \xrightarrow[\text{(medium)} \ \Delta_T]{\text{Reducing Agent}} M_n + L^-$$

$$(L = NO_3^-, C_2H_5O^-)$$

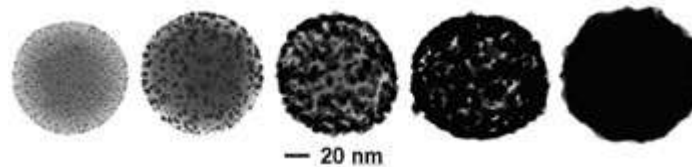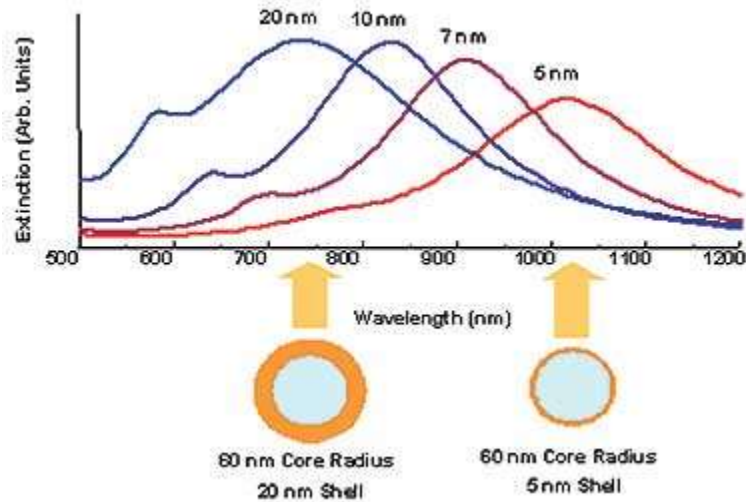$$(\text{Reducing Agent} = R - COH)$$
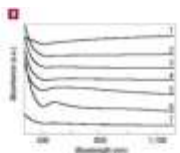
Construction of Core Shell Ag/Au@SiO$_2$ Nanoparticles

1. *Under vigorous stirring, 1 ml of the silver/ gold colloids solution was mixed with 250 mL of isopropanol and 25 mL of deionized water.*
2. *Immediately after the addition of 4 mL of 30% ammonium hydroxide, different amounts of tetraethoxysilane (TEOS) were added to the reaction mixture.*
3. *To obtain different silica layer thicknesses, TEOS solutions with a concentration between 50% and 100% was added to the suspension. The reaction was stirred at room temperature for 30 minutes and then was allowed to age without agitation at 4°C overnight.*
4. *Each suspension of silica-coated silver/gold nanoparticles was washed and centrifuged, followed by re-suspension in water. The thickness of the silica layers was determined from TEM images .*
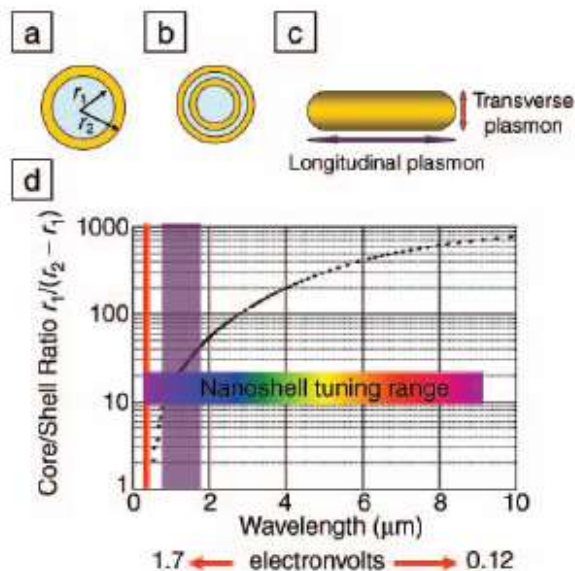
Core-Shell Nanoparticles

a
r_1
r_2

b

c
Transverse plasmon
Longitudinal plasmon

d

Core/Shell Ratio $r_1/(r_2 - r_1)$

1000
100
10
1

Nanoshell tuning range

0   2   4   6   8   10
Wavelength (μm)

1.7 ← electronvolts → 0.12

Figure 1. (a) Schematic illustration of a silica-core, gold-shell nanoshell, indicating inner (r_1) and outer (r_2) radii of the shell layers. (b) Depiction of a four-layer, concentric nanoshell. (c) Schematic illustration of a metallic nanorod. (d) Plot of nanoshell resonance as a function of core and shell dimensions, overlaid with reported spectral ranges of nanorod resonances (red, transverse plasmon; purple, longitudinal plasmon), and reported nanoshell and concentric nanoshell combined spectral range of plasmon response.
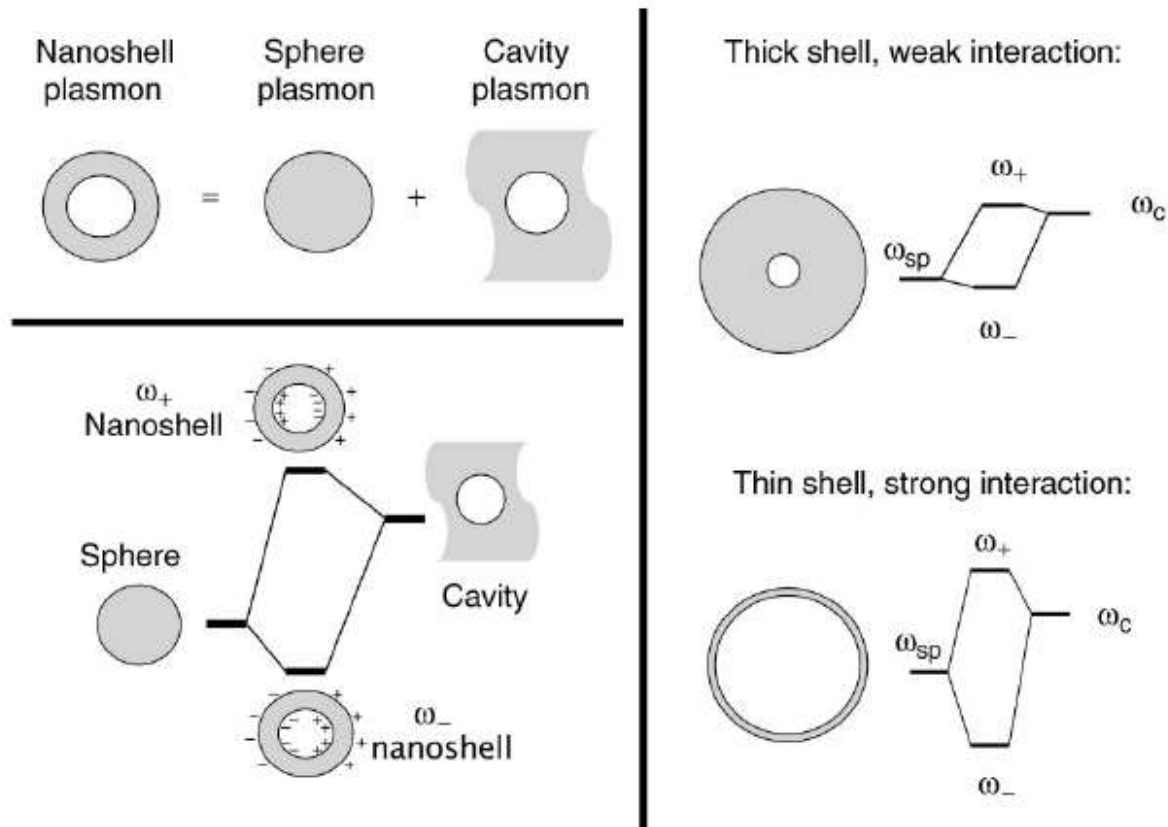
Nanoshell plasmon = Sphere plasmon + Cavity plasmon

ω_+ Nanoshell

Sphere

Cavity

ω_- nanoshell

Thick shell, weak interaction:

ω_+
ω_{sp}
ω_c
ω_-

Thin shell, strong interaction:

ω_+
ω_{sp}
ω_c
ω_-

Figure 2. Plasmon hybridization and the sphere–cavity model for nanoshells: the interaction between a sphere (resonance frequency, ω_{sp}) and a cavity plasmon (resonance frequency, ω_c) is tuned by varying the thickness of the shell layer of the nanoparticle. Two hybrid plasmon resonances, the ω_- "bright," or "bonding," plasmon and the ω_+ "dark," or "anti-bonding," plasmon resonances are formed. The lower-energy plasmon couples most strongly to the optical field.
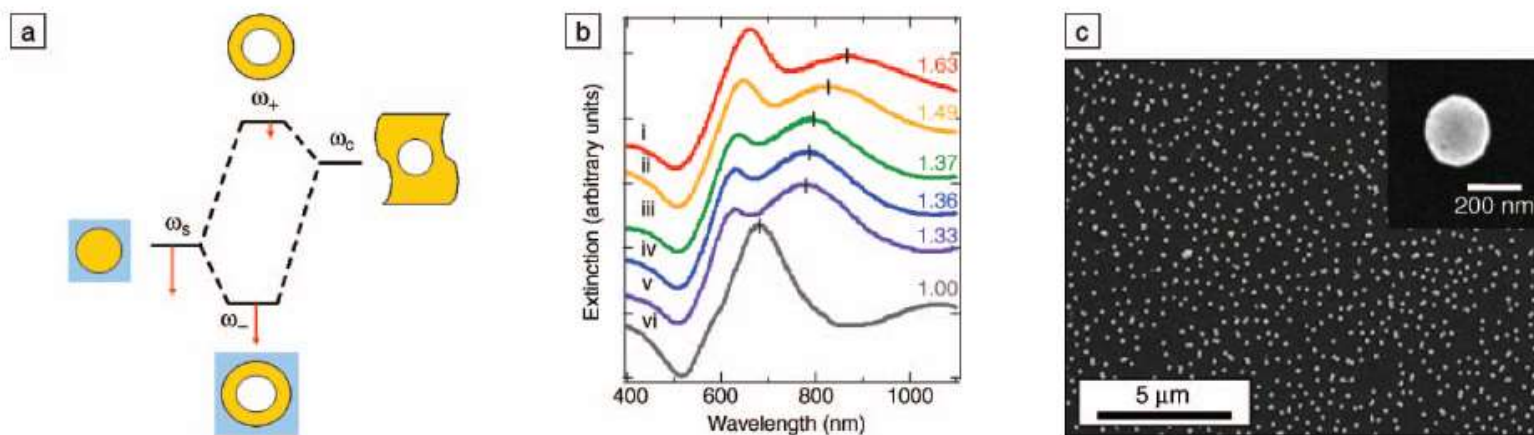
Figure 5. (a) Plasmon hybridization picture applied to surface plasmon resonance sensing with nanoshells: the low-energy "bonding" plasmon, ω_-, is sensitized to changes in its dielectric environment. The blue background schematically denotes the embedding medium for the nanoparticle. (b) Experimental curves showing plasmon resonance shifts for nanoshell-coated films in various media: (i) carbon disulfide, (ii) toluene, (iii) hexane, (iv) ethanol, (v) H$_2$O, and (vi) air. The index of refraction for each embedding medium is noted on the far right of the spectra. Spectra are offset for clarity. (c) Scanning electron micrograph of nanoshells deposited onto a poly(vinyl pyridine) functionalized glass surface, as used to acquire data in (b). Inset: individual nanoshell.

Preparation of Fe$_3$O$_4$@Ag/Au

1. *To the magnetic nanoparticle suspension obtained from commercial company, add 50 ml of a solution of Au (III) salt or Ag (I) salt at concentration of 0.01–1% mmol/L , shaking for 30 minutes, allowing Au (III) or Ag (I) ion to absorb on the surface of magnetic nanoparticle sufficiently,*
2. *Then adding 15–40 ml of reducing agent, such as hydroxylamine hydrochloride at concentration of 40 mmol/L, reacting for 5–40 minutes.*
3. *Further adding 1–10 ml of a solution of Au (III) salt or Ag (I) salt at concentration of 0.01–1%, shaking for 10 minutes, coating a reduced layer of gold or silver on the surface of the magnetic nanoparticle, forming super-paramagnetic composite particles having core/shell structure, separating magnetically, washing repeatedly with distilled water.*

.

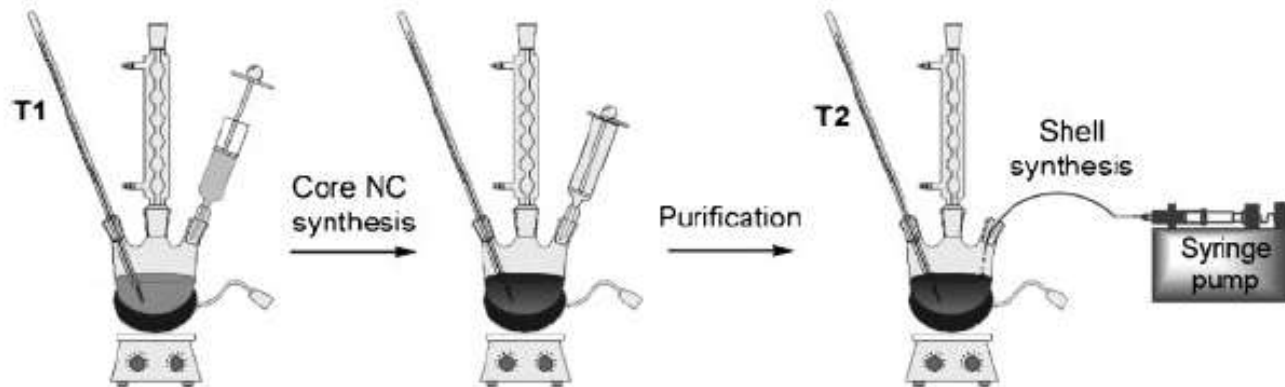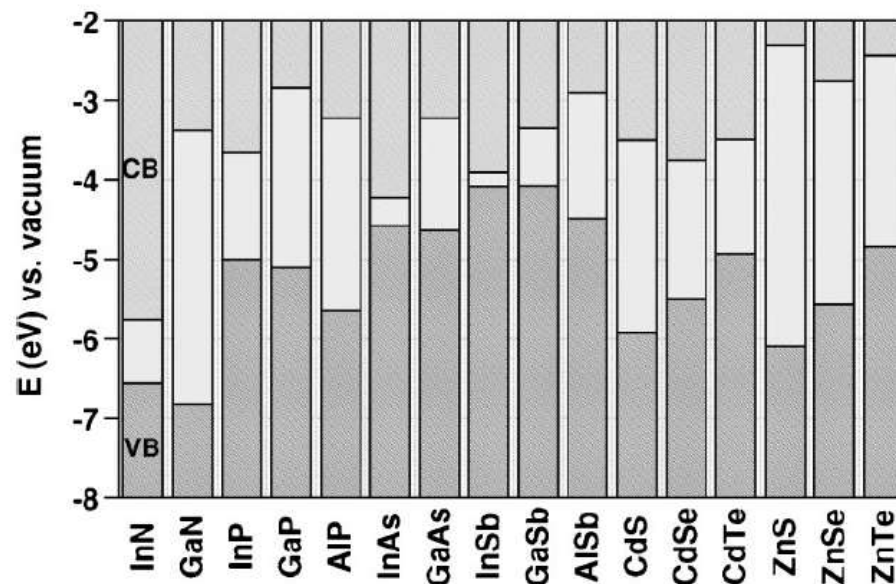# Synthesis of Quantum Dots

Figure 2. Two–step synthesis of core/shell nanocrystals.

Scheme 1. Electronic energy levels of selected III–V and II–VI semi-conductors using the valence-band offsets from Reference [12] (VB: valence band, CB: conduction band).
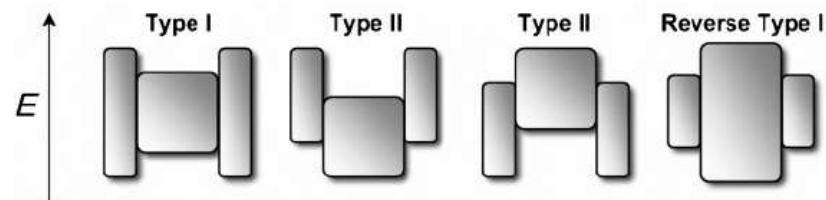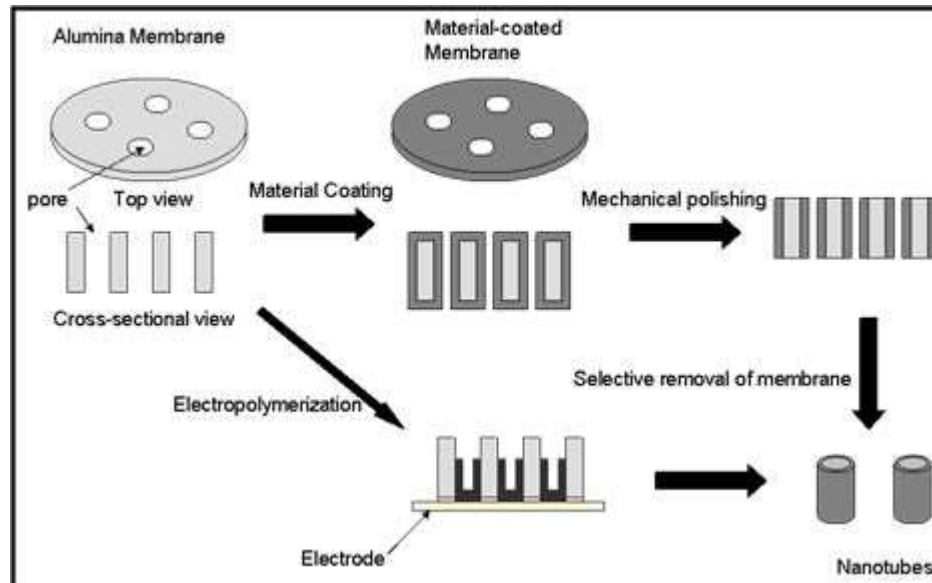

Figure 1. Schematic representation of the energy-level alignment in different core/shell systems realized with semiconductor NCs to date. The upper and lower edges of the rectangles correspond to the positions of the conduction- and valence-band edge of the core (center) and shell materials, respectively.
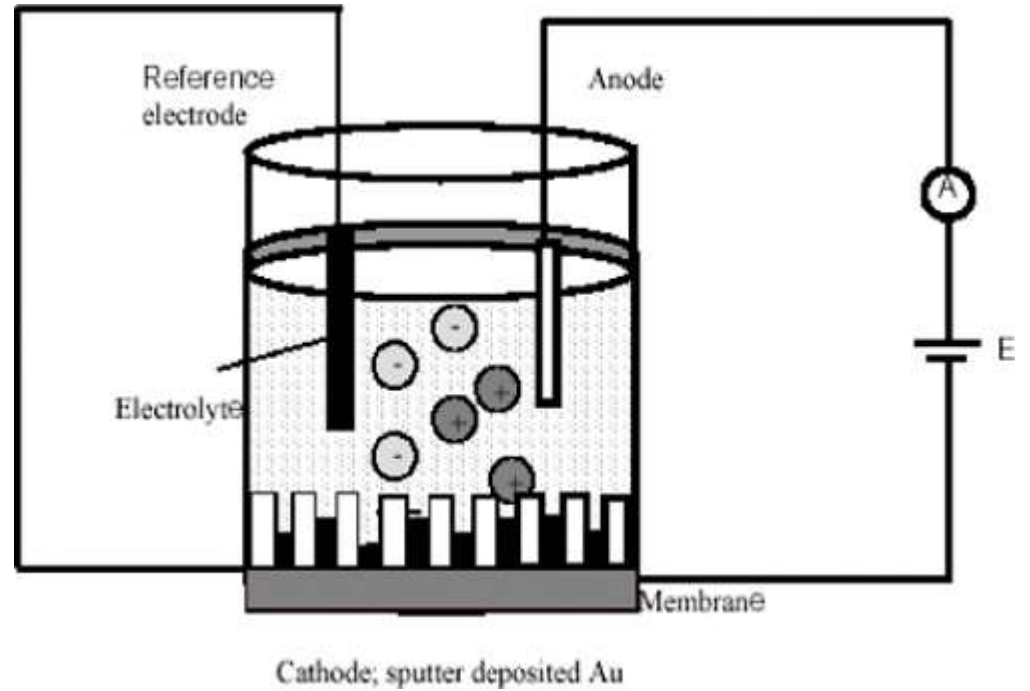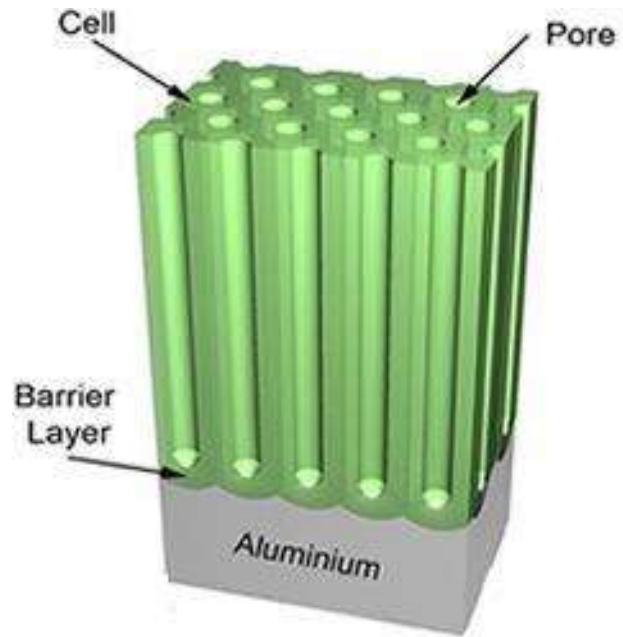
Template Synthesis
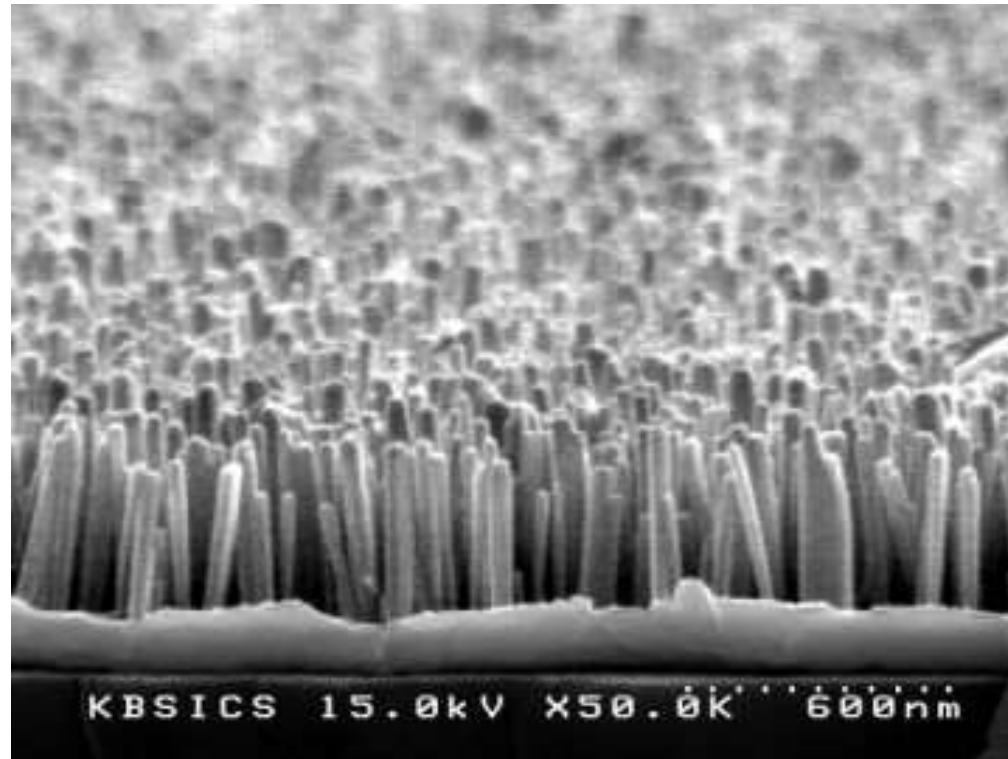
Porous Materials

- AAO

- MCM-41

Mobil Crystalline Materials, or MCM-41

Santa Barbara Amorphous type material, or SBA-15

- Micro: < 2nm

- Meso:

- Macro: > 50nm

AAO

Cell

Pore

Barrier Layer

Aluminium

Reference electrode

Anode

Electrolyte

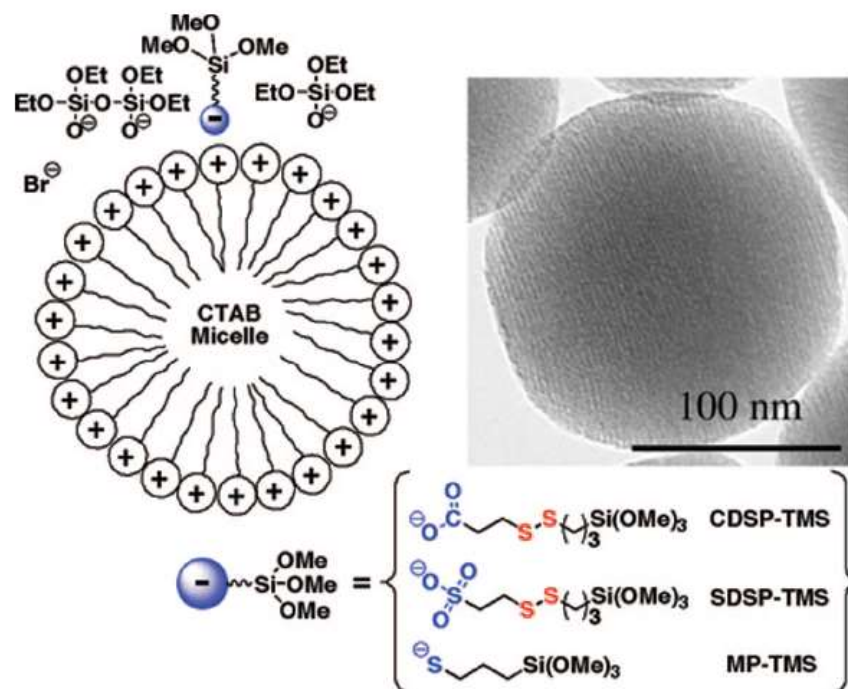Membrane

Cathode; sputter deposited Au

A

E

FIGURE 3. Schematic representation of the use of anionic organoalkoxysilanes for controlling the functionalization of the MSN materials. The MCM-41-type mesoporous channels are illustrated by the parallel stripes shown in the transmission electron microscopy (TEM) micrograph of the MSN–SH material. Reproduced with permission from ref 15. Copyright 2005, Royal Society of Chemistry.
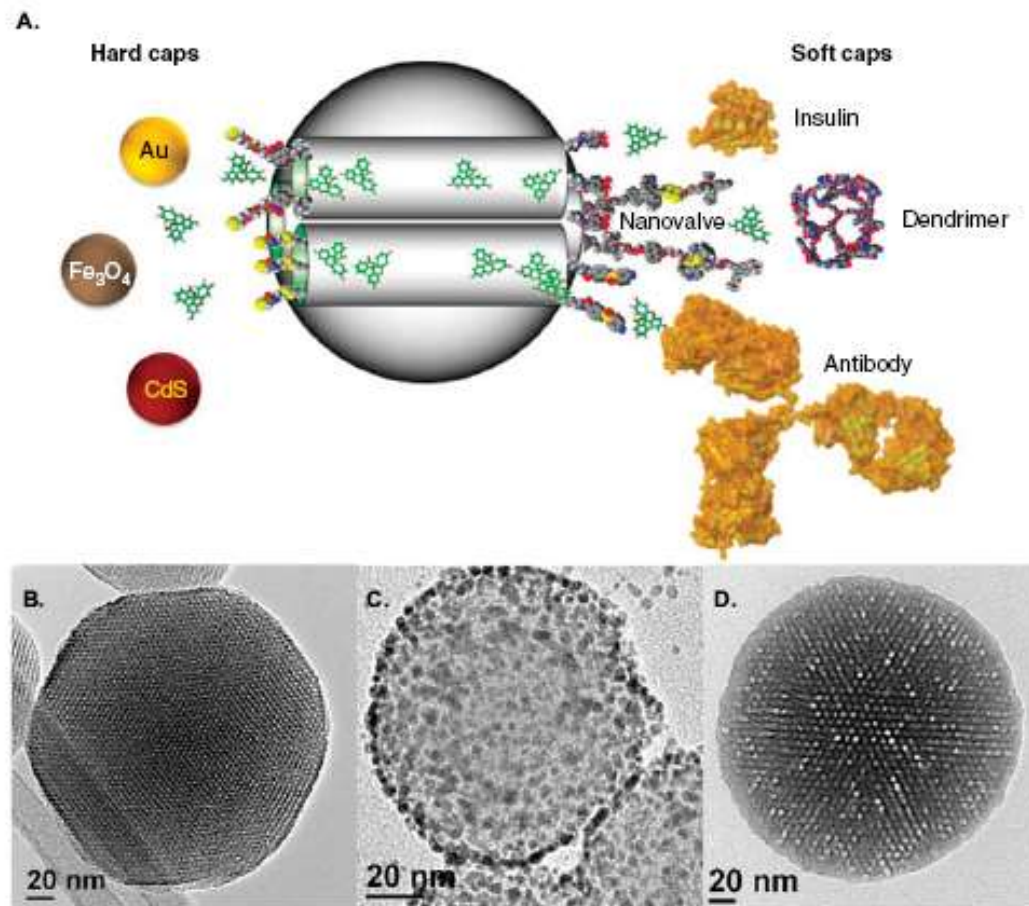
Figure 1. A. Schematic representation of a MSN loaded with drugs and capped with hard caps and soft caps highlighted in this review. Transmission electron microscopy images of **(B)** a MSN along the axis of the mesopores, **(C)** capped with hard (Au NP) and **(D)** with soft (polymer) caps.
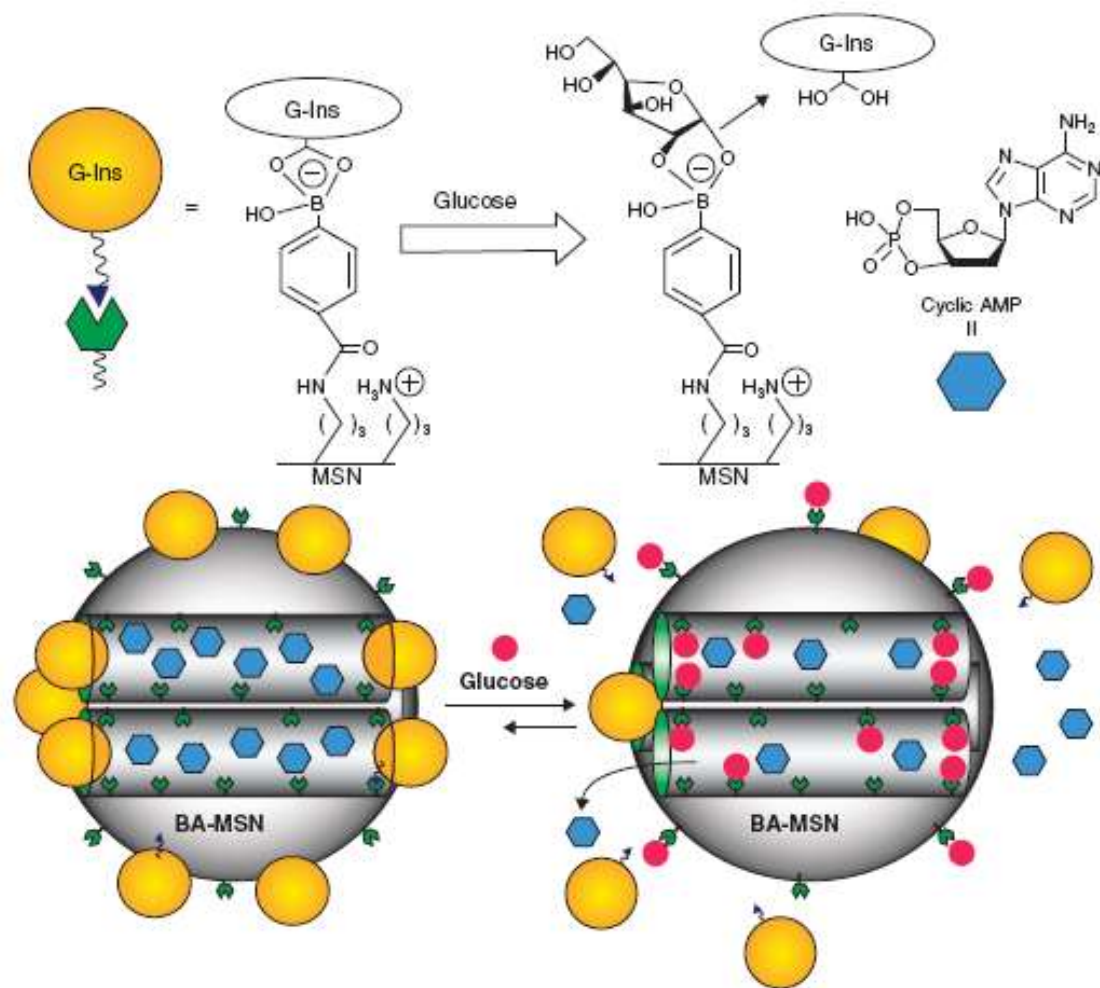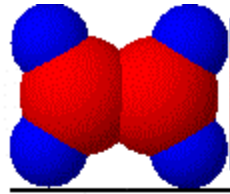
MSN: Mesoporous silica nanoparticle.

Figure 5. Schematic representation of the glucose-responsive MSN-based double delivery system for controlled release of bioactive G-Ins and cyclic AMP. The controlled release mechanism was achieved by means of the displacement reaction between blood glucose and G-Ins based on reversible boronic acid-diol complexation. High glucose concentration triggers the G-Ins uncapping and the release of cyclic AMP sequentially to diminish the higher than normal level of blood glucose.
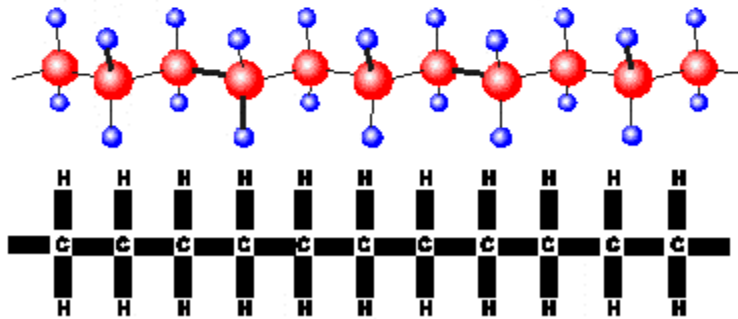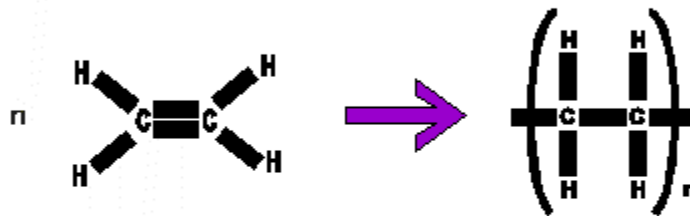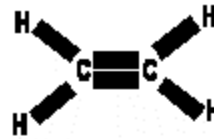
G-Ins: G-insulin; MSN: Mesoporous silica nanoparticle.

Polymer

a monomer   ethene

C_2H_4

a polymer   poly(ethene)

Block copolymer

| POLYSTYRENE BLOCK (end-block) | | RUBBER BLOCK (mid-block) | | POLYSTYRENE BLOCK (end-block) |

Phase Segregation

A-B diblock copolymer   +   C (inorganic precursor)

A

Thermal crosslinking

B + C

Nanostructured Inorganics
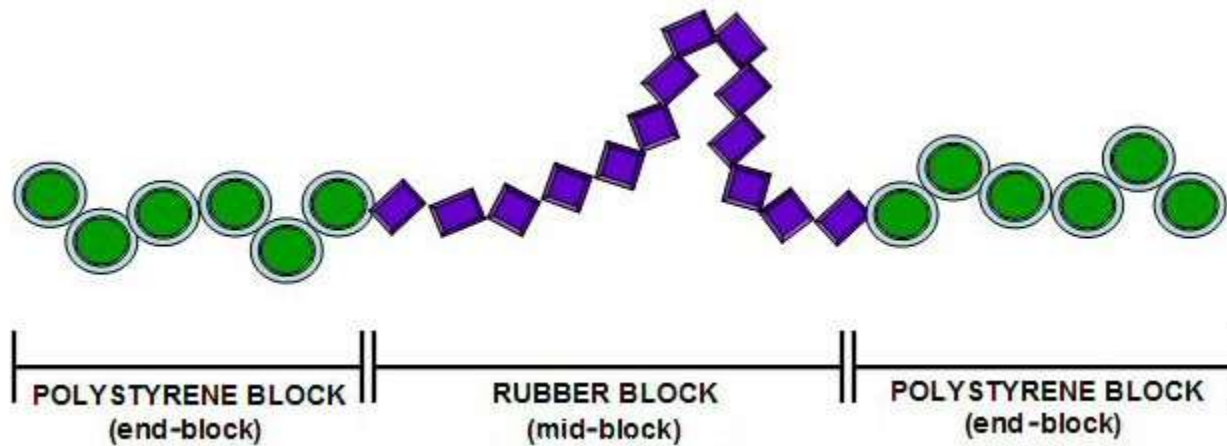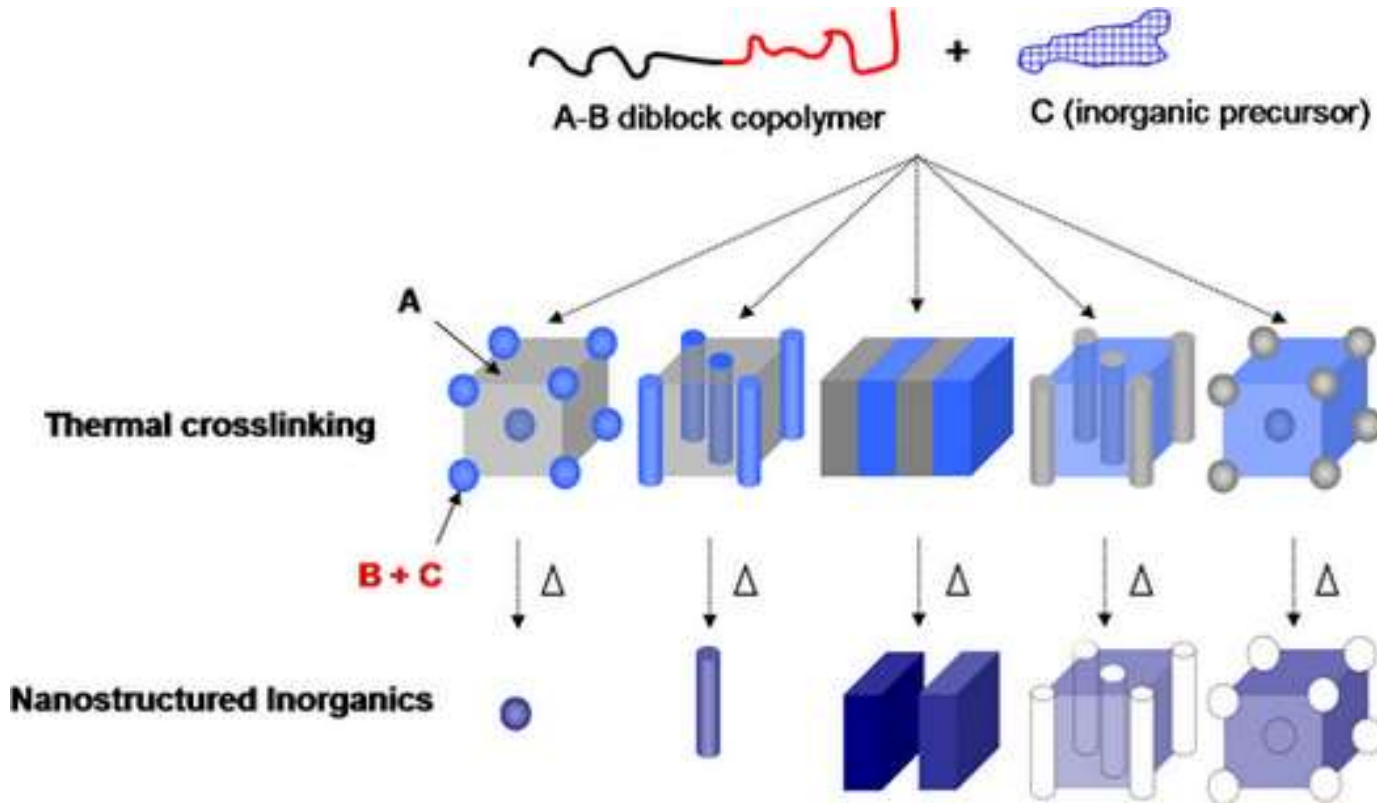
Self-Assembled Block-copolymer
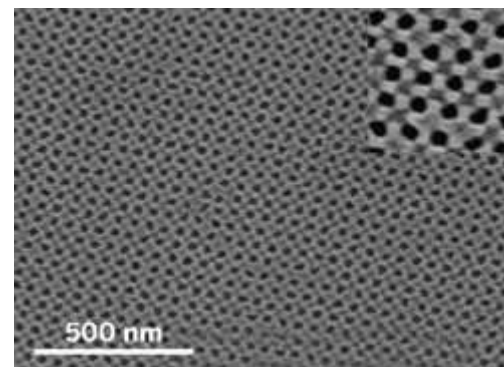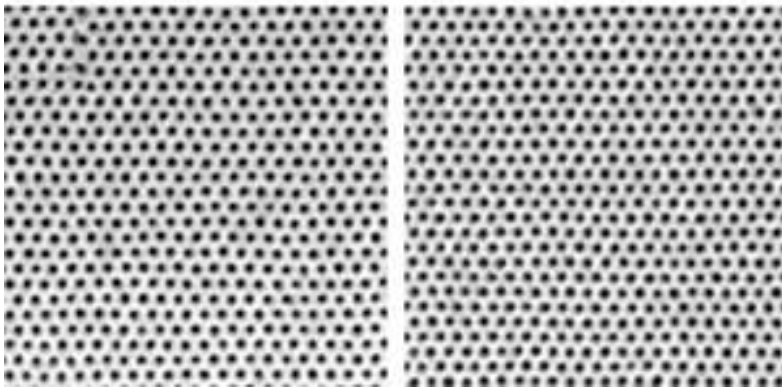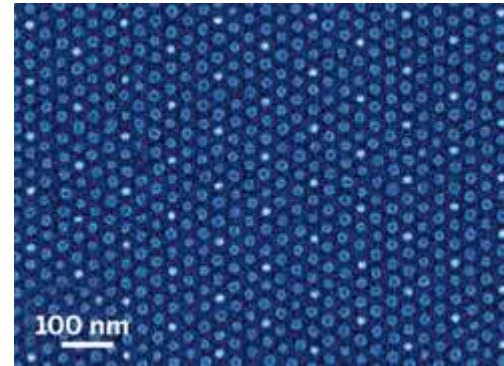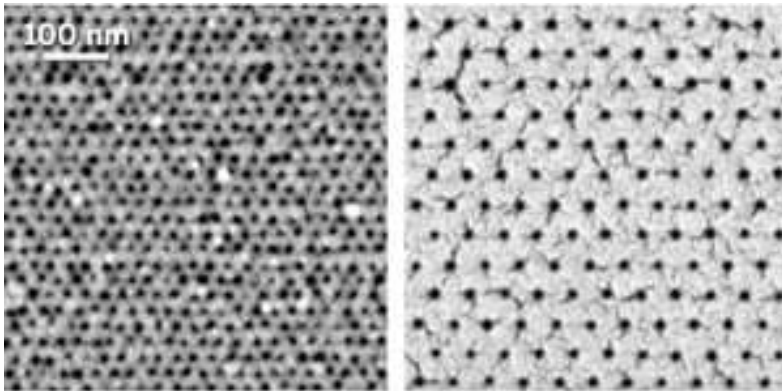
CNT
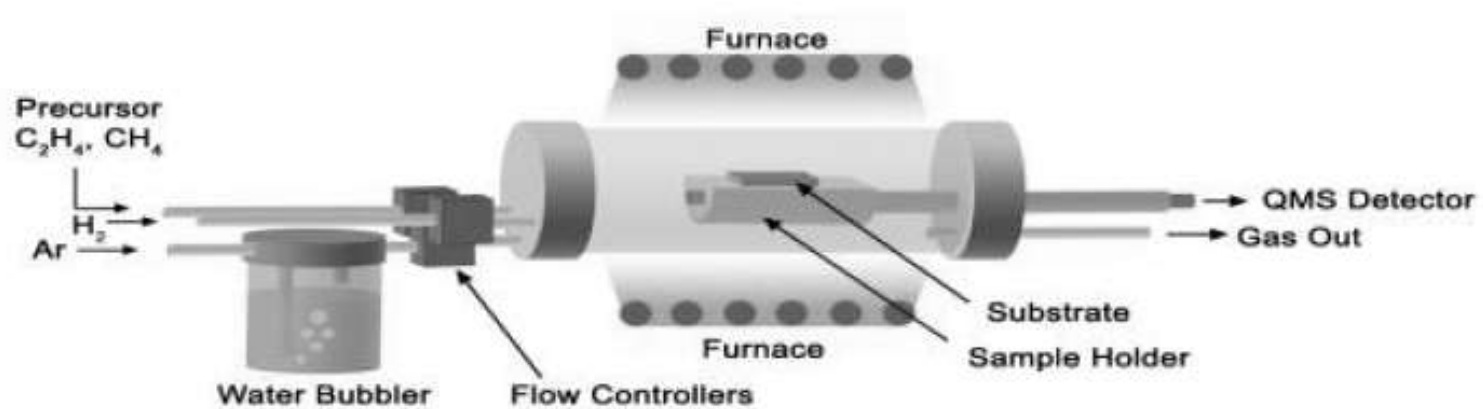
Fig. 1. Schematic of a CVD reactor for carbon nanotube growth. (Sketch by S. Yarmolenko from NCA&T State University)
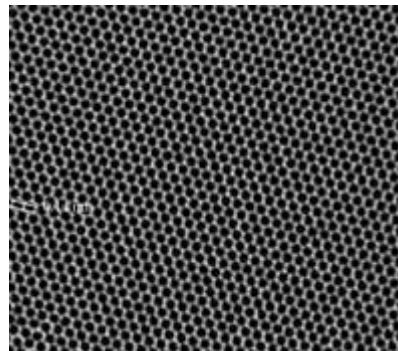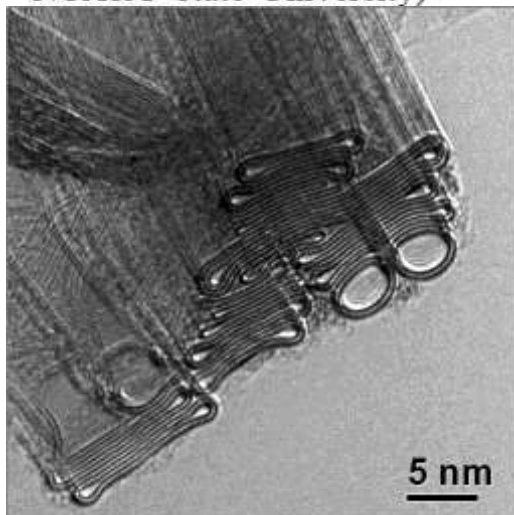
Surface Functionalization

- Recognition
  - Molecular Recognition
    - Protein
    - DNA
    - Saccharide
- Reporting/Detection
  - Dye
  - Quantum dots
  - SPR
  - SERS/LSPR
- Separation
  - Gel/Chromatography
  - Magnetic

- Surfaces
  - Gold and silver
  - Silicon oxide (glass)
  - Quantum dots
  - Polymer

Molecular Recognition
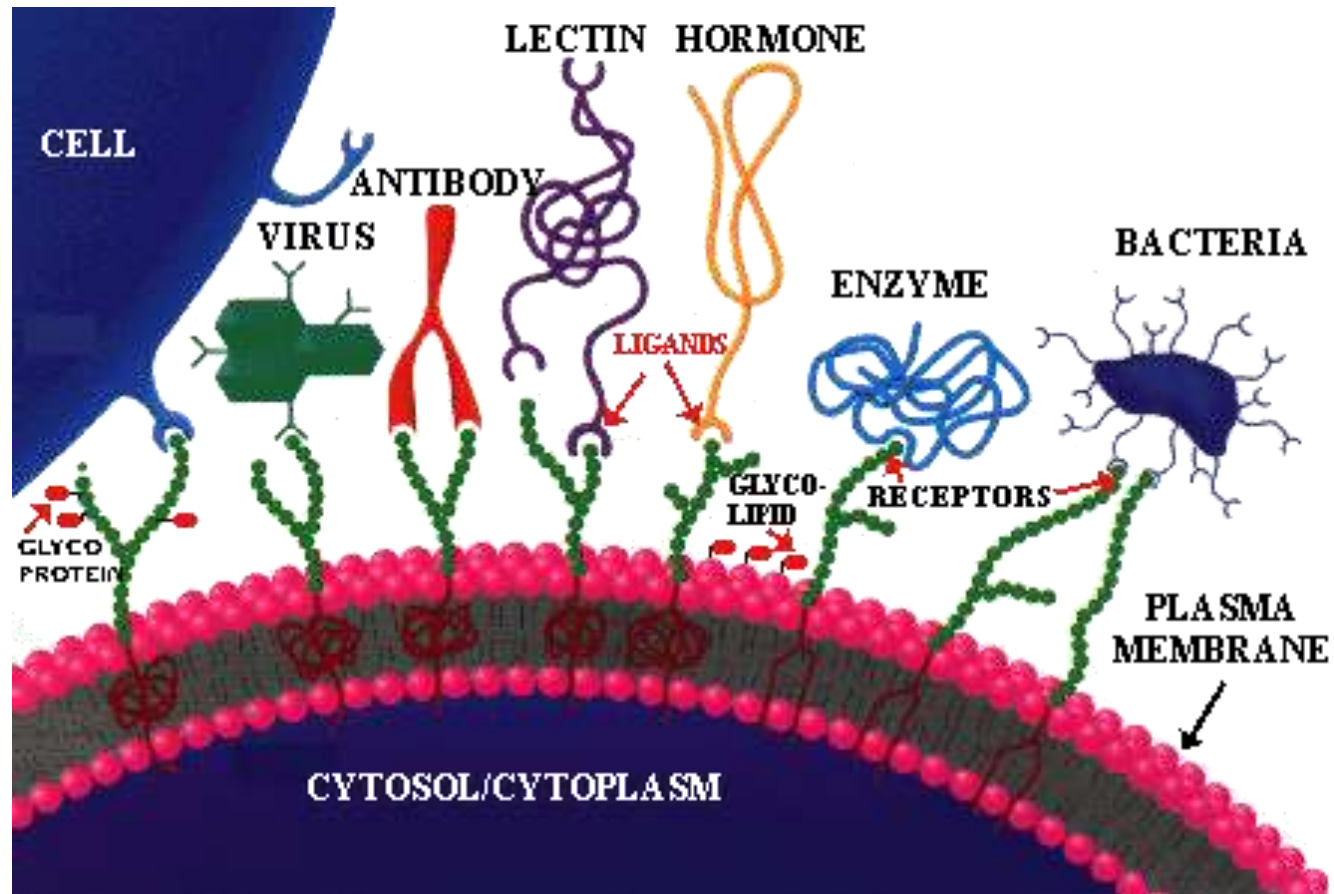
Carboxyl Presenting Surfaces
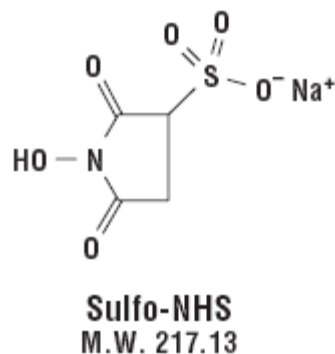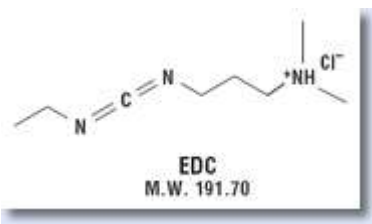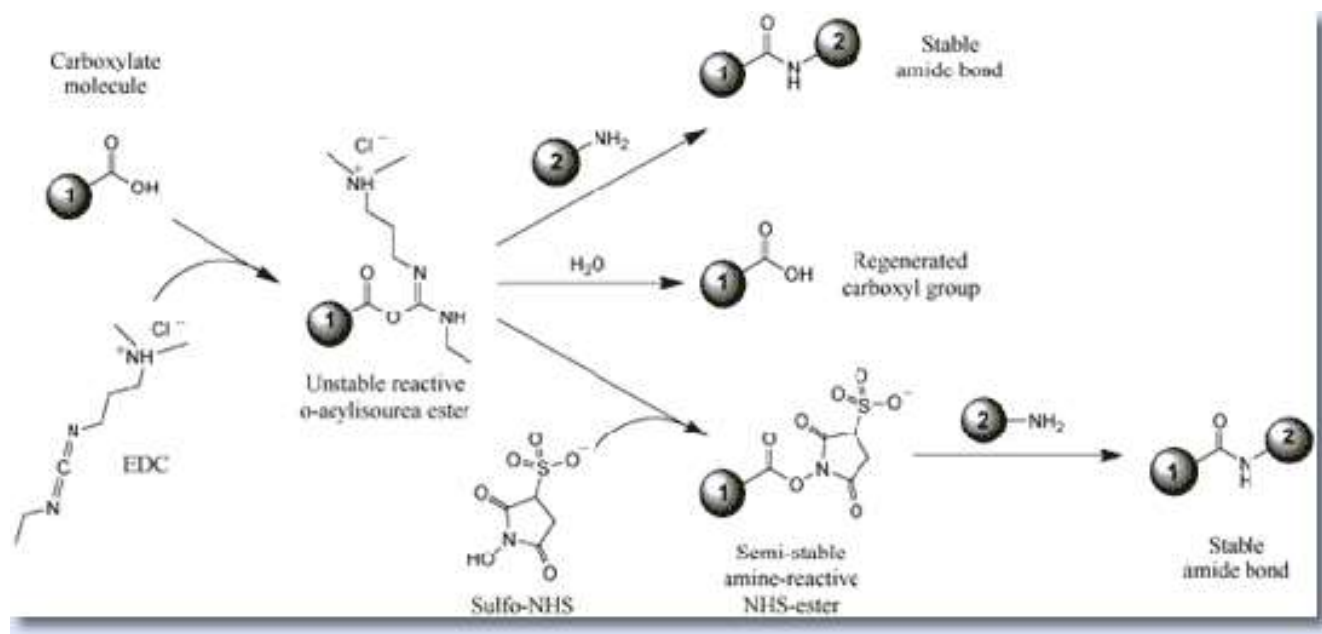
EDC (1-Ethyl-3-[3-dimethylaminopropyl]carbodiimide Hydrochloride)

Amine Presenting Surface
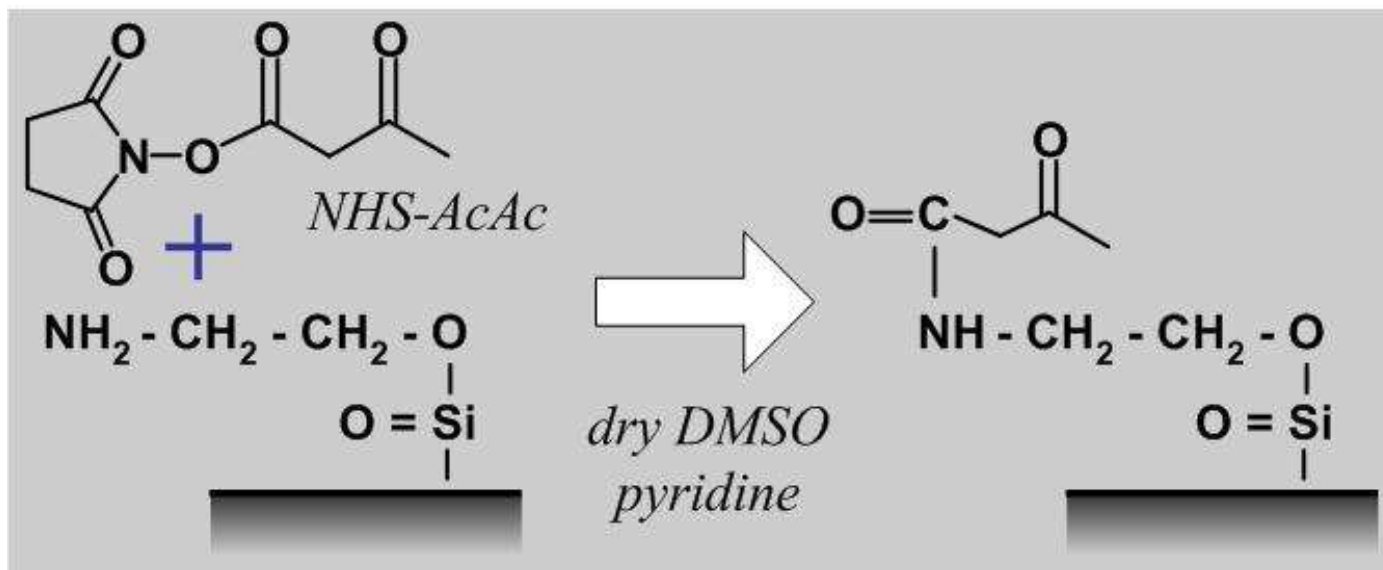
Scheme 1. Modular Design of Hydrophilic Ligands with Terminal Functional Groups Used in This Study
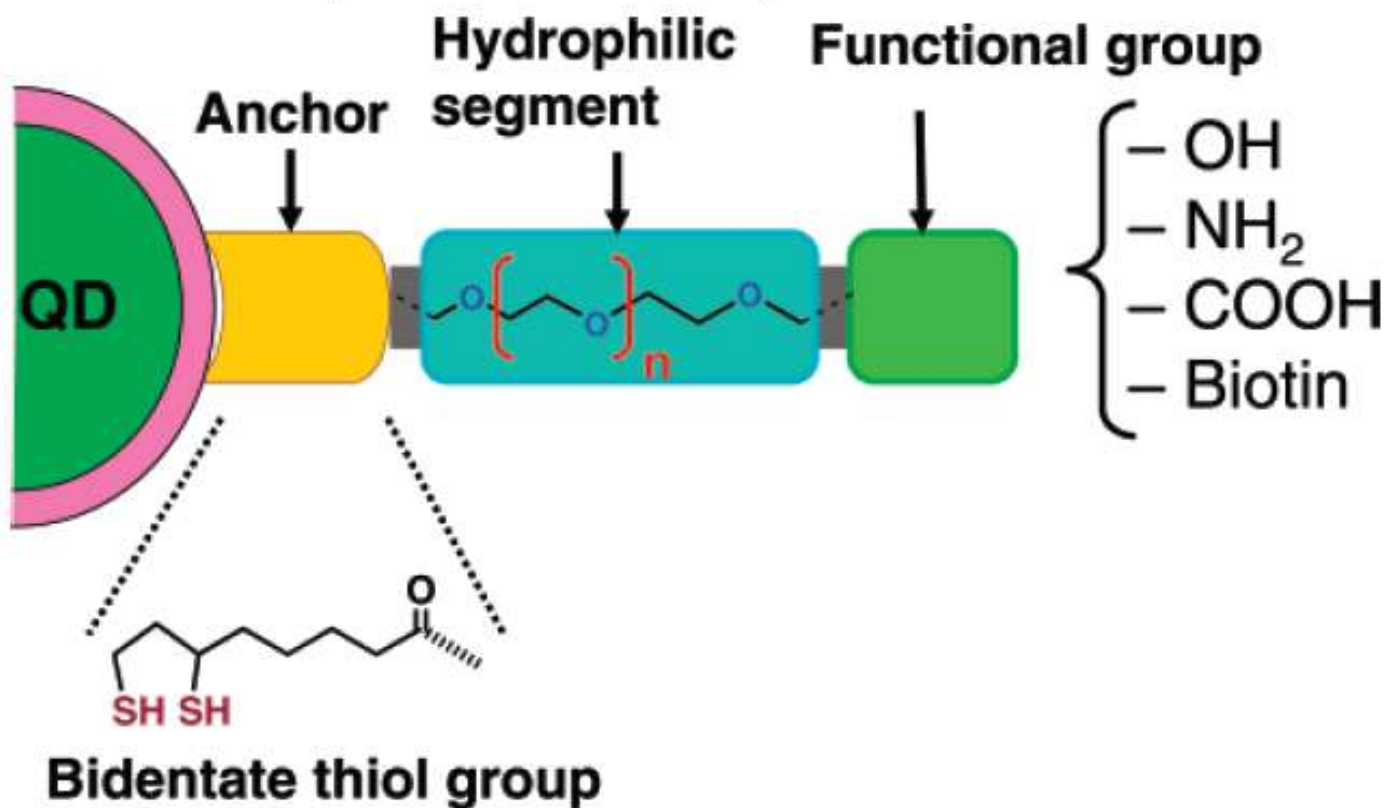
Sulfhydryl Labeling
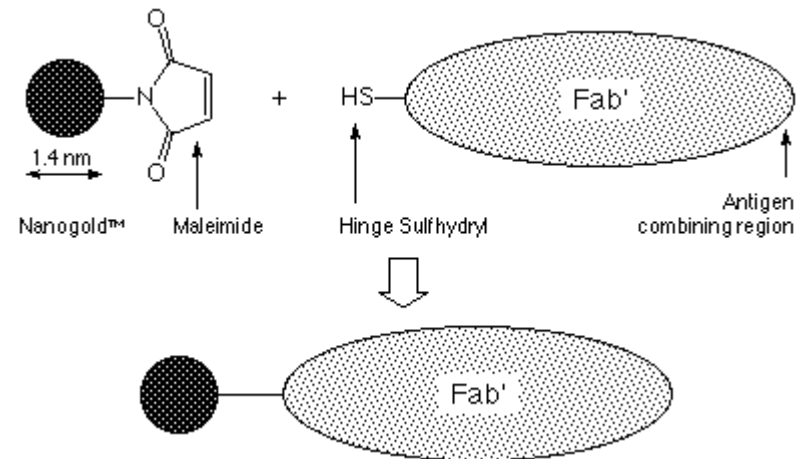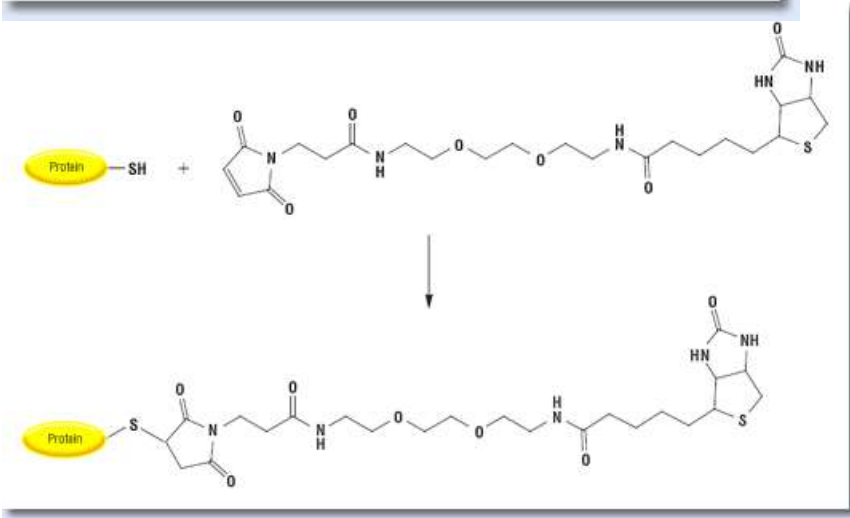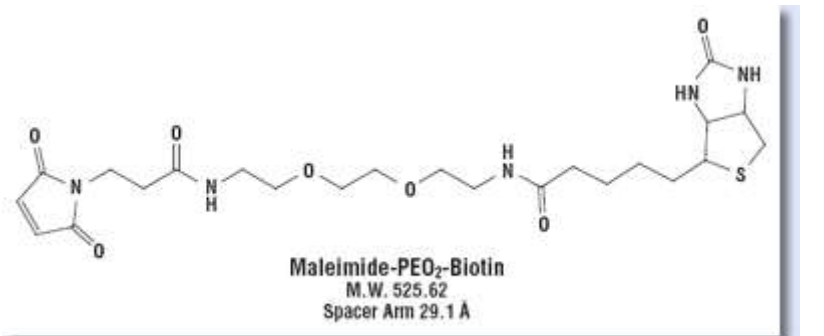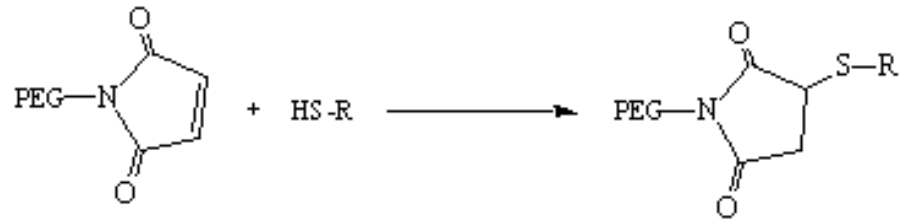
Silica Modification
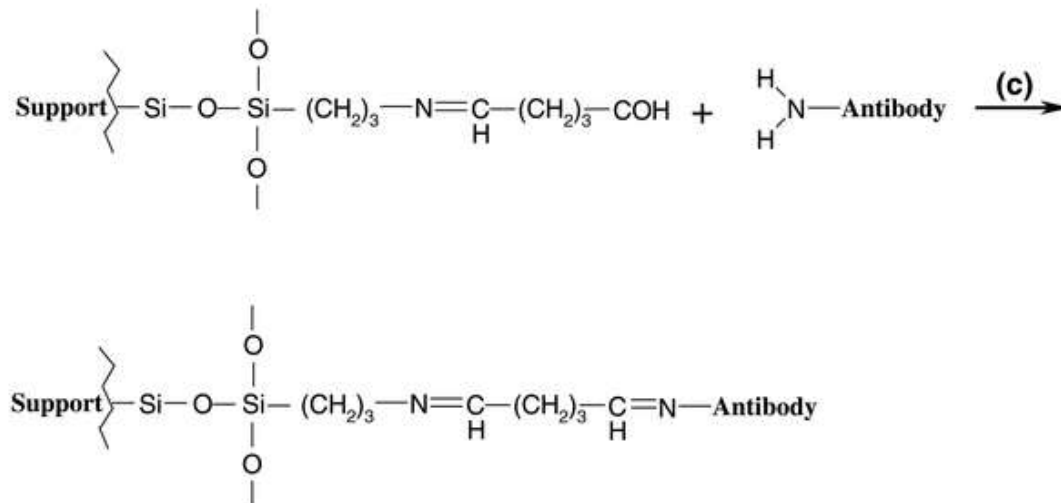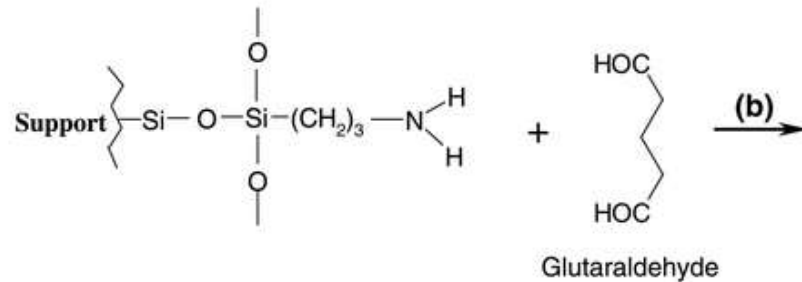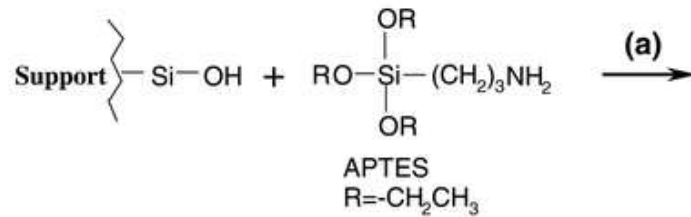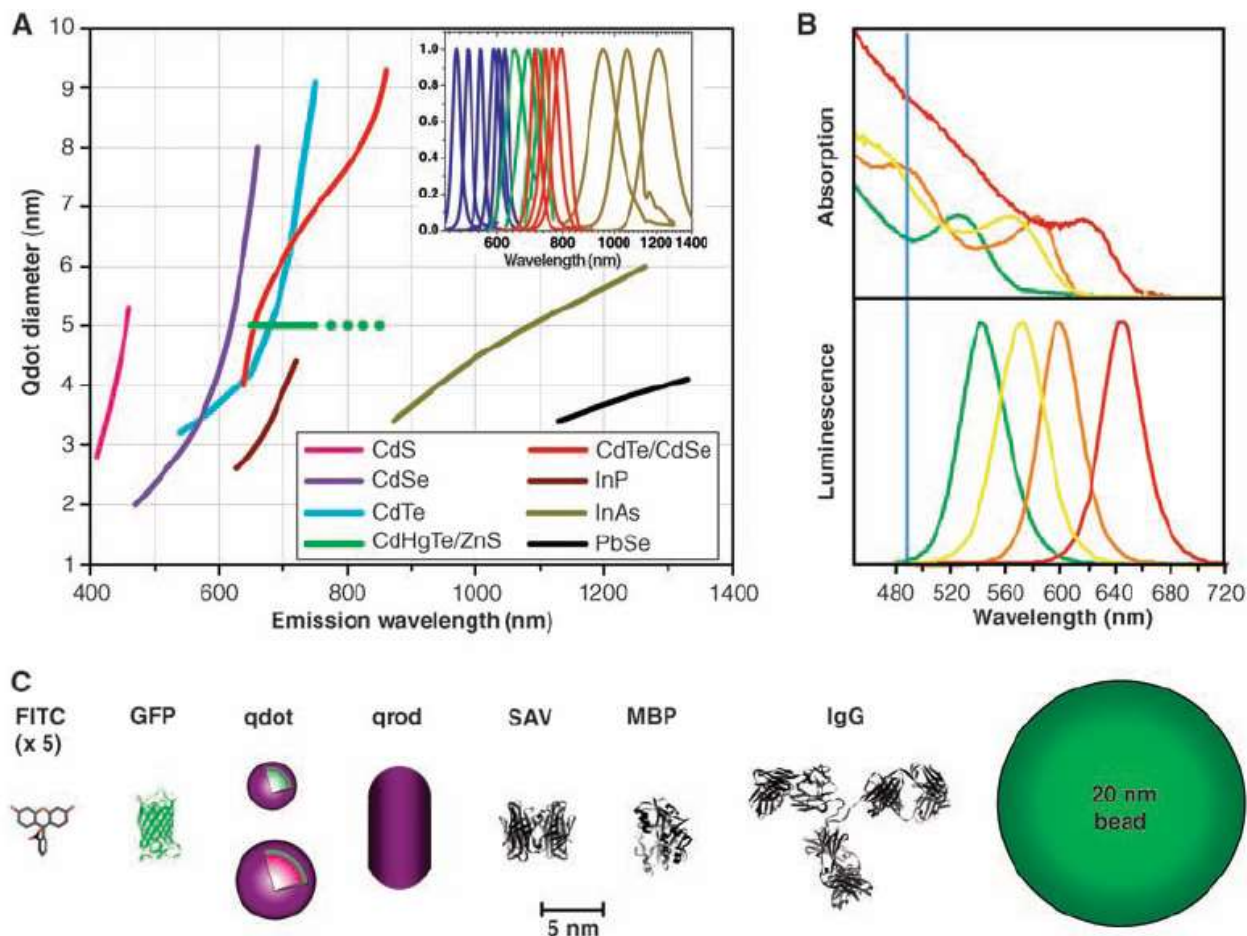
Fig. 1. (A) Emission maxima and sizes of quantum dots of different composition. Quantum dots can be synthesized from various types of semiconductor materials (II-VI: CdS, CdSe, CdTe...; III-V: InP, InAs...; IV-VI: PbSe...) characterized by different bulk band gap energies. The curves represent experimental data from the literature on the dependence of peak emission wavelength on qdot diameter. The range of emission wavelength is 400 to 1350 nm, with size varying from 2 to 9.5 nm (organic passivation/solubilization layer not included). All spectra are typically around 30 to 50 nm (full width at half maximum). Inset: Representative emission spectra for some materials. Data are from (*12, 18, 27, 76–82*). Data for CdHgTe/ZnS have been extrapolated to the maximum emission wavelength obtained in our group. **(B)** Absorption (upper curves) and emission (lower curves) spectra of four CdSe/ZnS qdot samples. The blue vertical line indicates the 488-nm line of an argon-ion laser, which can be used to efficiently excite all four types of qdots simultaneously. [Adapted from (*28*)] **(C)** Size comparison of qdots and comparable objects. FITC, fluorescein isothiocyanate; GFP, green fluorescent protein; qdot, green (4 nm, top) and red (6.5 nm, bottom) CdSe/ZnS qdot; qrod, rod-shaped qdot (size from Quantum Dot Corp.'s Web site). Three proteins—streptavidin (SAV), maltose binding protein (MBP), and immunoglobulin G (IgG)—have been used for further functionalization of qdots (see text) and add to the final size of the qdot, in conjunction with the solubilization chemistry (Fig. 2).
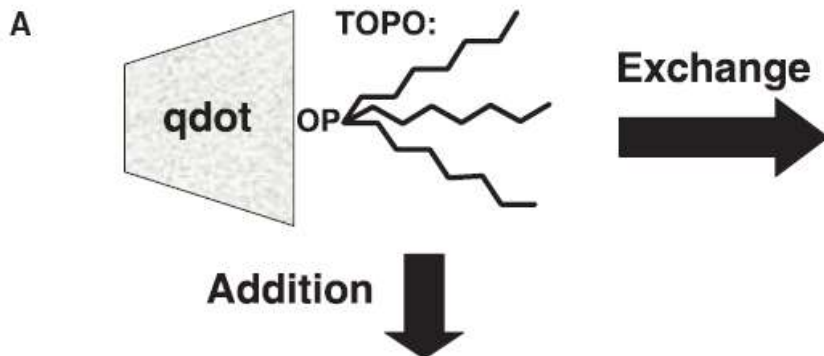
A
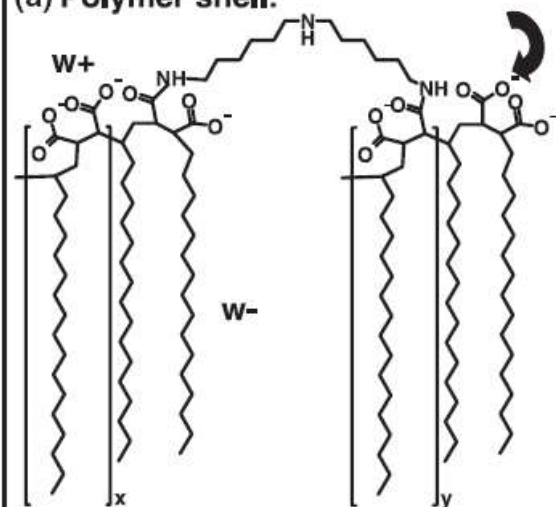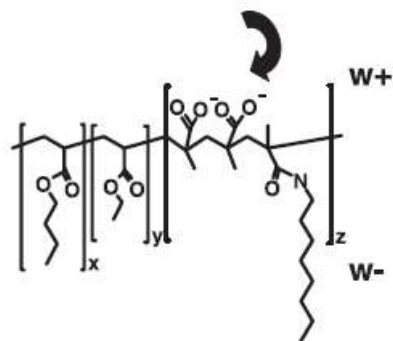
TOPO:

qdot

OP

Exchange

Addition

(a) Polymer shell:

W+

NH

NH

W−

x

y

(b) Triblock copolymer:

W+

x

y

z

W−

(c) Phospholipids:

W−

W+

(d) MAA: HS—COOH

(e) DTT: HS—SH

(f) DHLA:

SH SH

O−

(g) Oligomeric phosphine:

L

P

N

COOH

L

P

N

COOH

L

(h) Dendrons:

H_2N

H_2N

H_2N

NH_2

NH_2

OH OH

OH

OH

HO

HO

O−

HO

OH

O−

OH

SH HS

(i) Peptides:

H_2N

Cha**CC**Cha**CC**Cha**CC**Cha**GSESGGSESG**

(b) Thiol chelation

(a)

(c) Silanization

Ligand exchange

(d) Phospholipids

(e) Diblock copolymer

Hydrophobic interaction
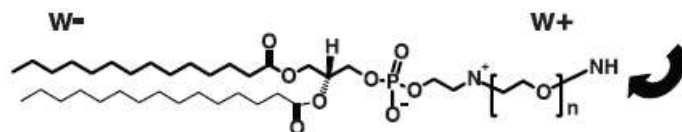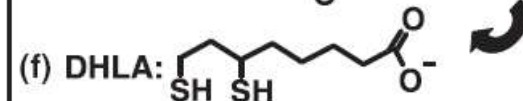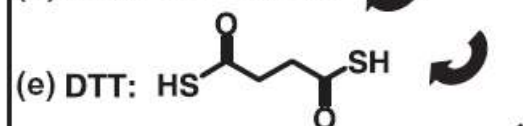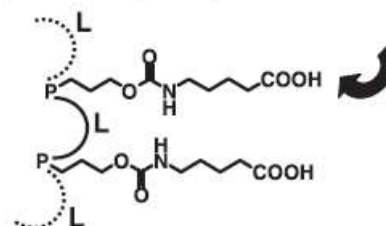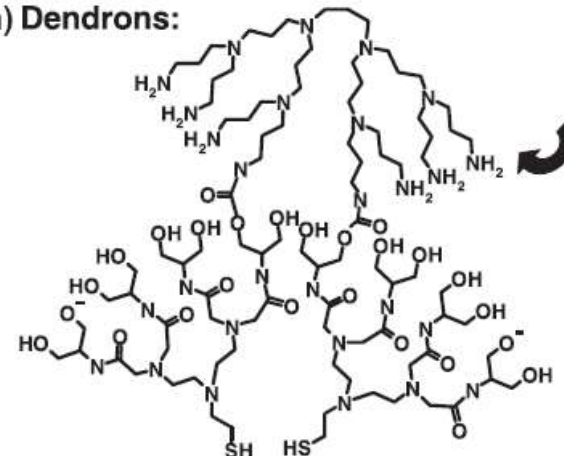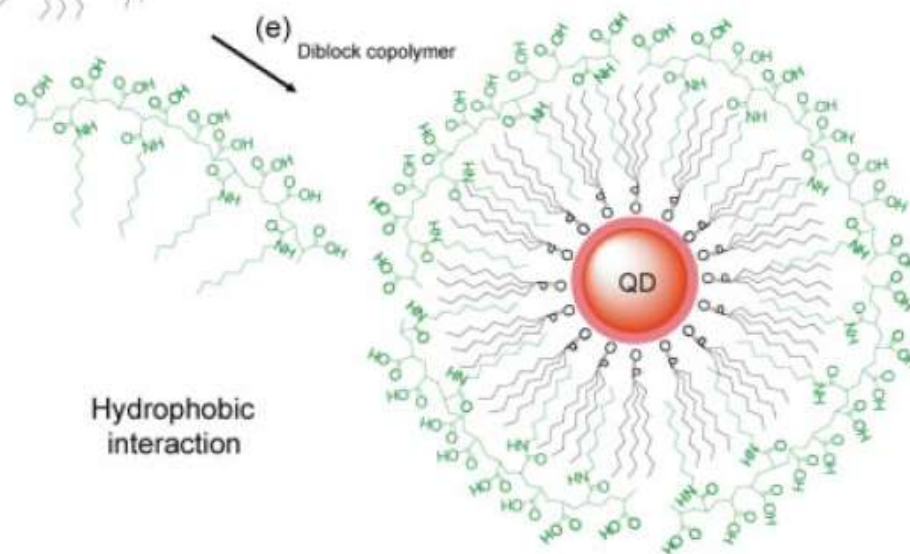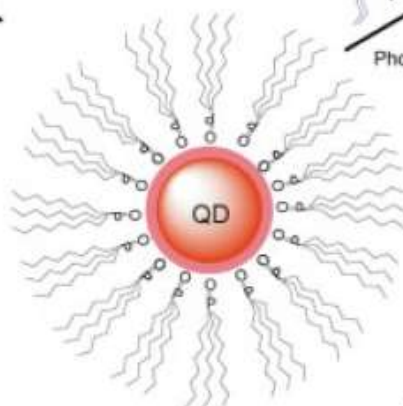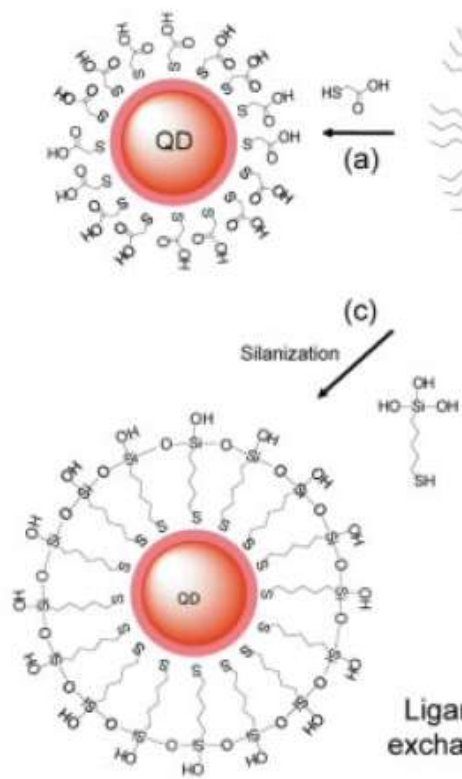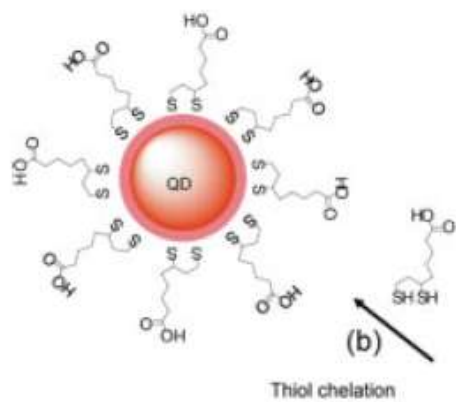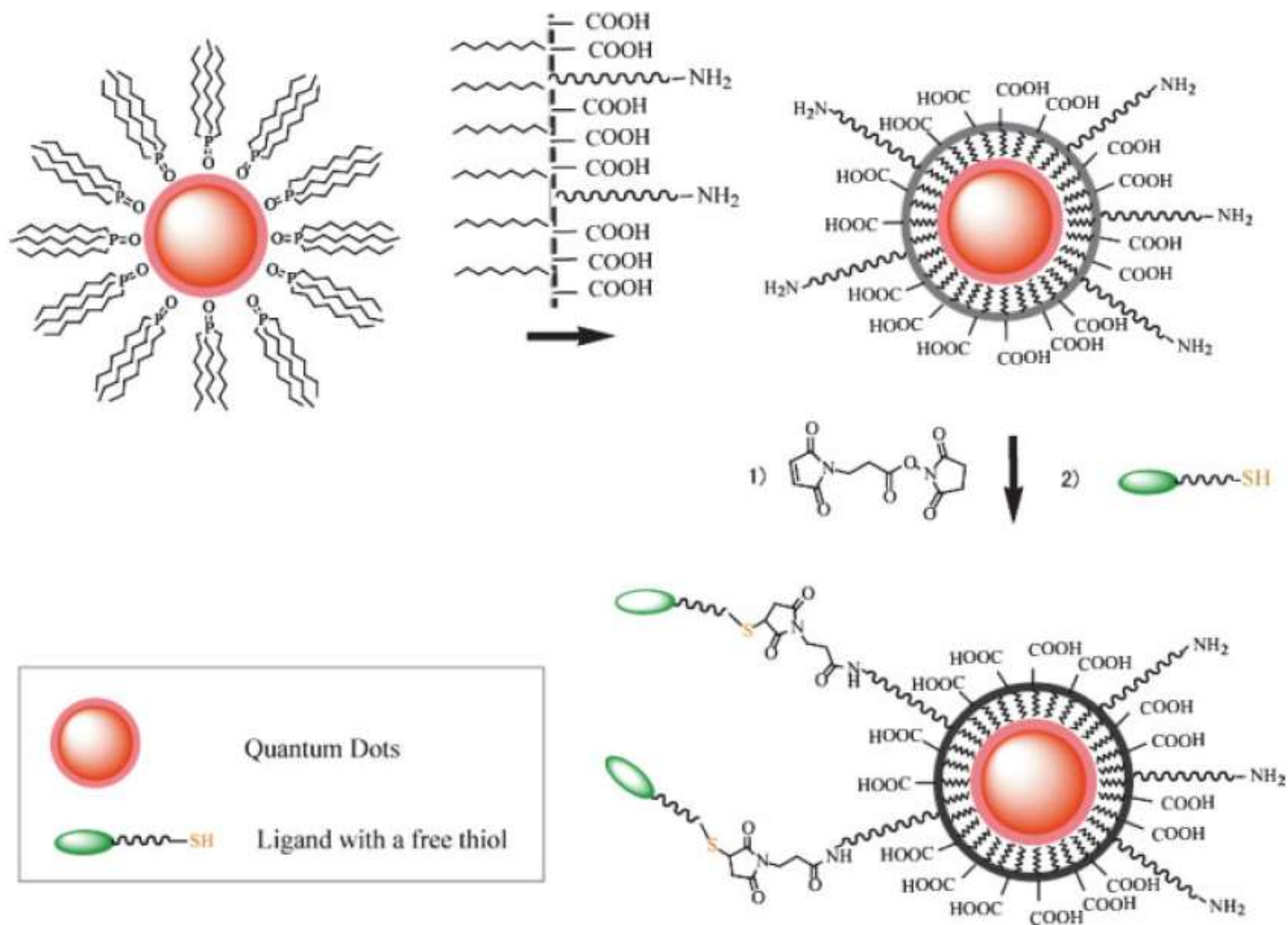
FIGURE 3 Maleimide functionalized QDs for conjugating thiol-containing ligands. TOPO stabilized QDs are coated with a primary amine functionalized tri-block amphiphilic copolymer for producing water-soluble QDs, which facilitate further conjugation to ligands with free thiols through bi-functional cross-linkers.

Nanomaterials for Biodiagnostic

- Nucleic Acid
  - Genetic information for identification
  - Diseases, bacterium, virus, pathogen
  - PCR with molecular fluorophore, State of the Art
  - Expansive, Non-portable, Non-multiplexing
- Proteins
  - Cancers and diseases, unusual high concentration of marker
  - ELISA (~pM) with molecular fluorophore
  - No PCR version

ELISA (Enzyme-Linked Immunosorbent Assay)

is a biochemical technique used mainly in immunology to detect the presence of an antibody or an antigen in a sample. It utilizes two antibodies, one of which is specific to the antigen and the other of which is coupled to an enzyme. This second antibody gives the assay its "enzyme-linked" name, and will cause a chromogenic or fluorogenic substrate to produce a signal.
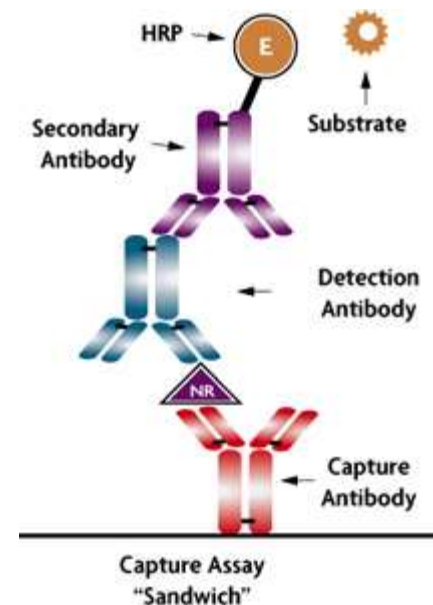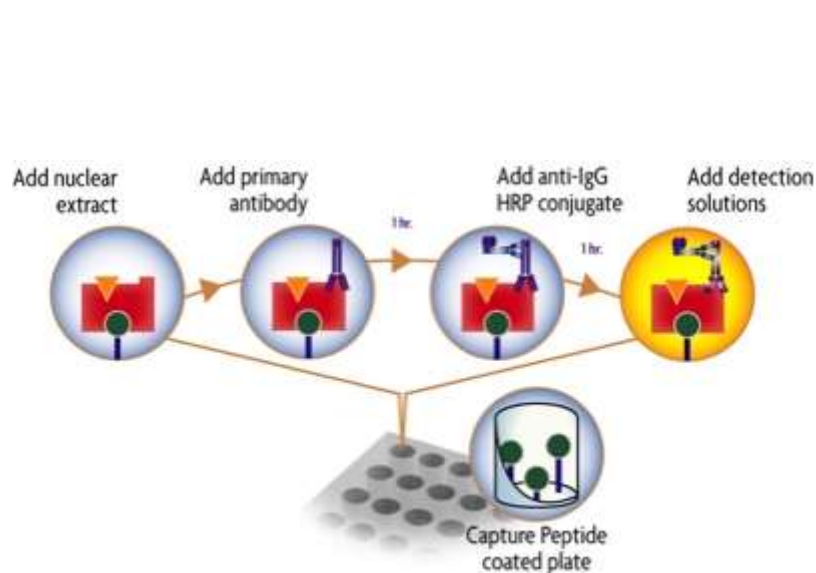
Why Nanomaterials?

- Molecular fluorophores
  - Limited spectral response
  - photostability
- Nanomaterials
  - Small size (1-100 nm)
  - Chemically tailorable physical properties
  - Unusual target binding properties
  - Structure robustness

Nanomaterial Detection

- Optical
- Electrical and electrochemical
- Magnetic
- Nanowire and Nanotubes
- Nanofabrication

Colorimetric Detection of DNA
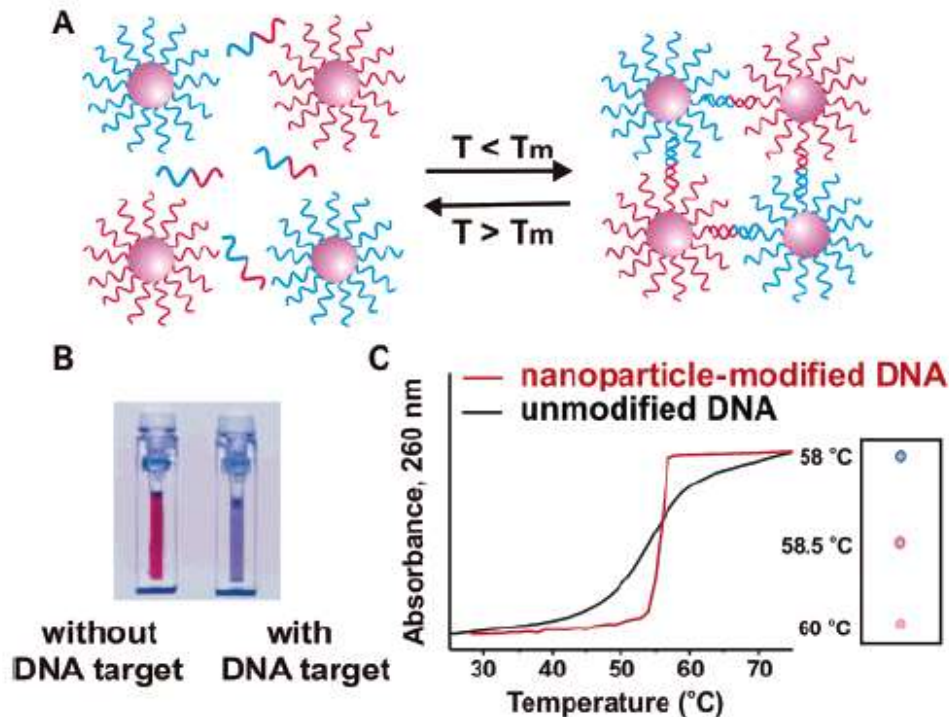
Figure 2. In the presence of complementary target DNA, oligonucleotide-functionalized gold nanoparticles will aggregate (A), resulting in a change of solution color from red to blue (B). The aggregation process can be monitored using UV–vis spectroscopy or simply by spotting the solution on a silica support (C). (Reprinted with permission from *Science* (http://www.aaas.org), ref 29. Copyright 1997 American Association for the Advancement of Science.)

A DNA-based method for rationally assembling nanoparticles into macroscopic materials

Chad A. Mirkin, Robert L. Letsinger, Robert C. Mucic & James J. Storhoff
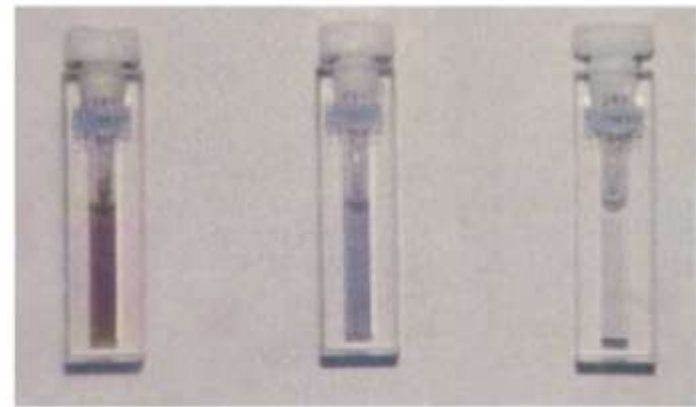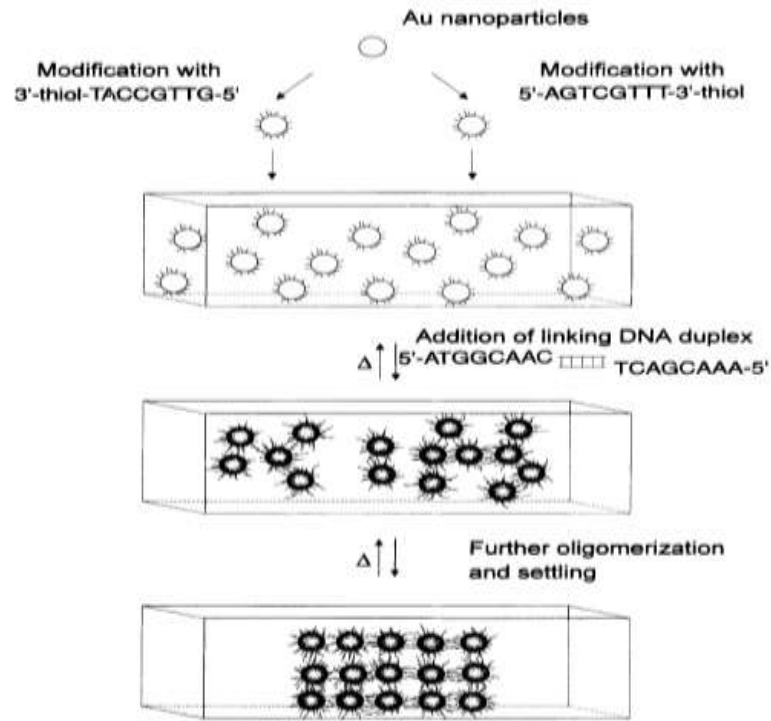
FIG. 2 Cuvettes with the Au colloids and the four DNA strands responsible for the assembly process. Left cuvette, at 80 °C with DNA-modified colloids in the unhybridized state; centre, after cooling to room temperature but before the precipitate settles; and right, after the polymeric precipitate settles to the bottom of the cuvette. Heating either of these cool solutions results in the reformation of the DNA-modified colloids in the unhybridized state (shown in the left cuvette).
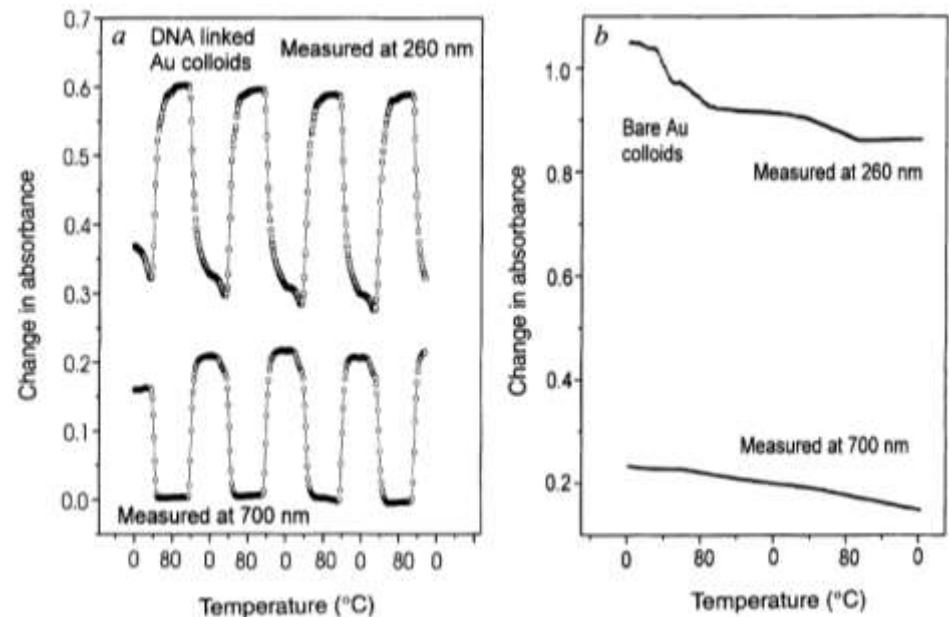
Selective Colorimetric Detection of Polynucleotides Based on the Distance-Dependent Optical Properties of Gold Nanoparticles

Robert Elghanian, James J. Storhoff, Robert C. Mucic, Robert L. Letsinger,* Chad A. Mirkin*
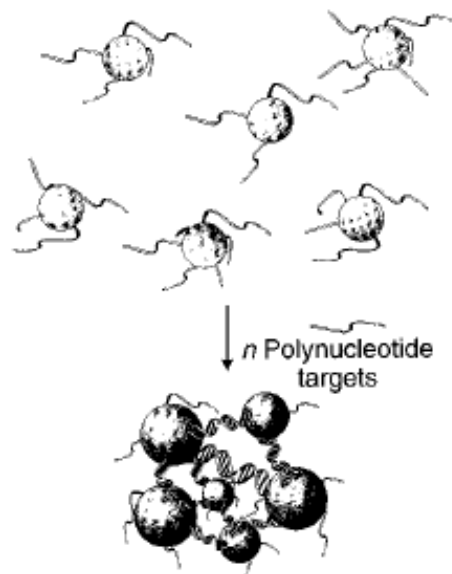
Fig. 1. Schematic representation of the concept for generating aggregates signaling hybridization of nanoparticle-oligonucleotide conjugates with oligonucleotide target molecules. The nanoparticles and the oligonucleotide interconnects are not drawn to scale, and the number of oligomers per particle is believed to be much larger than depicted.
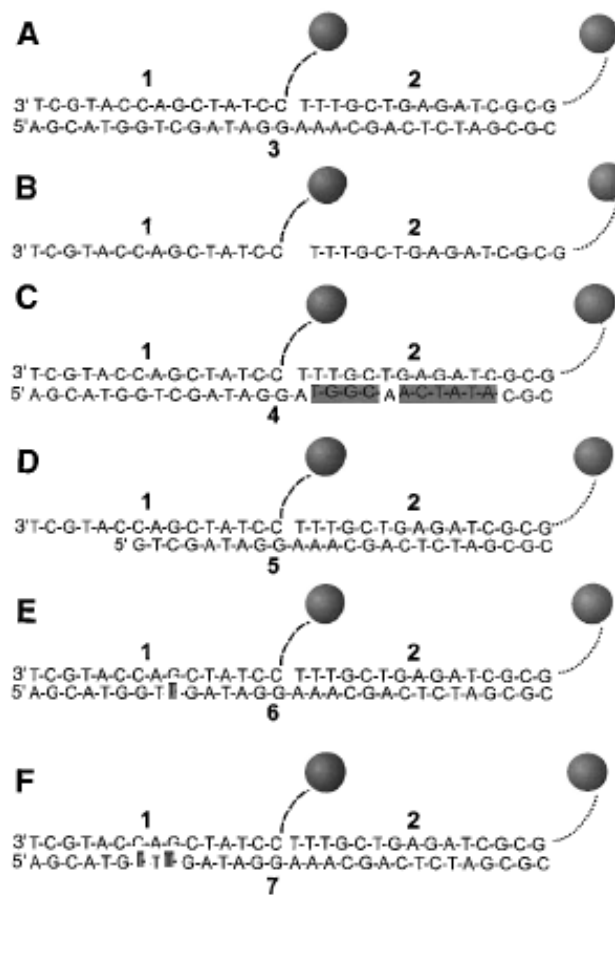
Fig. 2. Mercaptoalkyloligonucleotide-modified 13-nm Au particles and polynucleotide targets used for examining the selectivity of the nanoparticle-based colorimetric polynucleotide detection system. (A) Complementary target; (B) probes without the target; (C) a half-complementary target; (D) a 6-bp deletion; (E) a 1-bp mismatch; and (F) a 2-bp mismatch. For the sake of clarity, only two particles are shown; in reality a polymeric aggregate with many particles is formed. Dashed lines represent flexible spacer portions of the mercaptoalkyloligonucleotide strands bound to the nanoparticles; note that these spacers, because of their noncomplementary nature, do not participate in hybridization. The full sequences for the two probes, 1 and 2, which bind to targets 3 through 7, are

1-5′SH-$(CH_2)_6$- [CTA-ATC-CGC-ACA-G]$_{spacer}$

[CC-TAT-CGA-CCA-TGC-T]$_{probe}$

2-5′SH-$(CH_2)_6$-[ATG-GCA-ACT-ATA-C]$_{spacer}$

[GC-GCT-AGA-GTC-GTT-T]$_{probe}$
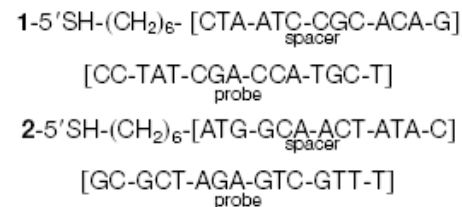
Fig. 3. (**A**) Comparison of the thermal dissociation curves for complexes of mercaptoalkyloligonucleotide-modified Au nanoparticles (black circles) and mercaptoalkyloligonucleotides without Au nanoparticles (red squares) with the complementary target, **3**, in hybridization buffer (0.1 M NaCl, 10 mM phosphate buffer, pH 7.0). For the first set (black circles), a mixture of 150 μl of each colloid conjugate and 3 μl of the target oligonucleotide in hybridization buffer (0.1 M

NaCl, 10 mM phosphate, pH 7.0) was frozen at the temperature of dry ice, kept for 5 min, thawed over a period of 15 min, and diluted to 1.0 ml with buffer (final target concentration, 0.02 μM). The absorbance was measured at 1-min intervals with a temperature increase of 1°C per minute. The increase in absorption at 260 nm (A_{260}) was ~0.3 absorption units (AU). In the absence of the oligonucleotide targets, the absorbance of the nanoparticles did not increase with increasing temperature. For the second set, the mercaptoalkyloligonucleotides and complementary target (each 0.33 μM) were equilibrated at room temperature in 1 ml of buffer, and the changes in absorbance with temperature were monitored as before. The increase in A_{260} was 0.08 AU. (**Insets**) Derivative curves for each set (15). (**B**) Spot test showing T_c (thermal transition associated with the color change) for the Au nanoparticle probes hybridized with complementary target. A solution prepared from 150 μl of each probe and 3 μl of the target (0.06 μM final target concentration) was frozen for 5 min, allowed to thaw for 10 min, transferred to a 1-ml cuvette, and warmed at 58°C for 5 min in the thermally regulated cuvette chamber of the spectrophotometer. Samples (3 μl) were transferred to a C_{18} reverse phase plate with an Eppendorf pipette as the temperature of the solution was increased incrementally 0.5°C at 5-min intervals.

A

1   2
3' T-C-G-T-A-C-C-A-G-C-T-A-T-C-C T-T-T-G-C-T-G-A-G-A-T-C-G-C-G
5' A-G-C-A-T-G-G-T-C-G-A-T-A-G-G-A-A-A-A-C-G-A-C-T-C-T-A-G-C-G-C
                              3

B

1   2
3' T-C-G-T-A-C-C-A-G-C-T-A-T-C-C   T-T-T-G-C-T-G-A-G-A-T-C-G-C-G

C

1   2
3' T-C-G-T-A-C-C-A-G-C-T-A-T-C-C T-T-T-G-C-T-G-A-G-A-T-C-G-C-G
5' A-G-C-A-T-G-G-T-C-G-A-T-A-G-G-A-T-G-G-C A-A-C-T-A-T-A C-G-C
                              4

D

1   2
3' T-C-G-T-A-C-C-A-G-C-T-A-T-C-C T-T-T-G-C-T-G-A-G-A-T-C-G-C-G
        5' G-T-C-G-A-T-A-G-G-A-A-A-A-C-G-A-C-T-C-T-A-G-C-G-C
                              5

E

1   2
3' T-C-G-T-A-C-C-A-G-C-T-A-T-C-C T-T-T-G-C-T-G-A-G-A-T-C-G-C-G
5' A-G-C-A-T-G-G-T-T-G-A-T-A-G-G-A-A-A-A-C-G-A-C-T-C-T-A-G-C-G-C
                              6

F

1   2
3' T-C-G-T-A-C-C-A-G-C-T-A-T-C-C T-T-T-G-C-T-G-A-G-A-T-C-G-C-G
5' A-G-C-A-T-G-T-T-G-A-T-A-G-G-A-A-A-A-C-G-A-C-T-C-T-A-G-C-G-C
                              7

Fig. 4. Selective polynucleotide detection for the target probes shown in Fig. 2: (**A**) complementary target; (**B**) no target; (**C**) complementary to one probe; (**D**) a 6-bp deletion; (**E**) a 1-bp mismatch; and (**F**) a 2-bp mismatch. Nanoparticle aggregates were prepared in a 600-μl thin-walled Eppendorf tube by addition of 1 μl of a 6.6 μM oligonucleotide target to a mixture containing 50 μl of each probe (0.06 μM final target concentration). The mixture was frozen (5 min) in a bath of dry ice and isopropyl alcohol and allowed to warm to room temperature. Samples were then transferred to a temperature-controlled water bath, and 3-μl aliquots were removed at the indicated temperatures and spotted on a C_{18} reverse phase plate.

Colloidal Au-Enhanced Surface Plasmon Resonance for Ultrasensitive Detection of DNA Hybridization

Lin He, Michael D. Musick, Sheila R. Nicewarner, Frank G. Salinas, Stephen J. Benkovic, Michael J. Natan, and Christine D. Keating*

Scheme 1. SPR Surface Assembly

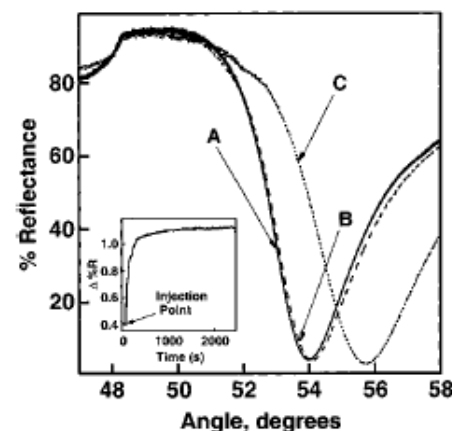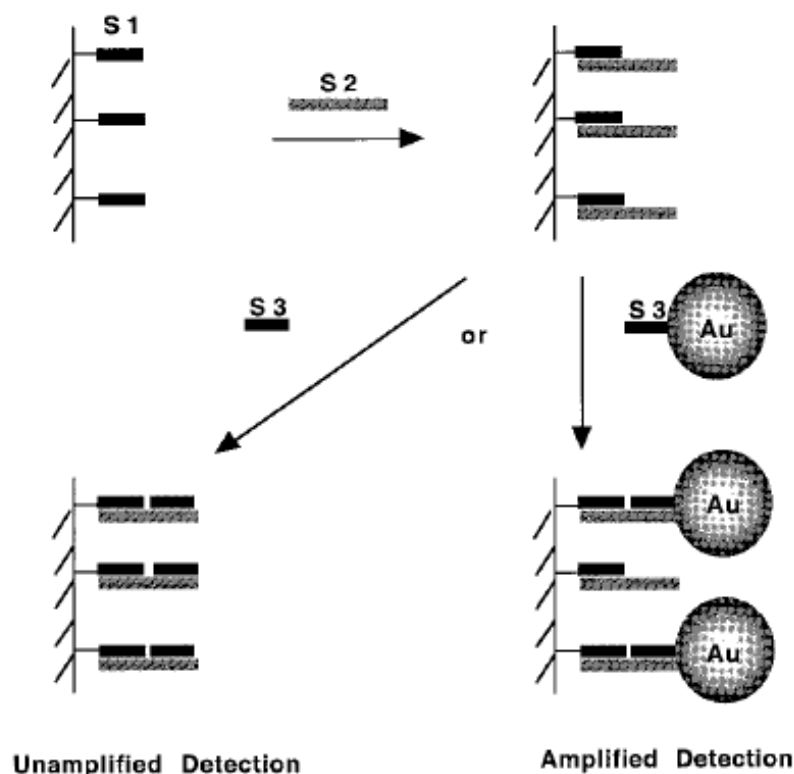**Figure 1.** SPR curves of surfaces prepared in sequential steps as illustrated in Scheme 1: a MHA-coated Au film modified with a 12-mer oligonucleotide S1(A), after hybridization with its complementary 24-mer target S2 (B), and followed by introduction of S3:Au conjugate (C) to the surface. Inset: surface plasmon reflectance changes at 53.2° for the oligonucleotide-coated Au film measured during a 60-min exposure to S3:Au conjugates.

Scheme 2. SPR Surface Assembly in the Digestion Experiment

- Au d = 12 nm Au colloid
- biotin
- Streptavidin
- Hinf 1
- ds DNA
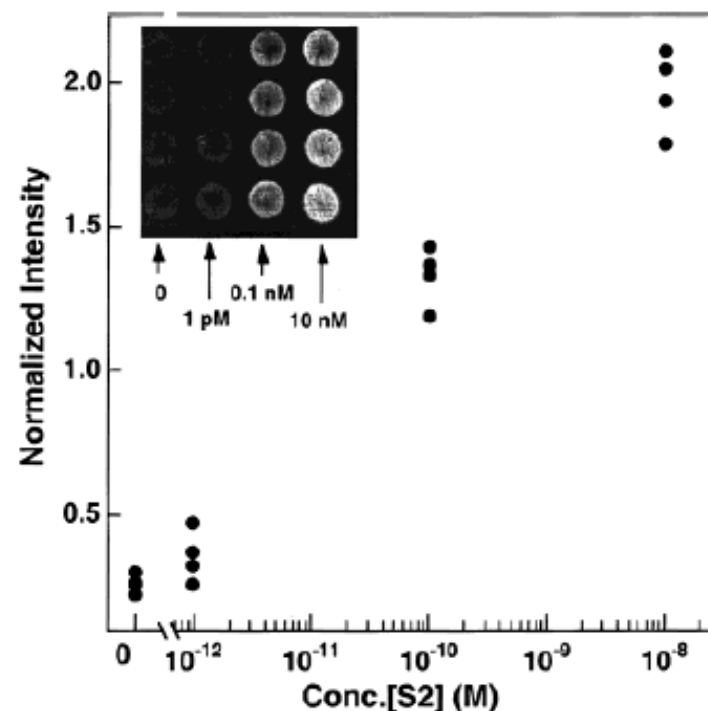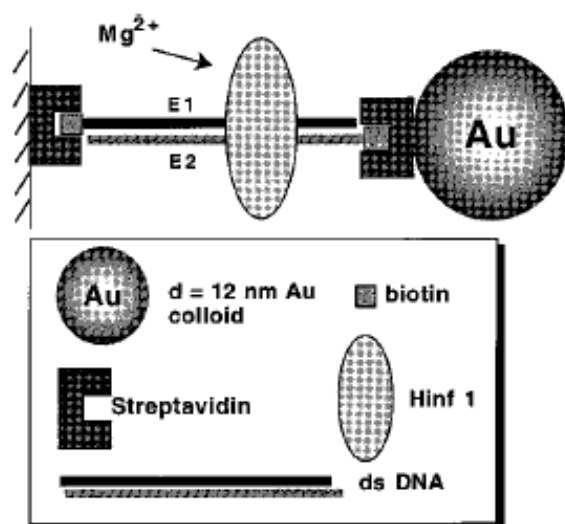
Figure 5. Plot of normalized intensity of SPR reflectance as a function of logarithmic concentration of the analyte 24-mer oligo (S2). Each spot represents one data point at the corresponding concentration. CCD parameters: exposure time = 0.3 s, 16 bit resolution, spot size = 4.5 mm in diameter. Inset: a 2-D SPR image of a Au surface derivatized with 20 μL of buffer blank, 1 pM, 0.1 nM, and 10 nM S2 oligos (from left to right, respectively).

Self-Assembled Nanoparticle Probes for Recognition and Detection of Biomolecules

Dustin J. Maxwell, Jason R. Taylor, and Shuming Nie*,[†]
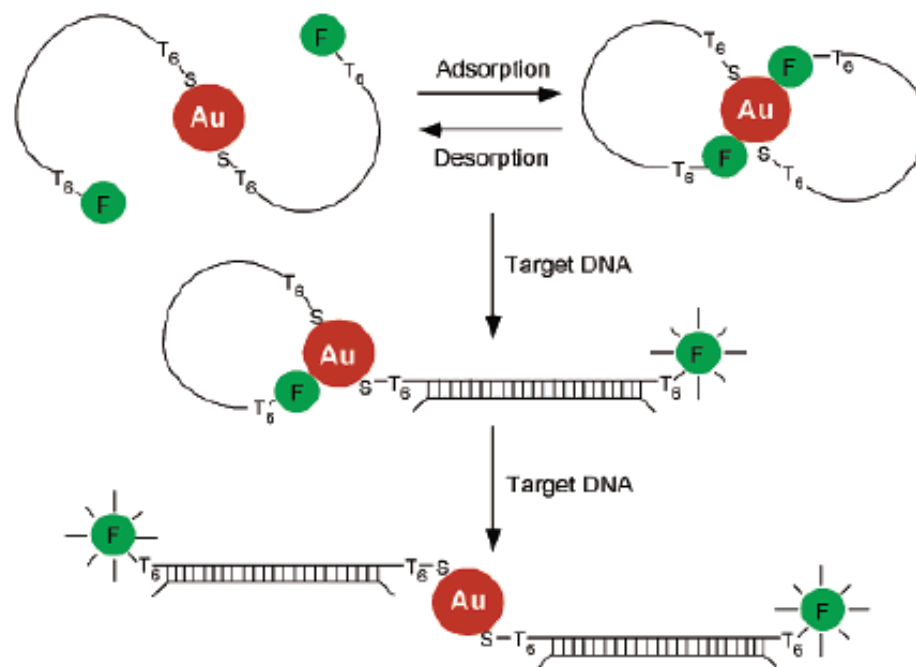
Figure 1. Nanoparticle-based probes and their operating principles. Two oligonucleotide molecules (oligos) are shown to self-assemble into a constrained conformation on each gold particle (2.5 nm diameter). A T_6 spacer (six thymines) is inserted at both the 3′- and 5′-ends to reduce steric hindrance. Single-stranded DNA is represented by a single line and double-stranded DNA by a cross-linked double line. In the assembled (closed) state, the fluorophore is quenched by the nanoparticle. Upon target binding, the constrained conformation opens, the fluorophore leaves the surface because of the structural rigidity of the hybridized DNA (double-stranded), and fluorescence is restored. In the open state, the fluorophore is separated from the particle surface by about 10 nm. See text for detailed explanation. Au, gold particle; F, fluorophore; S, sulfur atom.

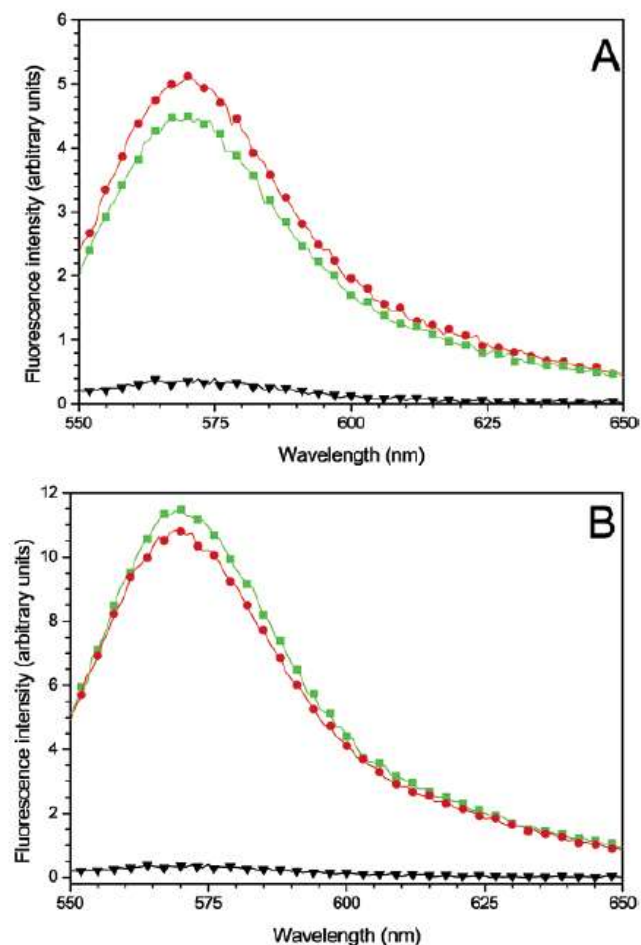**Figure 5.** Fluorescence responses and the lack of sequence recognition abilities observed for nonthiolated nanoparticle probes. (A) Fluorescence spectra of nonthiolated probes generated by a complementary target (red curve), a noncomplementary target (green curve), and no target (black curve). These probes are considered nonfunctional because they do not recognize specific DNA sequences. (B) Fluorescence signals obtained from the supernatant solution when the probes were treated with a complementary target (red curve) or a noncomplementary target (green curve). The result revealed that the oligos were released into solution by nonspecific adsorption of the target on the particle surface. With a thiol group, this release was not observed (little or no signal in solution, black curve in B). The nonfunctional probes were prepared in the same way as the functional probes, except that the 3'-end thiol group was deleted. The intensity differences for the red and green curves were within experimental errors and had no particular significance.

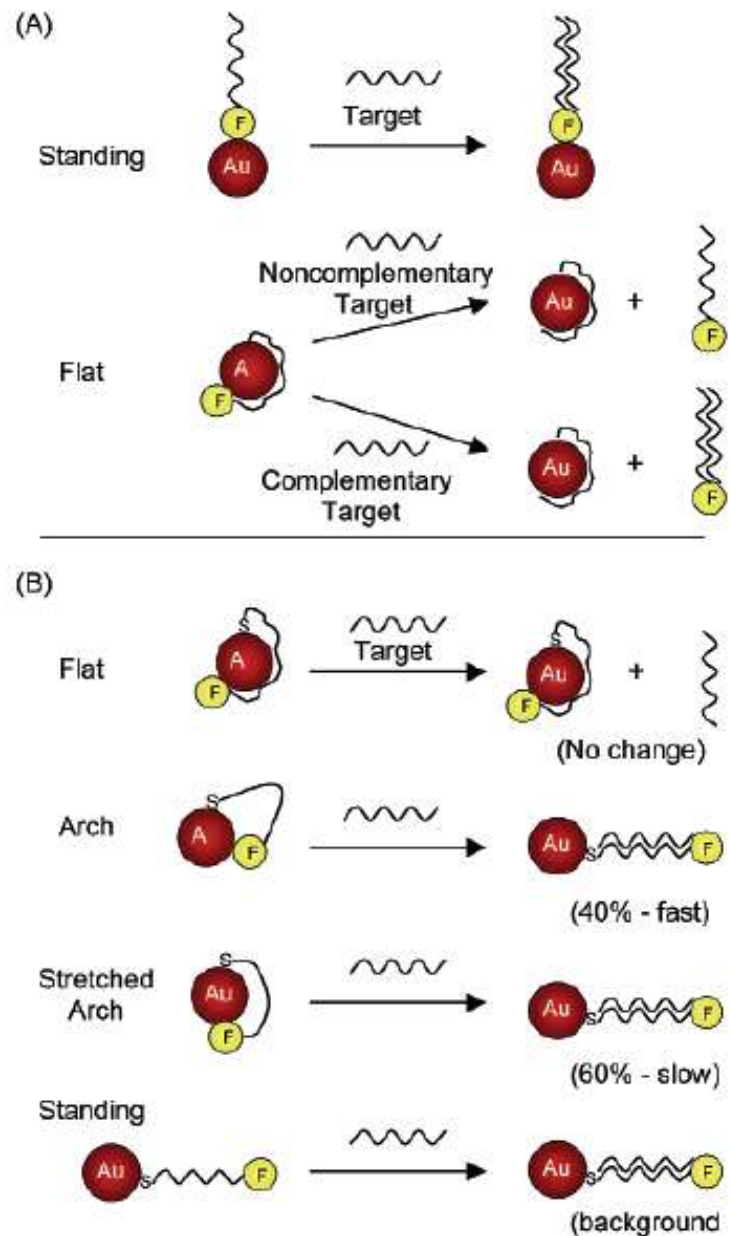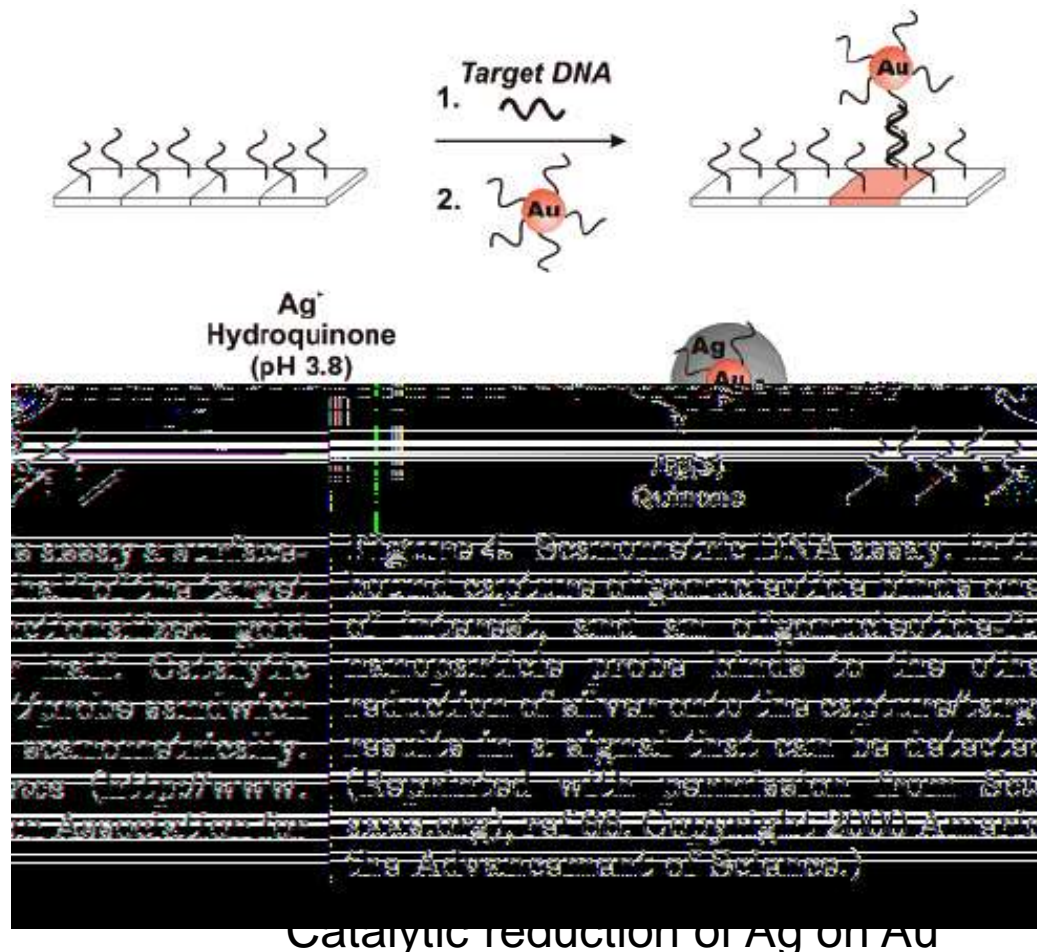
Figure 6. Schematic illustration of possible configurations for (a) nonthiolated and (b) thiolated oligonucleotides adsorbed on colloidal gold nanocrystals. Detailed discussion in text.
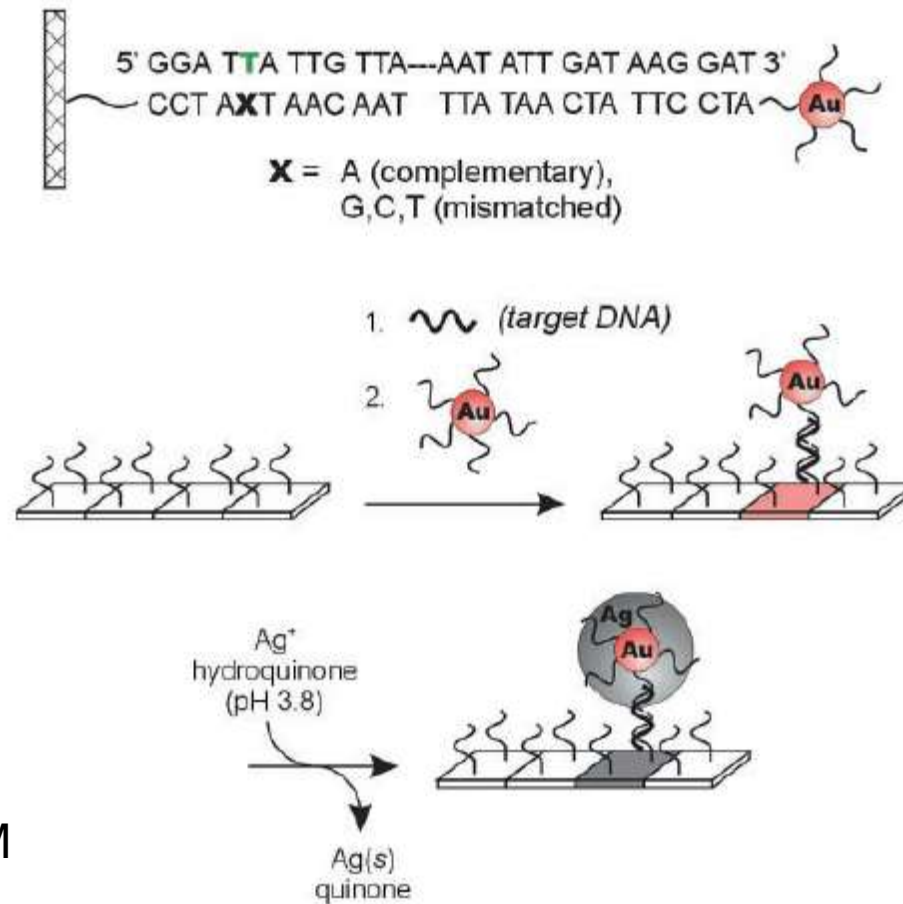
Silver Amplification

Catalytic reduction of Ag on Au

Scanometric DNA Array Detection with Nanoparticle Probes

T. Andrew Taton,[1,2] Chad A. Mirkin,[1,2]* Robert L. Letsinger[1]*

50 fM => 0.2 fM

Fig. 1. Images of 7 mm by 13 mm, oligonucleotide-functionalized, float glass slides, obtained with a flatbed scanner. (**A**) Slide before hybridization of target and nanoparticle probe. (**B**) A slide identical to (A) after hybridization with oligonucleotide target (10 nM) and then nanoparticle probes (5 nM in particles). The pink color derives from the Au nanoparticle probes. (**C**) A slide identical to (B) after exposure to silver amplification solution for 5 min. (**D**) Slide before hybridization of target and nanoparticle probe. (**E**) A slide identical to (D) after hybridization with target (100 pM) and then nanoparticle probe (5 nM). The extinction of the submonolayer of nanoparticles is too low to be observed visually or with a flatbed scanner. (**F**) A slide identical to (E) after exposure to silver amplification solution for 5 min. Slide (F) is lighter than slide (C), indicating a lower concentration of target. (**G**) A control slide exposed to 5 nM nanoparticle probe and then exposed to silver amplification solution for 5 min. No darkening of the slide is observed. (**H**) Graph of 8-bit gray scale values as a function of target concentration. The gray scale values were taken from flatbed scanner images of oligonucleotide-functionalized glass surfaces that had been exposed to varying concentrations of oligonucleotide target, labeled with 5 nM oligonucleotide probe and immersed in silver amplification solution. For any given amplification time, the grayscale range is limited by surface saturation at high grayscale values and the sensitivity of the scanner at low values. Therefore, the dynamic range of this system can be adjusted by means of hybridization and amplification conditions (that is, lower target concentrations require longer amplification periods). Squares: 18-base capture-target overlap (5), 8× PBS hybridization buffer [1.2 M NaCl and 10 mM NaH_2PO_4/Na_2HPO_4 buffer (pH 7)], 15 min amplification time. Circles: 12-base capture-target overlap, 8× PBS hybridization buffer, 10 min amplification time. Triangles: 12-base capture-target overlap, 2× PBS hybridization buffer [0.3 M NaCl, 10 mM NaH_2PO_4/Na_2HPO_4 buffer (pH 7)], 5 min amplification time. The lowest target concentration that can be effectively distinguished from the background baseline is 50 fM.
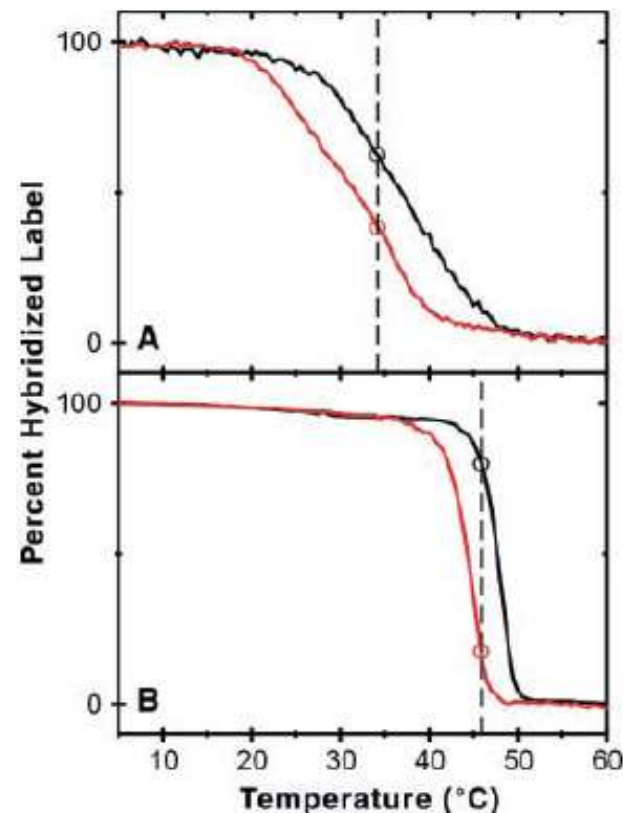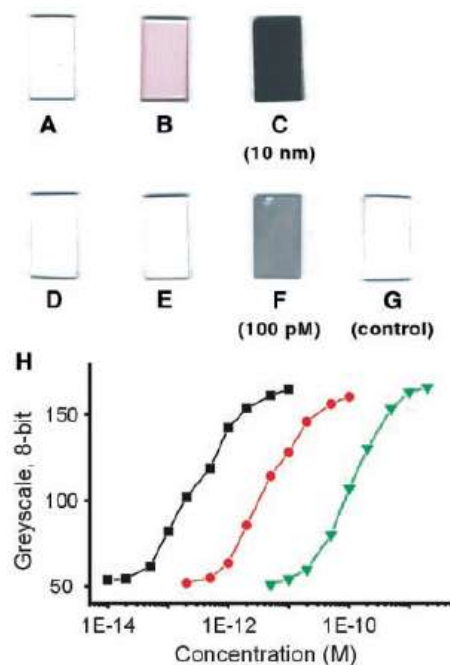
Fig. 3. (Left) Nanoparticle-labeled arrays developed at different stringency temperatures. Model oligonucleotide arrays (with the capture sequences shown in Scheme 1) were treated with oligonucleotide target and nanoparticle probes, followed by a 2-min buffer wash at the temperatures shown and subsequent silver amplification (*13*). Images were obtained with an Epson Expression 636 (600 dots per inch) flatbed scanner (Epson America, Long Beach, California). The darkened border indicates the array that showed optimum selectivity for the perfectly complementary target; at this temperature, the ratio of background-subtracted, 8-bit gray scale values for elements A:G:T:C, obtained from histogram averages in Adobe Photoshop (Adobe Systems, San Jose, California), is 96:9:7:6. **(Right)** Fluorophore-labeled arrays washed at different stringency temperatures. Model oligonucleotide arrays identical to those shown at left were treated with oligonucleotide target and Cy3-labeled oligonucleotide probes, followed by a 2-min buffer wash at the temperatures shown. Images were obtained with a ScanArray Confocal Microarray Scanner (GSI Lumonics, Billerica, Massachusetts). The darkened border indicates the array that showed the highest selectivity for the perfectly complementary target, as calculated by the QuantArray Analysis software package (GSI Lumonics); at this temperature, the intensity ratio (in percent, with the intensity of the X = A element at 15°C set to 100%) for elements A:G:T:C is 18:7:1:1.
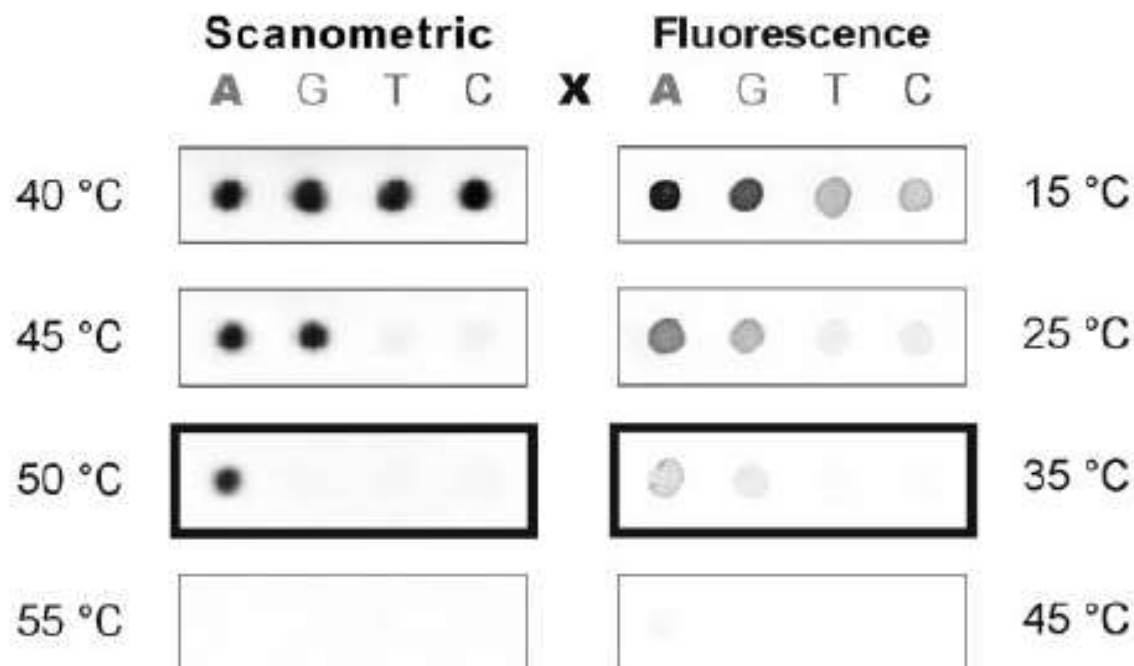
Nanoparticles with Raman Spectroscopic Fingerprints for DNA and RNA Detection

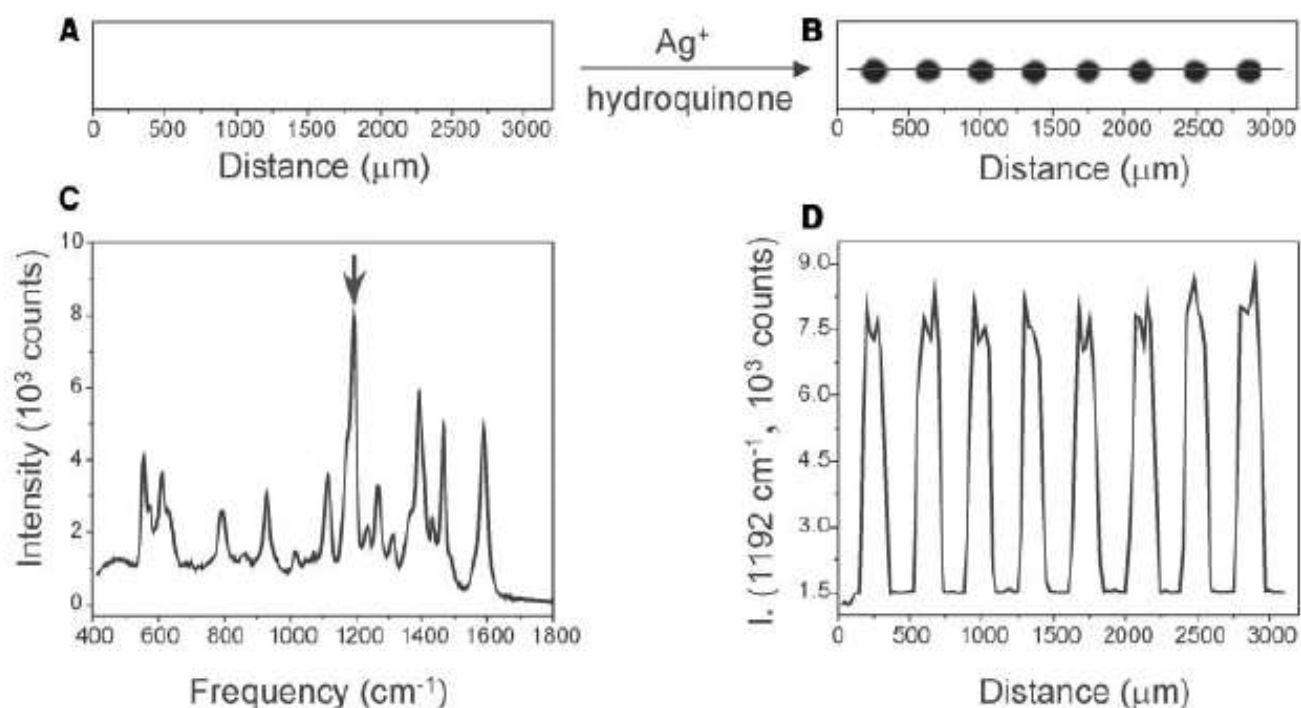YunWei Charles Cao, Rongchao Jin, Chad A. Mirkin*
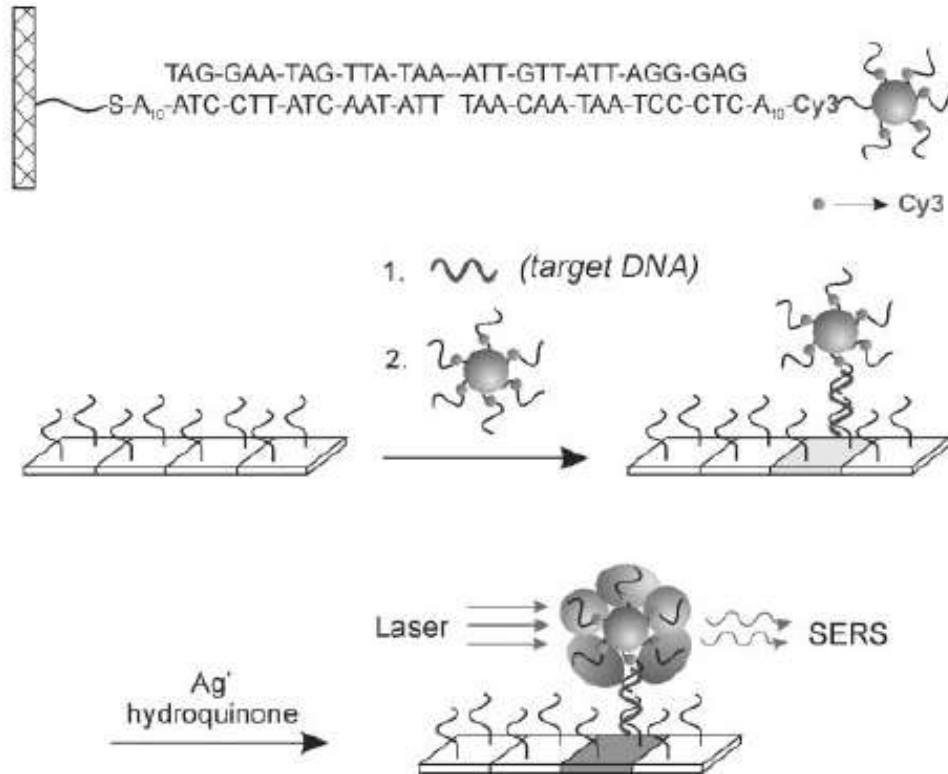
1 fM

Fig. 1. Flatbed scanner images of microarrays hybridized with nanoparticles (**A**) before and (**B**) after Ag enhancing. (**C**) A typical Raman spectrum acquired from one of the Ag spots. (**D**) A profile of Raman intensity at 1192 cm^{-1} as a function of position on the chip; the laser beam from the Raman instrument is moved over the chip from left to right as defined by the line in (**B**).
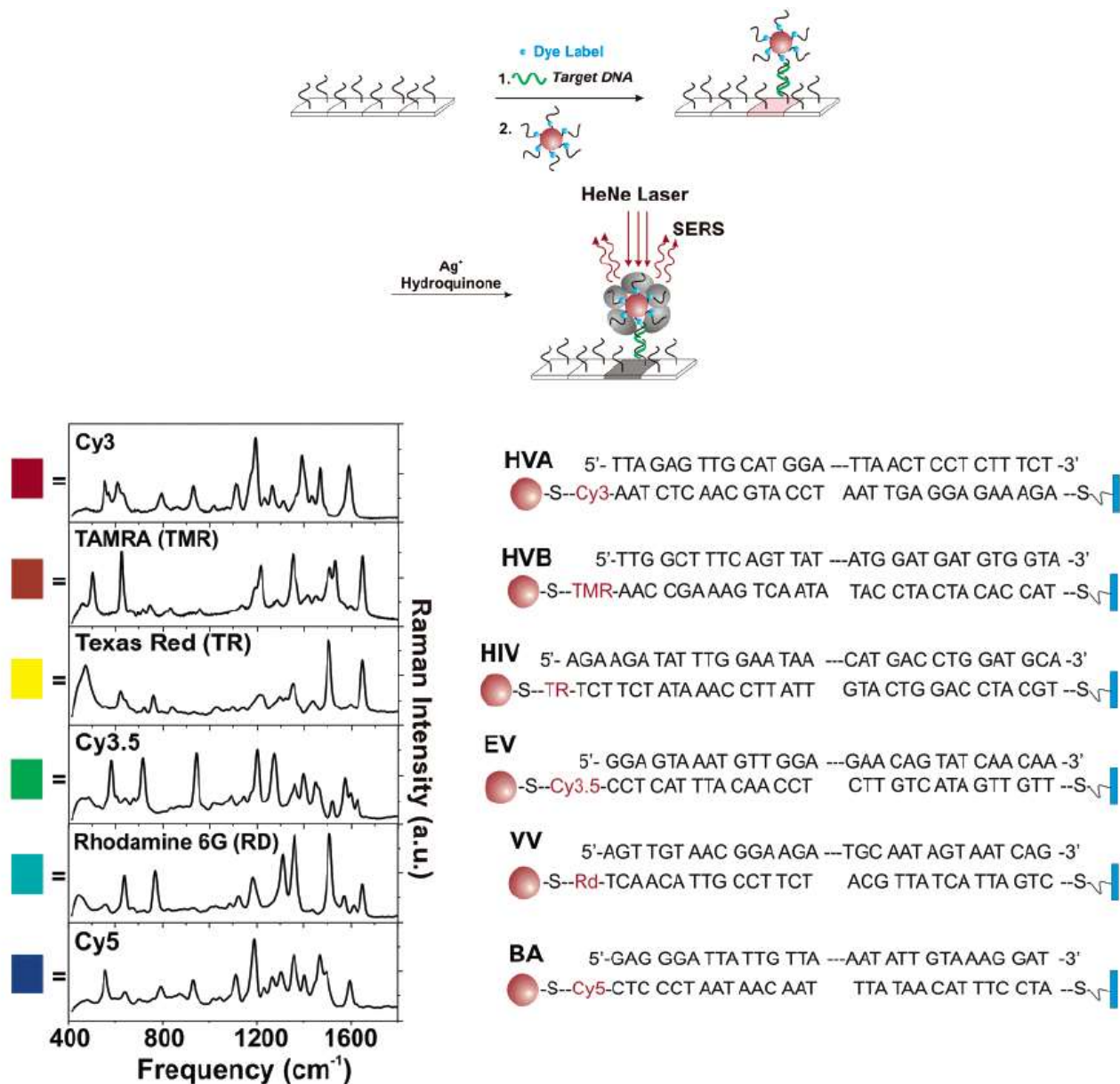
Figure 5. If Raman dyes (blue spheres) are attached to the labeling probe in the scanometric assay, the targets can be encoded and detected via the Raman signal of their labels. (Reprinted with permission from *Science* (http://www.aaas.org), ref 68. Copyright 2002 American Association for the Advancement of Science.)
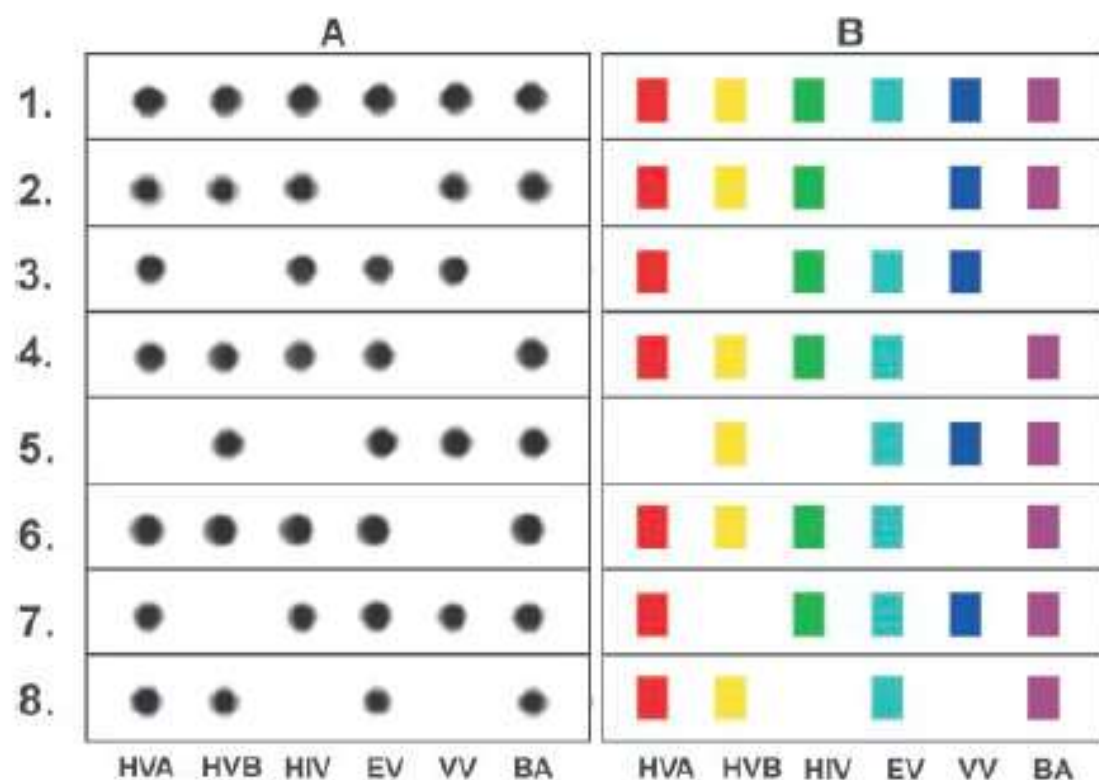
Fig. 3. (A) Flatbed scanner images of Ag-enhanced microarrays and (B) corresponding Raman spectra. The colored boxes correlate with the color-coded Raman spectra in Fig. 2. No false-positives or false-negatives were observed.

Bio-Bar-Code-Based DNA Detection with PCR-like Sensitivity

Jwa-Min Nam, Savka I. Stoeva, and Chad A. Mirkin*

Target DNA (anthrax): 5′ GGATTATTGTTAAATATTGATAAGGAT 3′
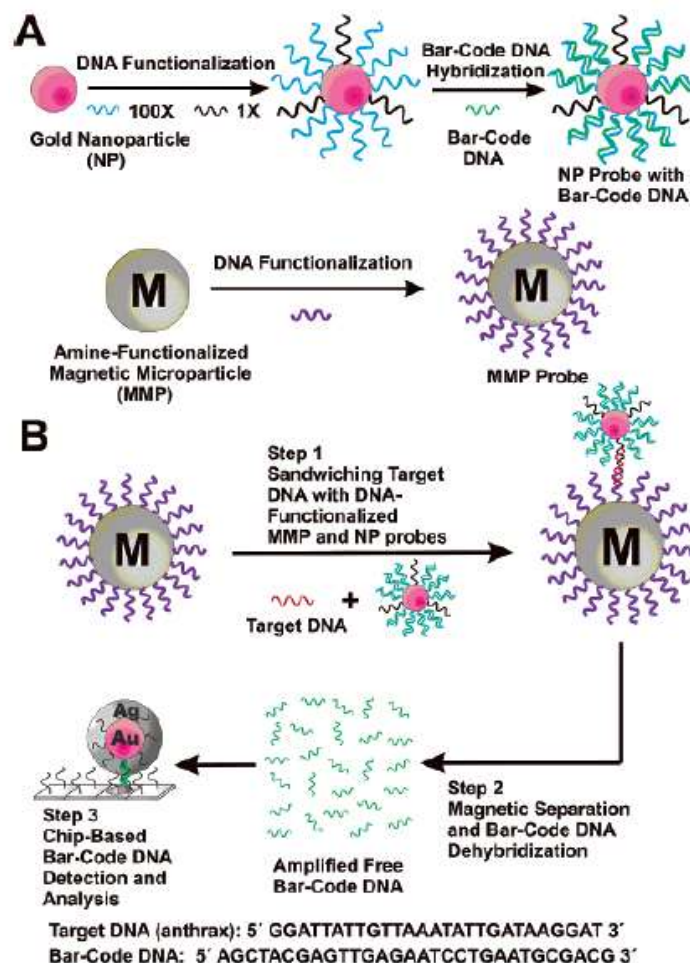Bar-Code DNA: 5′ AGCTACGAGTTGAGAATCCTGAATGCGACG 3′

Figure 1. The DNA-BCA assay. (A) Nanoparticle and magnetic micro-particle probe preparation. (B) Nanoparticle-based PCR-less DNA amplification scheme.
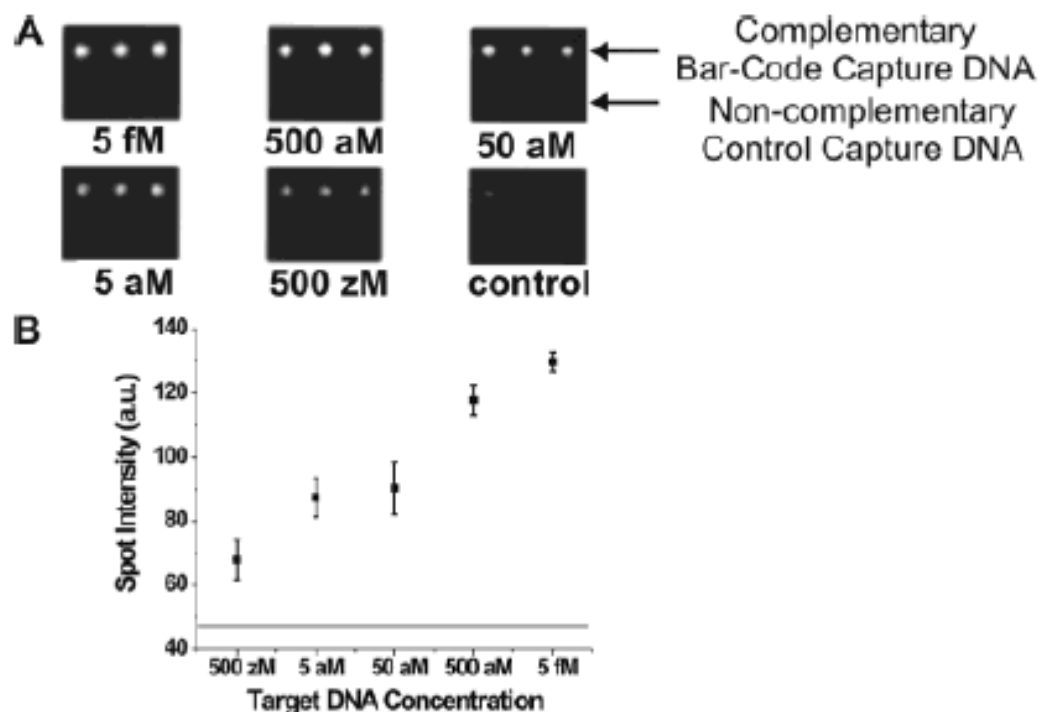
Figure 2. Amplified anthrax bar-code DNA detection with the Verigene ID system. (A) Anthrax bar-code DNA detection with 30 nm NP probes. (B) Quantitative data of spot intensities with 30 nm NP probes (Adobe Photoshop, Adobe Systems, Inc., San Jose, CA). The horizontal line represents control signal intensity (47 ± 2).
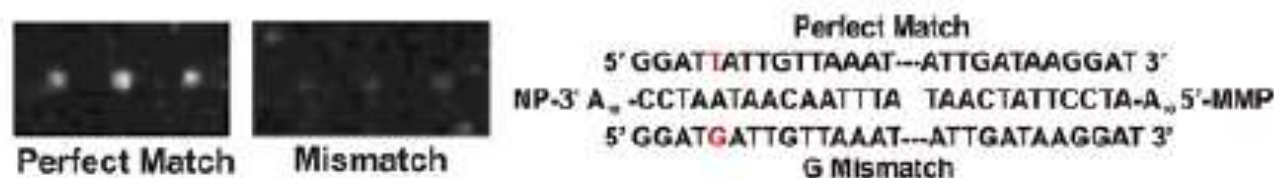

Figure 3. Single base mismatch experiment.

Nanoparticle-Based Bio–Bar Codes for the Ultrasensitive Detection of Proteins

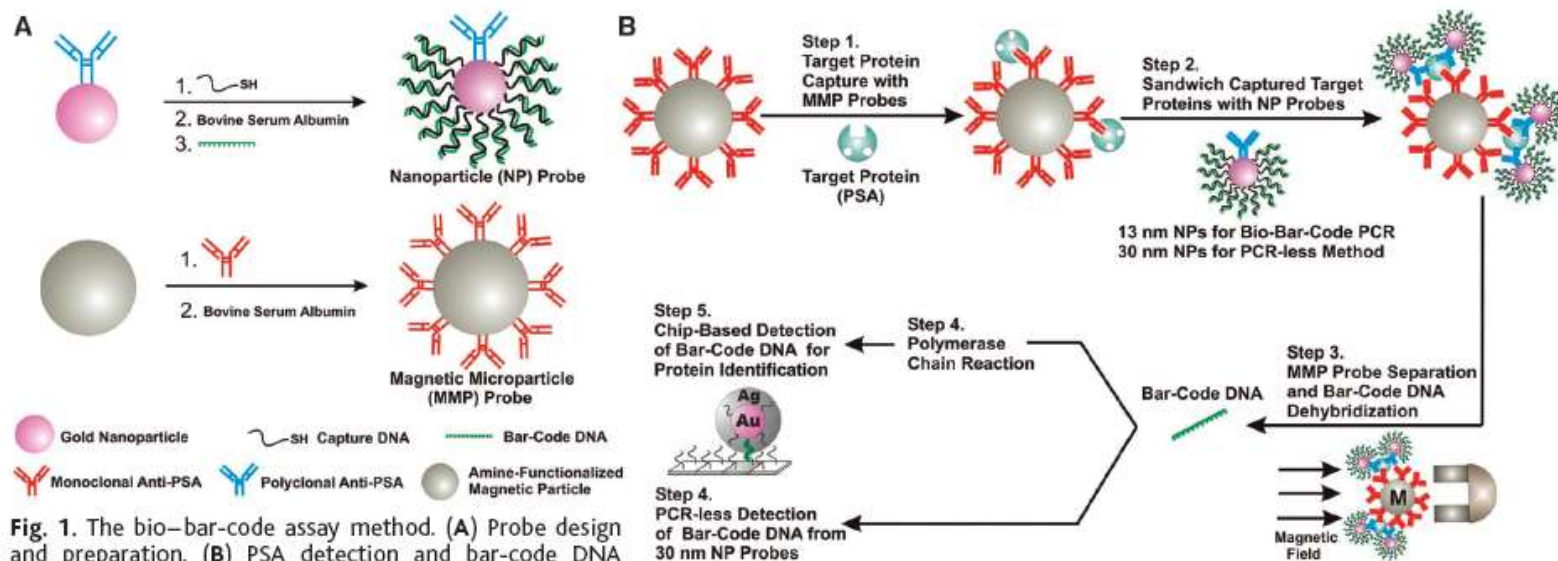Jwa-Min Nam,* C. Shad Thaxton,* Chad A. Mirkin†

Fig. 1. The bio–bar-code assay method. (**A**) Probe design and preparation. (**B**) PSA detection and bar-code DNA amplification and identification. In a typical PSA-detection experiment, an aqueous dispersion of MMP probes functionalized with mAbs to PSA (50 μl of 3 mg/ml magnetic probe solution) was mixed with an aqueous solution of free PSA (10 μl of PSA) and stirred at 37°C for 30 min (Step 1). A 1.5-ml tube containing the assay solution was placed in a BioMag microcentrifuge tube separator (Polysciences, Incorporated, Warrington, PA) at room temperature. After 15 s, the MMP-PSA hybrids were concentrated on the wall of the tube. The supernatant (solution of unbound PSA molecules) was removed, and the MMPs were resuspended in 50 μl of 0.1 M phosphate-buffered saline (PBS) (repeated twice). The NP probes (for 13-nm NP probes, 50 μl at 1 nM; for 30-nm NP probes, 50 μl at 200 pM), functionalized with polyclonal Abs to PSA and hybridized bar-code DNA strands, were then added to the assay solution. The NPs reacted with the PSA immobilized on the MMPs and provided DNA strands for signal amplification and protein identification (Step 2). This solution was vigorously stirred at 37°C for 30 min. The MMPs were then washed with 0.1 M PBS with the magnetic separator to isolate the mag-

netic particles. This step was repeated four times, each time for 1 min, to remove everything but the MMPs (along with the PSA-bound NP probes). After the final wash step, the MMP probes were resuspended in NANOpure water (50 μl) for 2 min to dehybridize bar-code DNA strands from the nanoparticle probe surface. Dehybridized bar-code DNA was then easily separated and collected from the probes with the use of the magnetic separator (Step 3). For bar-code DNA amplification (Step 4), isolated bar-code DNA was added to a PCR reaction mixture (20-μl final volume) containing the appropriate primers, and the solution was then thermally cycled (20). The bar-code DNA amplicon was stained with ethidium bromide and mixed with gel-loading dye (20). Gel electrophoresis or scanometric DNA detection (24) was then performed to determine whether amplification had taken place. Primer amplification was ruled out with appropriate control experiments (20). Notice that the number of bound NP probes for each PSA is unknown and will depend upon target protein concentration.
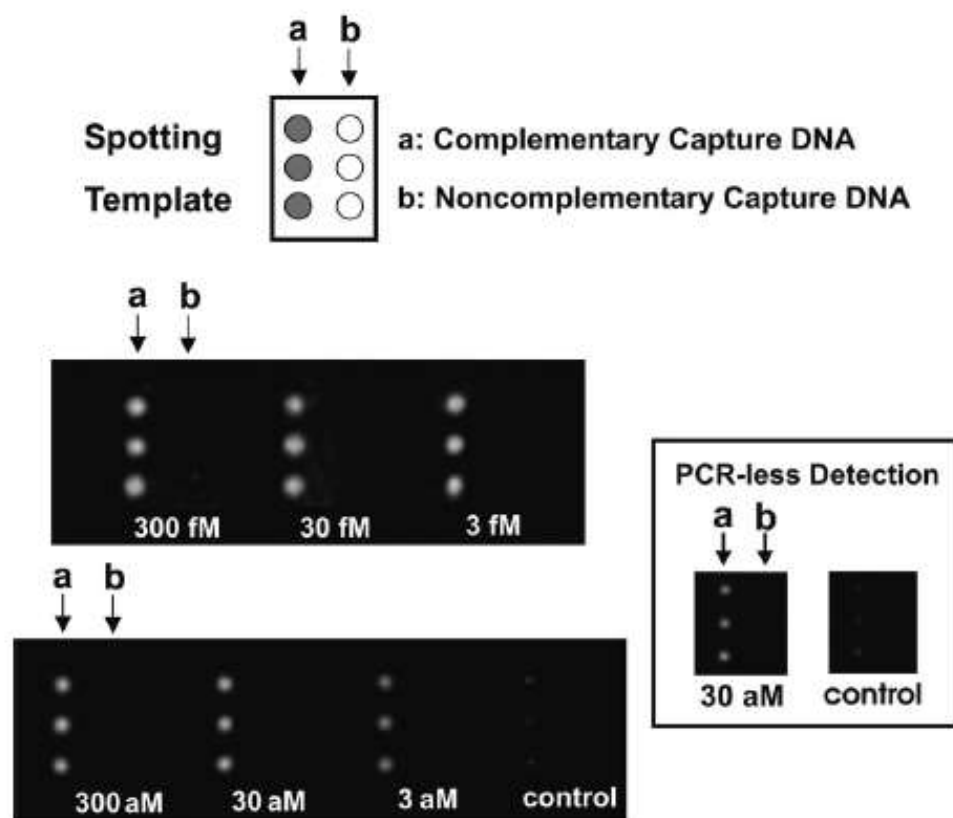
Spotting Template

a: Complementary Capture DNA

b: Noncomplementary Capture DNA

300 fM   30 fM   3 fM

300 aM   30 aM   3 aM   control

PCR-less Detection

30 aM   control

Fig. 2. Scanometric detection of PSA-specific bar-code DNA. PSA concentration (sample volume of 10 μl) was varied from 300 fM to 3 aM and a negative control sample where no PSA was added (control) is shown. For all seven samples, 2 μl of antidinitrophenyl (10 pM) and 2 μl of β-galactosidase (10 pM) were added as background proteins. Also shown is PCR-less detection of PSA (30 aM and control) with 30 nm NP probes (inset). Chips were imaged with the Verigene ID system (20).

Table 1. Detection Limits of Nucleic Acid Assays[a]

	assay	ss DNA	PCR products	genomic DNA
nanostructure-based methods	colorimetric[29] (cross-linked Au nanoparticles)	~10 nM		
	colorimetric[36] (non-cross-linked Au nanoparticles)	60 nM		
	magnetic relaxation[97] (iron oxide nanoparticles)	20 pM		
	electrochemical[96] (nanoparticles)	270 pM		
	scanometric[35,66,67] (Au nanoparticles with Ag amplification)	50 fM	100 aM[b]	200 fM
	Raman spectroscopy[68] (Au nanoparticles with Ag amplification)	~1 fM		
	electrical[93] (Au nanoparticles with Ag amplification)	500 fM		
	electrical[99] (Si nanowire)	10 fM		
	electrical[103] (carbon nanotube)	54 aM		
	resonant light-scattering[61−66] (metal nanoparticles)	170 fM[b]		33 fM
	fluorescence[56] (ZnS and CdSe quantum dots)	2 nM		
	surface plasmon resonance[41] (Au nanoparticles)	10 pM		
	quartz crystal microbalance[94] (Au nanoparticles)	~1 fM		
	laser diffraction[42] (Au nanoparticles)	~50 fM		
	fluorescence[45] (fluorescent nanoparticles)	~1 fM		
	bio-bar-code amplification[71] (Au nanoparticles with Ag amplification)	500 zM		
other non-enzymatic based methods	fluorescence[35] (molecular fluorophores)		~600 fM[b]	
	fluorescence (dendrimer amplification)[134]		2.5 μg	
	electrochemical amplification[136] (electroactive reporter molecules)	100 aM		

[a] Detection limits can vary based on target length and sequence; therefore, it is difficult to compare assays without testing them using identical targets and conditions. [b] Values taken from ref 34.

Table 2. Detection Limits of Protein Assays

	assay	target	protein in saline	protein in serum
nanostructure-based methods	optical[72] (Au nanoshells)	rabbit IgG	0.88 ng/mL ($\sim$4.4 pM)[a]	0.88 ng/mL ($\sim$4.4 pM)[a]
	optical[74] (Au nanoparticles)	IgE and IgG1	$\sim$20 nM	
	magnetic relaxation[98] (iron oxide nanoparticles)	adenovirus (ADV) and herpes simplex virus (HSV)	100 ADV/ 100 μL	50 HSV/ 100 μL
	scanometric[79] (Au nanoparticles with Ag amplification)	mouse IgG	200 pM	
	Raman[82] (Au nanoparticles with Raman labels)	prostate-specific antigen		30 fM
	surface plasmon resonance[83,84] (triangular Ag particles on surfaces)	streptavidin(S A) and anti-biotin (AB)	$\sim$1 pM SA and $\sim$700 pM AB	
	electrical[110] (single-walled carbon nanotubes)	10E3 antibody to U1A RNA splicing factor	$\sim$1 nM	
	electrical[20] (Si nanowires)	streptavidin	10 pM	
	bio-bar-code amplification[75] (Au nanoparticles with Ag amplification)	prostate-specific antigen	30 aM (3 aM)[b]	(30 aM)[b]
molecular fluorophore methods	enzyme-linked immunosorbent assay	various	pM range	pM range
electrochemical methods	electrochemical amplification[137] (oligonucleotide reporter molecules)	IgG	13 fM	
enzyme-based amplification methods	immuno-PCR[76]	bovine serum albumin	2 fM	
	rolling circle amplification[77]	prostate-specific antigen	3 fM	

[a] Reported in ng/mL; authors converted to molar concentration for ease of comparison. [b] These values are the lower limits when PCR is used to amplify the bar-code DNA prior to scanometric detection of bar codes.
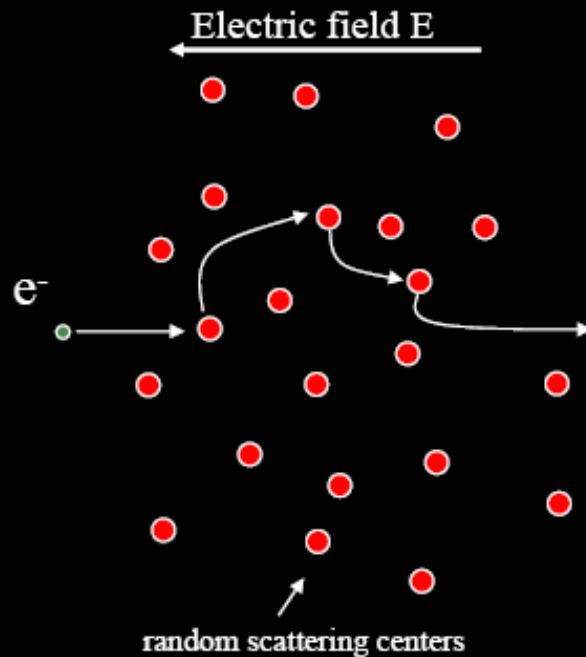
Surface Plasmon
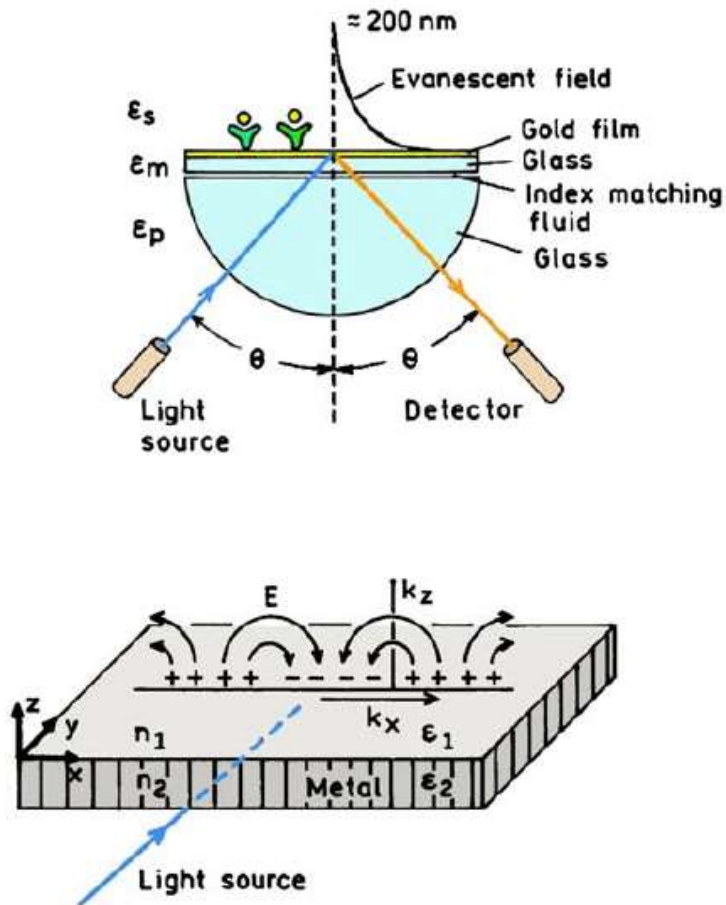
Figure 3. Schematics of an SPR experiment (top) and of the light-induced surface plasmons (bottom).

Drift: Drude model

Electric field E

e⁻

random scattering centers
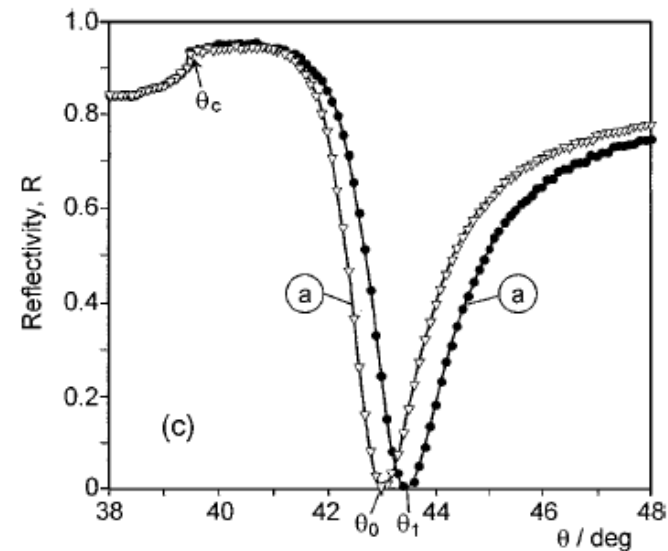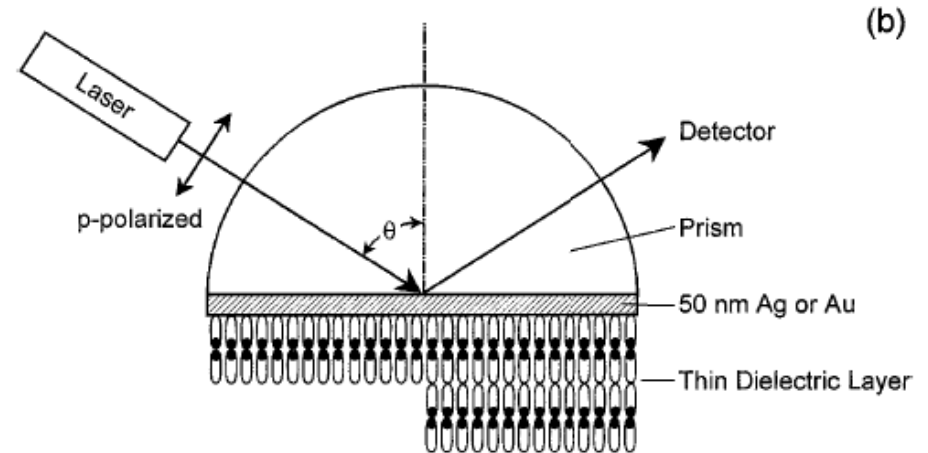
$$F = ma$$

$$eE = m\frac{\partial v}{\partial t}$$

$$v_{avg} = \underbrace{\frac{e\,\tau}{m}}_{\mu} E$$

$$j = ne\,v_{avg} = \underbrace{\frac{ne^2\tau}{m}}_{\sigma} E$$

$$m\frac{\partial}{\partial t}\langle\vec{v}\rangle = q\vec{E} - \gamma\langle\vec{v}\rangle$$

$$\sigma(\omega) = \frac{\sigma_0}{1 + i\omega\tau}$$

AC Dielectric Response

$$\varepsilon_m = 1 - \frac{\omega_p^2}{\omega^2}$$

Plasma frequency

polarizability of a small metal sphere with dielectric function $\varepsilon(\lambda)$

$$\alpha = R^3 \frac{\varepsilon - 1}{\varepsilon + 2}.$$

$$\varepsilon = \varepsilon_b + 1 - \frac{\omega_p^2}{\omega^2 + i\omega\gamma},$$

$$\alpha = \frac{R^3(\varepsilon_b \omega^2 - \omega_p^2) + i\omega\gamma\varepsilon_b}{[(\varepsilon_b + 3)\omega^2 - \omega_p^2] + i\omega\gamma(\varepsilon_b + 3)}.$$

$$\omega_R = \frac{\omega_p}{\sqrt{\varepsilon_b + 3}}$$

$$\gamma(\varepsilon_b + 3).$$

E

ε_0 (dielectric)

ε_M (metal)

$\varepsilon_M = -2\mathrm{Re}\,(\varepsilon_0)$

absorption

Surface plasmon resonance

Energy

$$\varepsilon_{eff} = \varepsilon_0 + 3N\varepsilon_0 \frac{\varepsilon_M - \varepsilon_0}{\varepsilon_M + 2\varepsilon_0}$$

ε_{inter}

ε_{exp}

ε_{intra}

Silver

Dielectric function (ε_1)

Energy (eV)
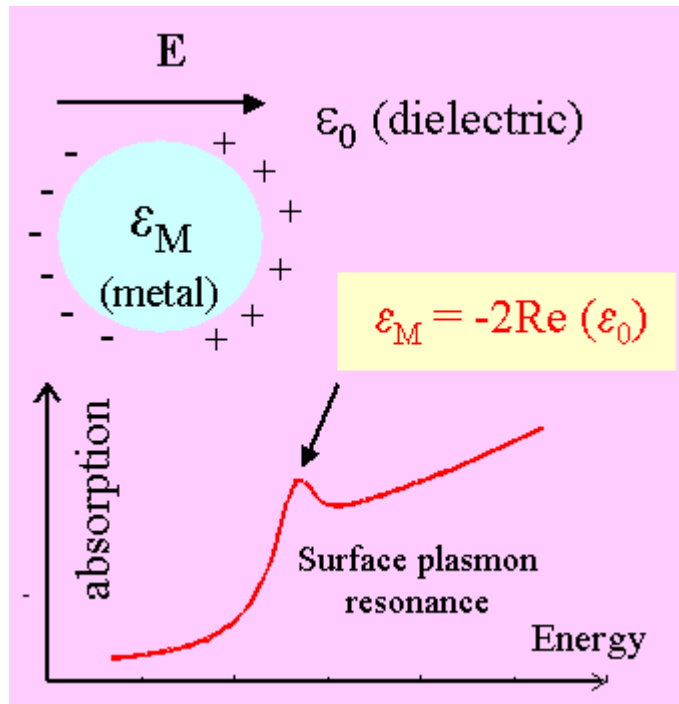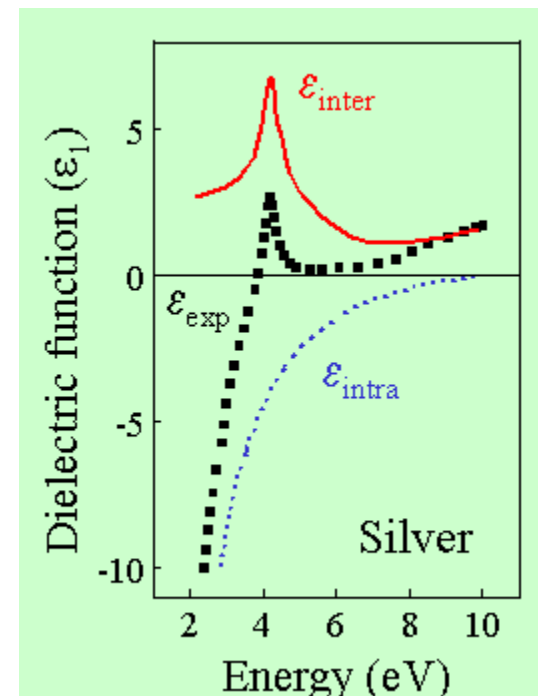
Biomolecular Binding in Real Time

SPR (Surface Plasmon Resonance) Detection System

Gold-Dextran Surfaces

Sensor Chip

Lot No:
00245

Biosensor

Microfluidic System

Flow Cell

Polarizer

Collimated White Light Source

Prism

Gold Film

Narrow Band Interference Filter

CCD Camera
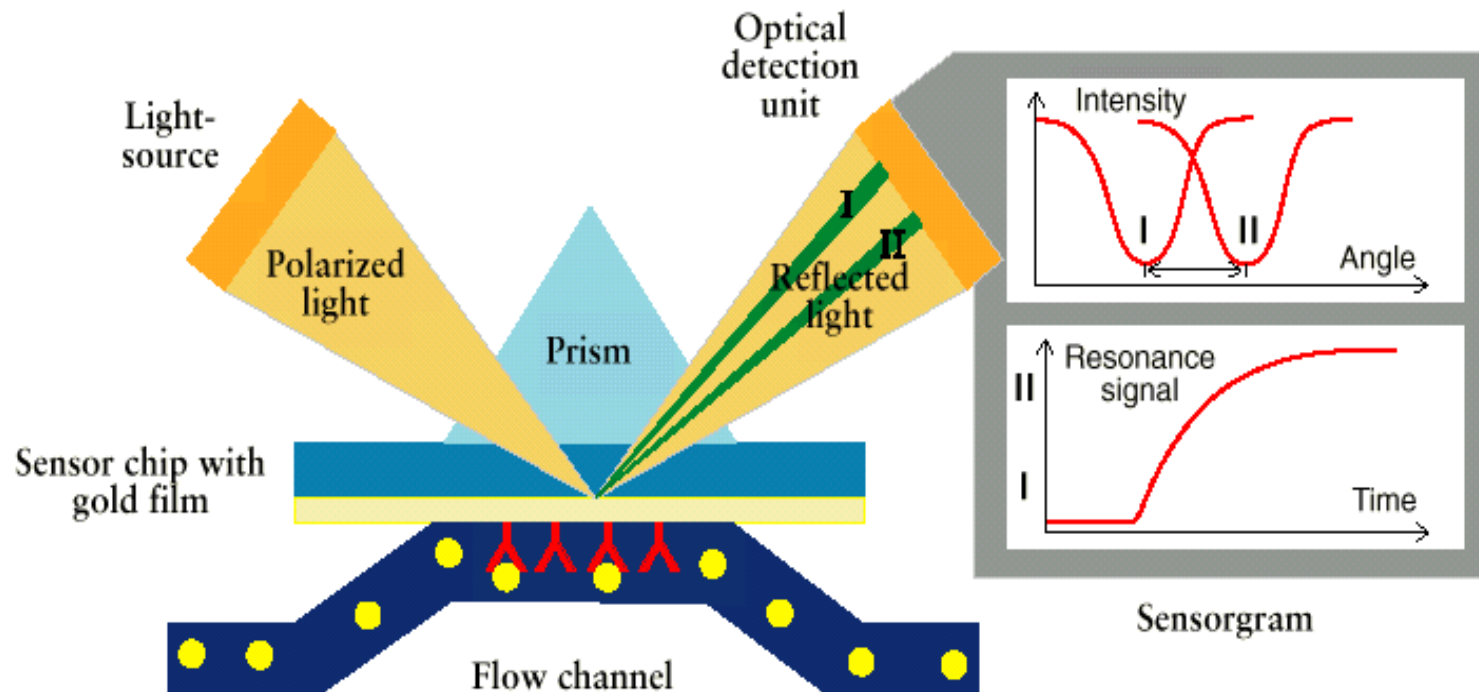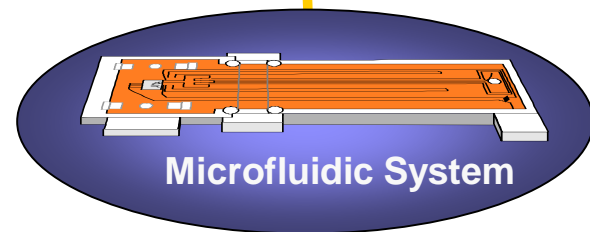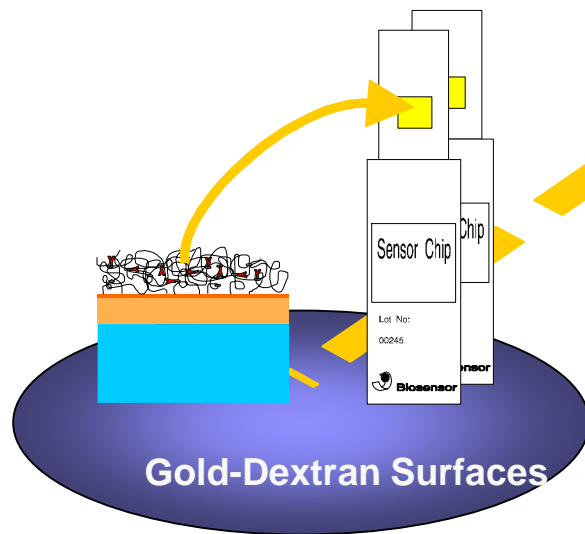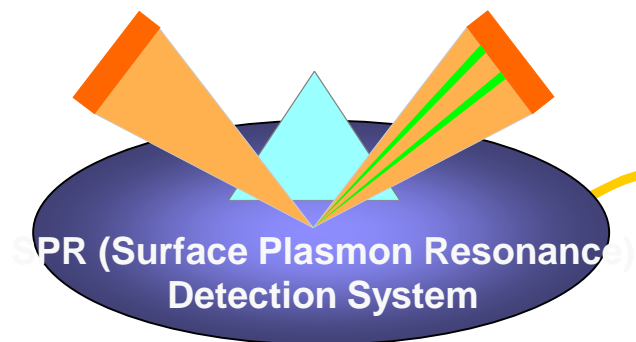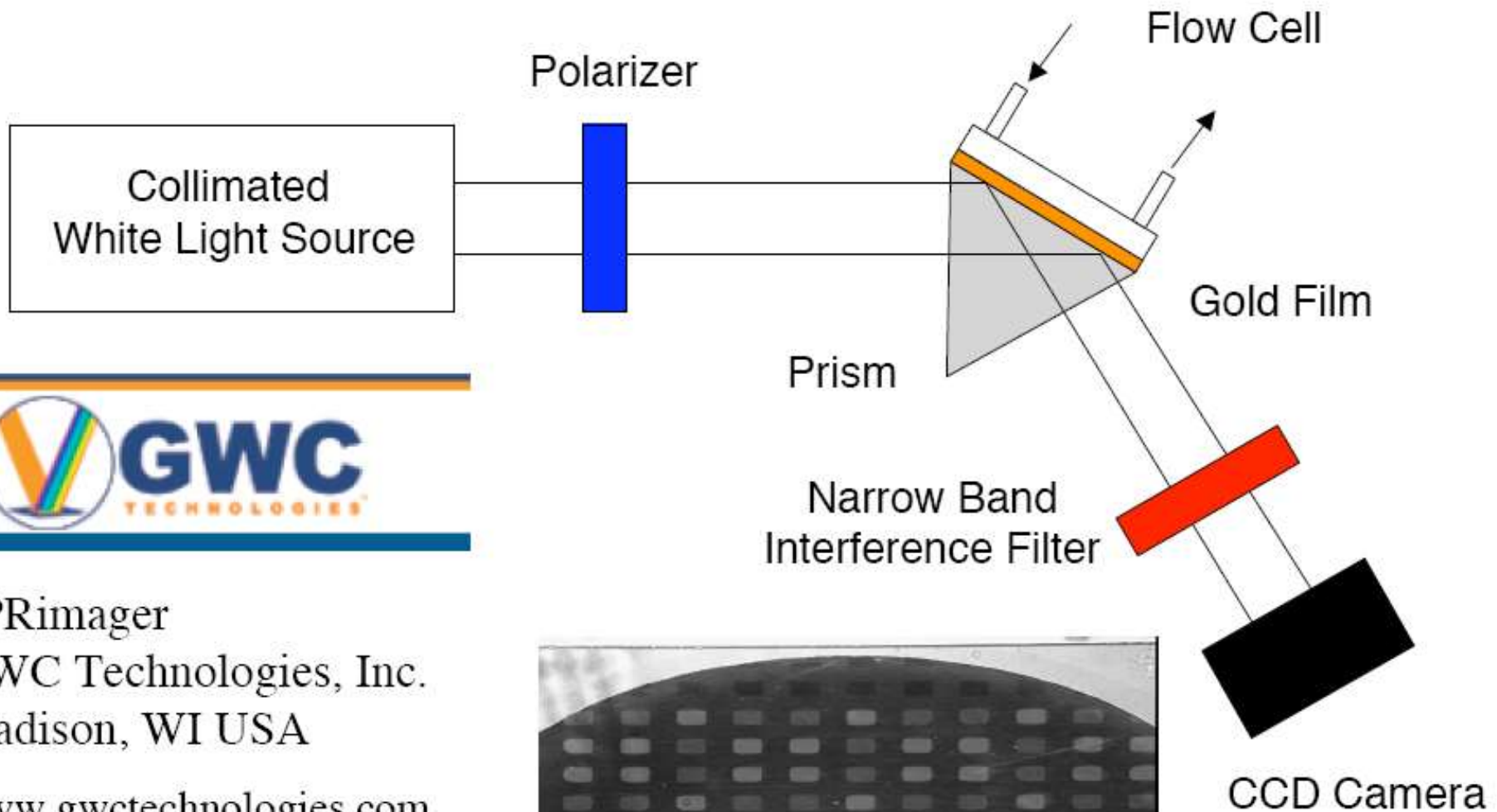
SPRimager
GWC Technologies, Inc.
Madison, WI USA

www.gwctechnologies.com

Raw Image
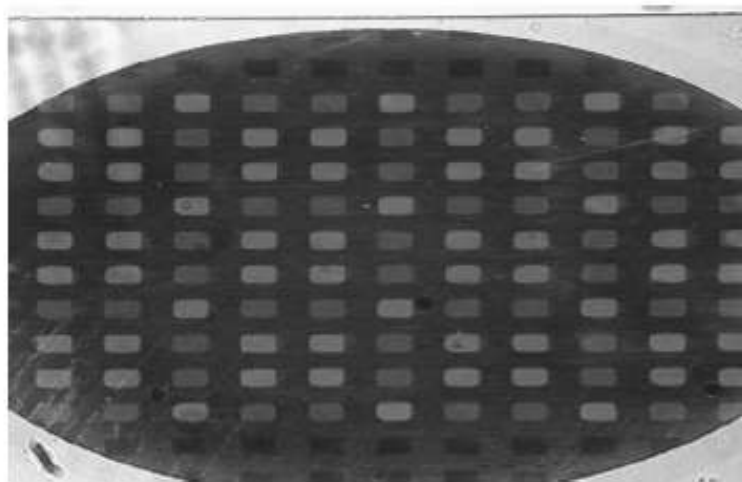
Localized Plasmon
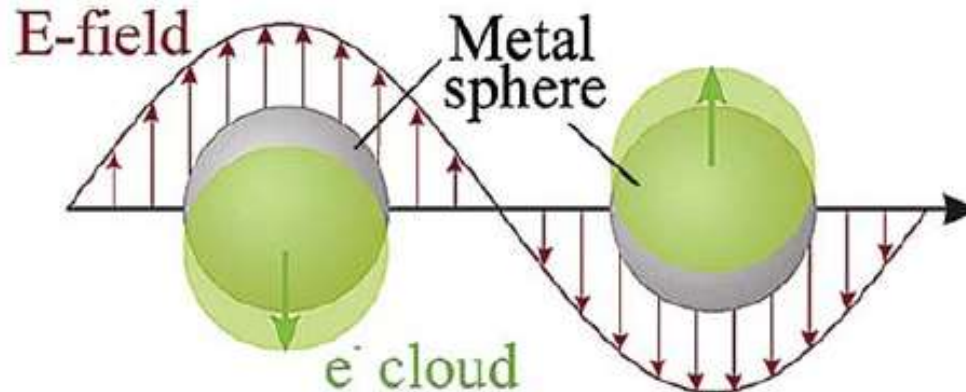
Figure 6. Schematic of plasmon oscillation for a sphere. From [39].
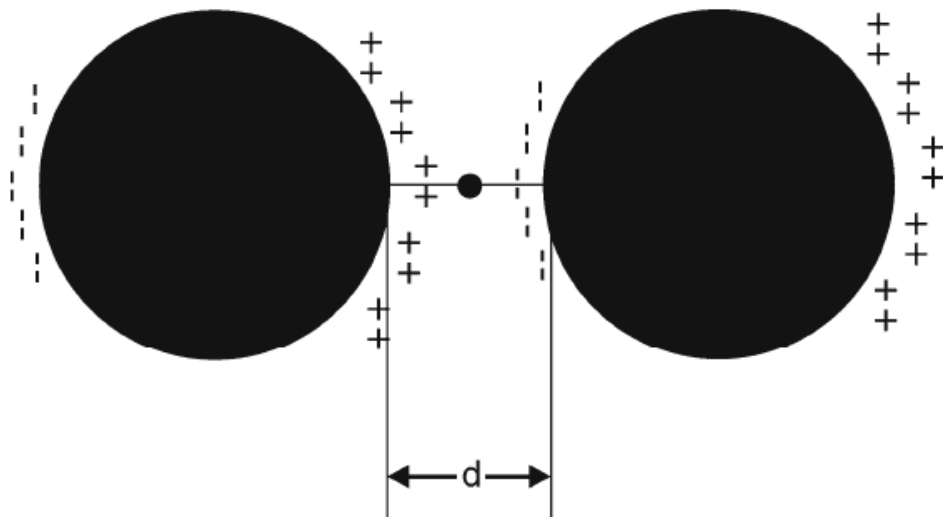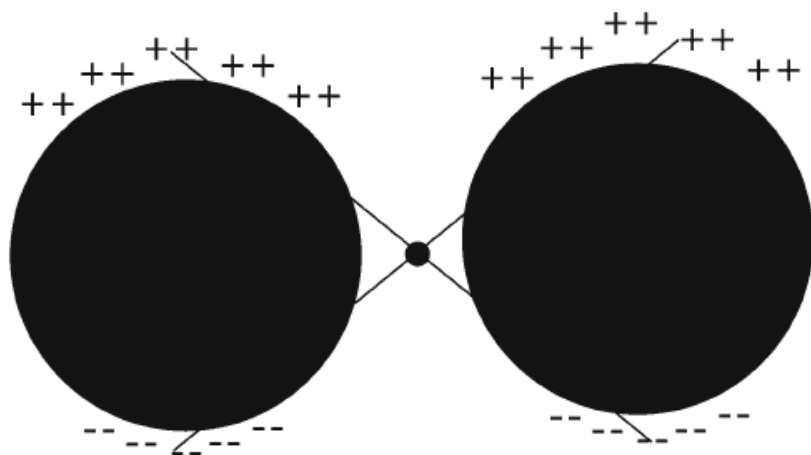
field enhancement

$E_s = gE_0$, where E_0 is the magnitude of the incident field

$$E_R \propto \alpha_R E_s \propto \alpha_R g E_0$$

$$E_{SERS} \propto \alpha_R gg' E_0$$

$$I_{SERS} \propto |\alpha_R|^2 |gg'|^2 I_0$$

$$g \cong g'$$

$$|E_L|^4 = |g|^4.$$

Probing Single Molecules and Single Nanoparticles by Surface-Enhanced Raman Scattering

Shuming Nie* and Steven R. Emory

Fig. 1. Single Ag nanoparticles imaged with evanescent-wave excitation. Total internal reflection of the laser beam at the glass-liquid interface was used to reduce the laser scattering background. The instrument setup for evanescent-wave microscopy was adapted from Funatsu et al. (11). The images were directly recorded on color photographic film (ASA-1600) with a 30-s exposure by a Nikon 35-mm camera attached to the microscope. (A) Unfiltered photograph showing scattered laser light from all particles immobilized on a polylysine-coated surface. (B) Filtered photographs taken from a blank Ag colloid sample (incubated with 1 mM NaCl and no R6G analyte molecules). (C) and (D) Filtered photographs taken from a Ag colloid sample incubated with 2×10^{-11} M R6G. These images were selected to show at least one Raman scattering particle. Different areas of the cover slip were rapidly screened, and most fields of view did not contain visible particles. (E) Filtered photograph taken from Ag colloid incubated with 2×10^{-10} M R6G. (F) Filtered photograph taken from Ag colloid incubated with 2×10^{-9} M R6G. A high-performance bandpass filter was used to remove the scattered laser light and to pass Stokes-shifted Raman signals from 540 to 580 nm (920 to 2200 cm^{-1}). Continuous-wave excitation at 514.5 nm was provided by an Ar ion laser. The total laser power at the sample was 10 mW. Note the color differences between the scattered laser light in (A) and the red-shifted light in (C) through (F).
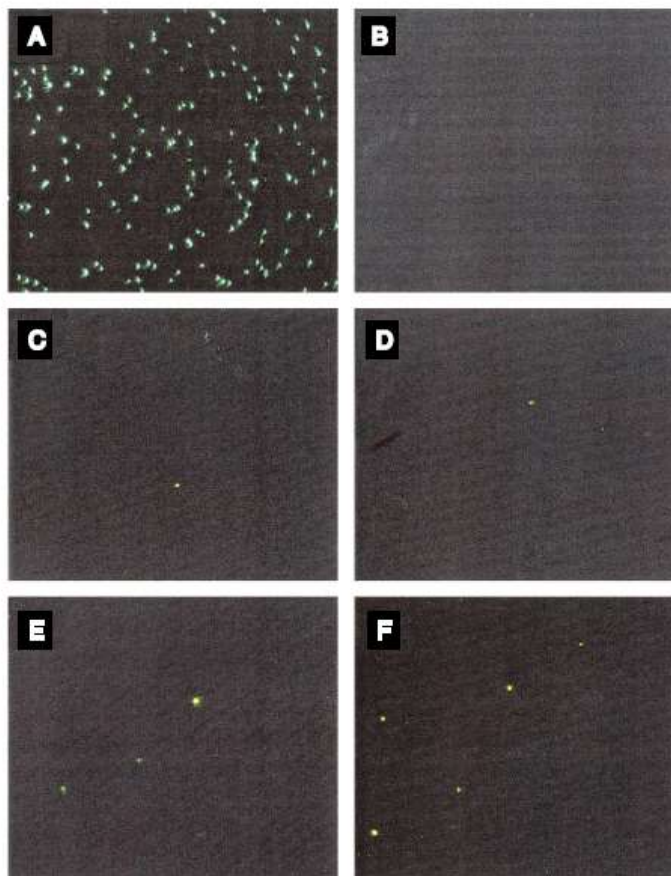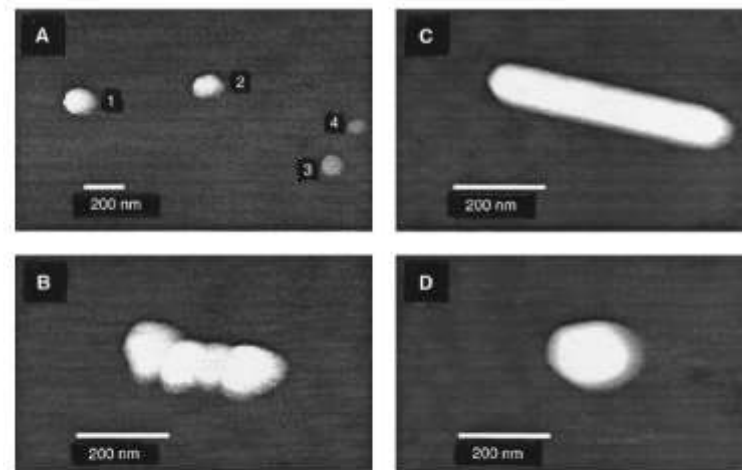

Fig. 2. Tapping-mode AFM images of screened Ag nanoparticles. (A) Large area survey image showing four single nanoparticles. Particles 1 and 2 were highly efficient for Raman enhancement, but particles 3 and 4 (smaller in size) were not. (B) Close-up image of a hot aggregate containing four linearly arranged particles. (C) Close-up image of a rod-shaped hot particle. (D) Close-up image of a faceted hot particle.

Fig. 3. Surface-enhanced Raman spectra of R6G obtained with a linearly polarized confocal laser beam from two Ag nanoparticles. The R6G concentration was 2×10^{-11} M, corresponding to an average of 0.1 analyte molecule per particle. The direction of laser polarization and the expected particle orientation are shown schematically for each spectrum. Laser wavelength, 514.5 nm; laser power, 250 nW; laser focal radius, ~250 nm; integration time, 30 s. All spectra were plotted on the same intensity scale in arbitrary units of the CCD detector readout signal.
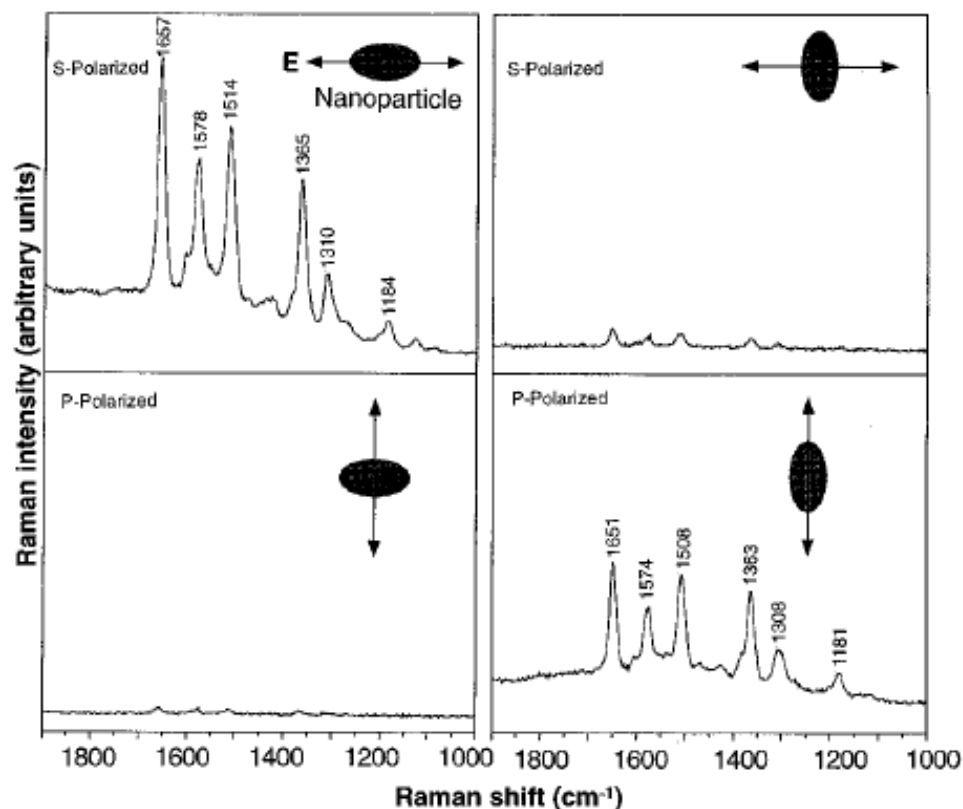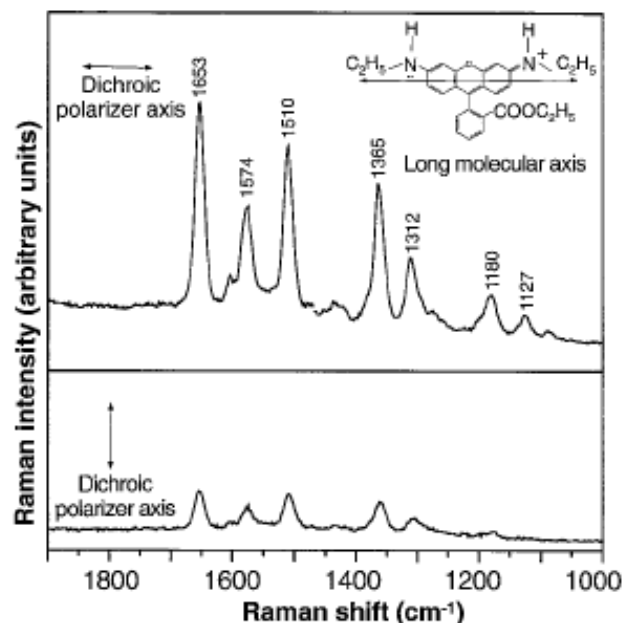
Fig. 4. Emission-polarized surface-enhanced Raman signals of R6G observed from a single Ag nanoparticle with a polarization-scrambled confocal laser beam. A dichroic sheet polarizer was rotated 90° to select Raman scattering signals polarized parallel (upper spectrum) or perpendicular (lower spectrum) to the long molecular axis of R6G. (**Inserts**) Structure of R6G, the electronic transition dipole (along the long axis when excited at 514.5 nm), and the dichroic polarizer orientations. Other conditions as in Fig. 3.

troscopic signatures of adsorbed molecules. For single rhodamine 6G molecules adsorbed on the selected nanoparticles, the intrinsic Raman enhancement factors were on the order of 10^{14} to 10^{15}, much larger than the ensemble-averaged values derived from conventional measurements. This enormous enhancement leads to vibrational Raman signals that are more intense and more stable than single-molecule fluorescence.

Electromagnetic contributions to single-molecule sensitivity in surface-enhanced Raman scattering
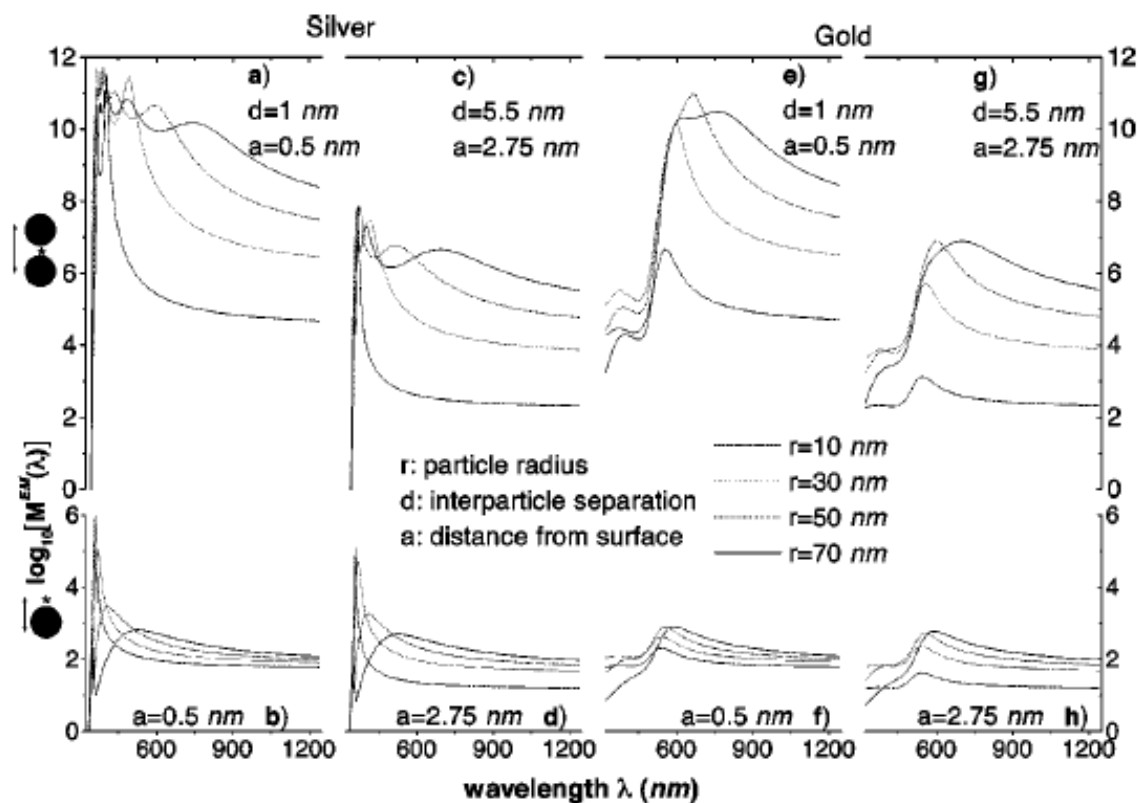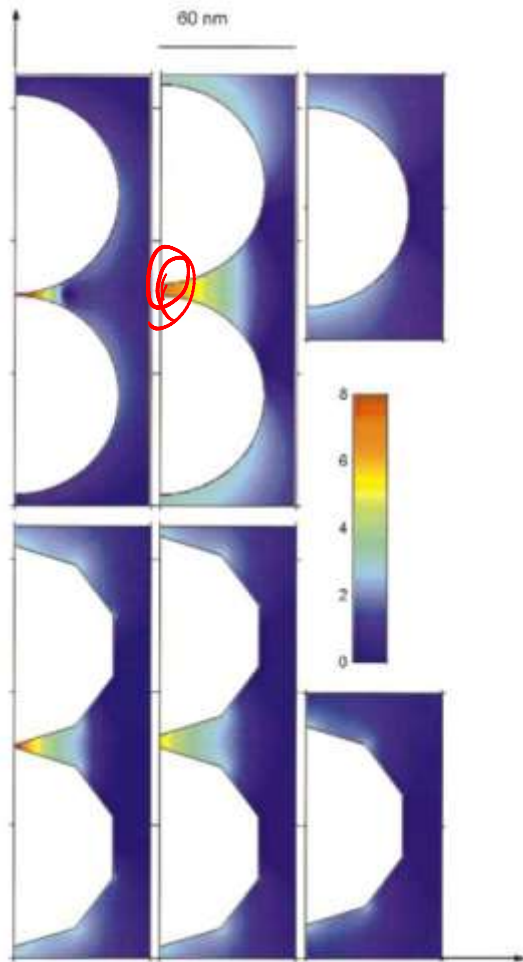
FIG. 3. (Color) EM-enhancement factor M^{EM} at a cross section through six different silver particle configurations. The wavelength of the incident field is $\lambda = 514.5$ nm with vertical polarization. The left-hand column illustrates the EM enhancement for dimer configurations of two spheres (top) and two polygons (bottom) with a separation of 1 nm. The middle column shows the same situation, but with a separation distance of 5.5 nm. The right-hand column shows the case of an isolated single particle. All particles share a common largest dimension of 90 nm. Note that the color scale from dark blue to dark red is logarithmic, covering the interval $10^0 < M^{EM} < 10^8$. Regions with enhancement outside this interval are shown in dark blue and dark red, respectively.
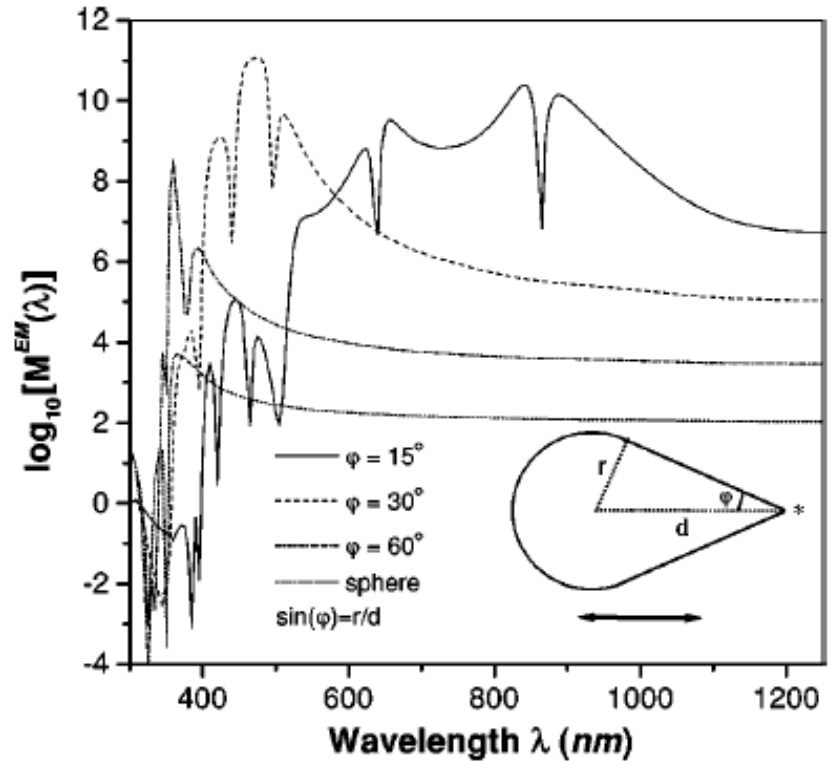
FIG. 5. EM-enhancement factor for a rotationally symmetric silver droplet as a function of the angle defining the opening edge ϕ. The field is polarized parallel to the axis of the droplet and the evaluation position (star) is located 0.5 nm outside the tip. As the droplet becomes sharper the enhancement increases several orders of magnitude.

Nanosphere Arrays with Controlled Sub-10-nm Gaps as Surface-Enhanced Raman Spectroscopy Substrates
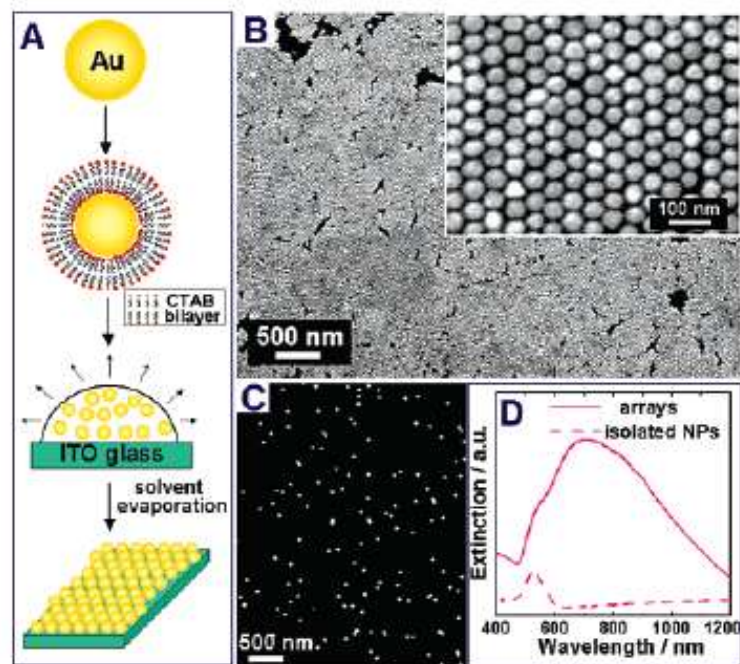
Figure 1. (A) Schematic illustration of the fabrication of sub-10-nm gap Au NP arrays. (B) SEM image of the arrays. (C) SEM image of monolayer of isolated Au NPs on ITO glass. (D) Vis−NIR extinction spectrum of the monolayer of isolated Au NPs and arrays.
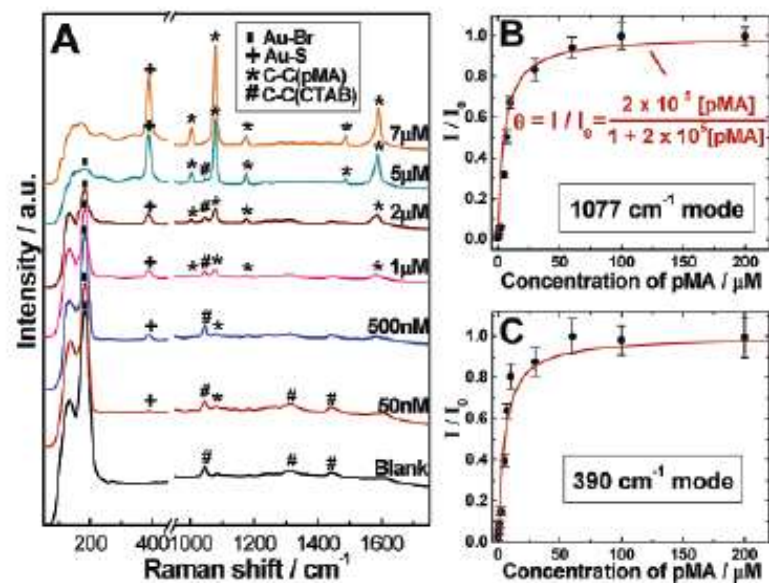

Figure 2. (A) SERS spectra of 5 μL of pMA with different concentrations deposited on the NP arrays. The excitation laser wavelength is 785 nm. Adsorption isotherm of pMA on the NP arrays obtained according to (B) 1077 and (C) 390 cm^{-1} modes in the SERS spectra. I_0 is the peak intensity of a saturated pMA monolayer.
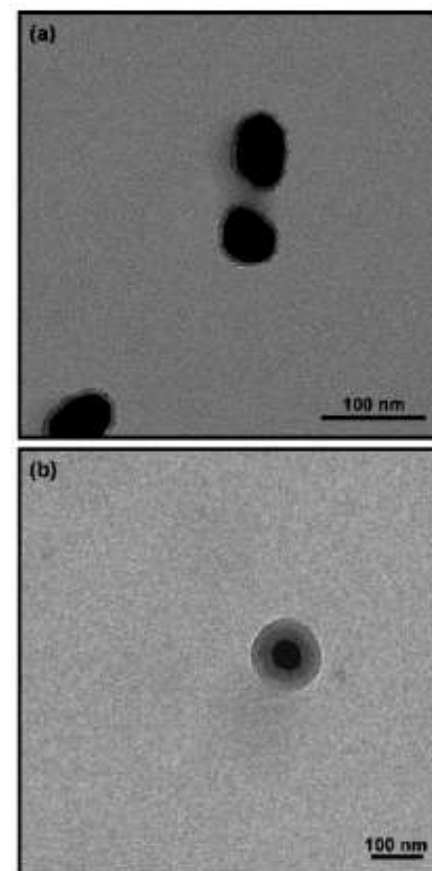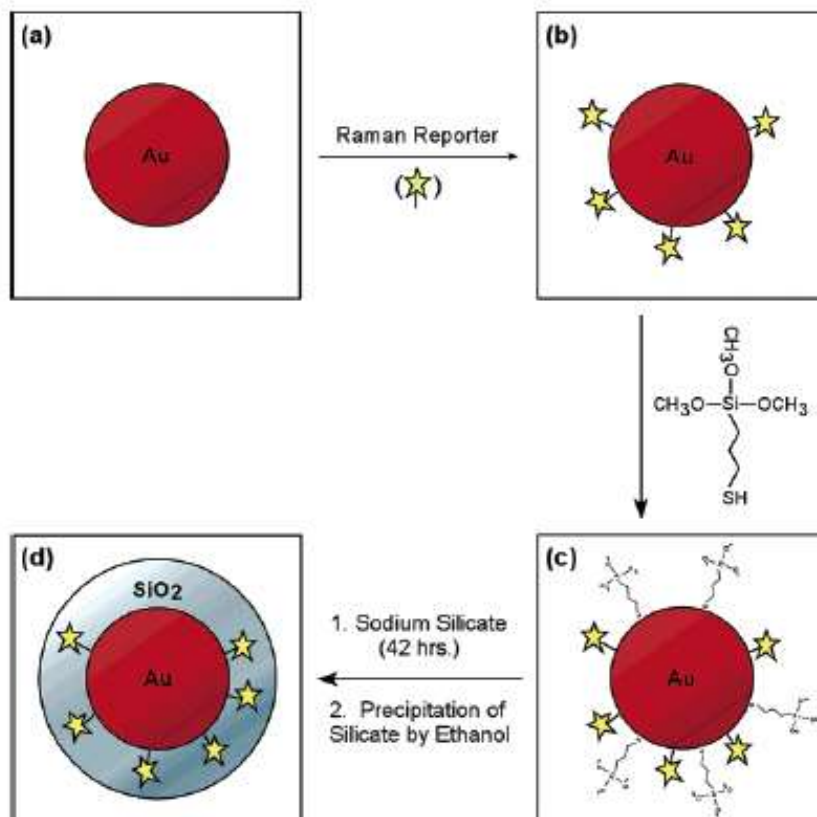
band arises from a coalescence of the dimer plasmon resonances

Profiling the Near Field of a Plasmonic Nanoparticle with Raman-Based Molecular Rulers
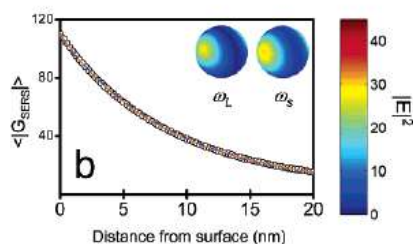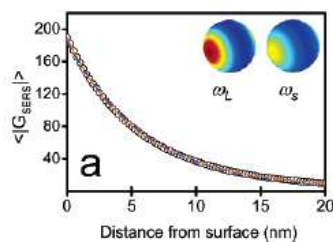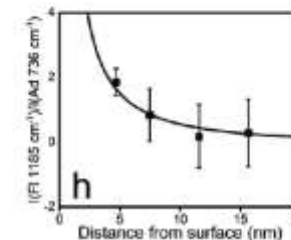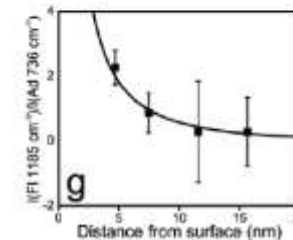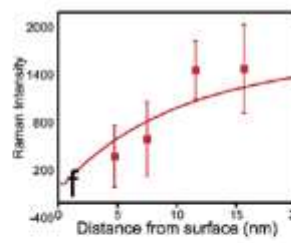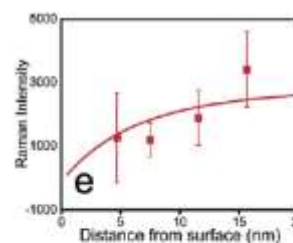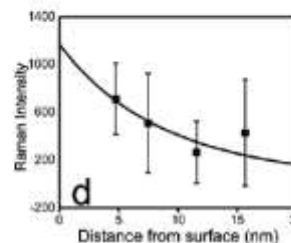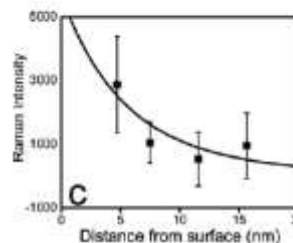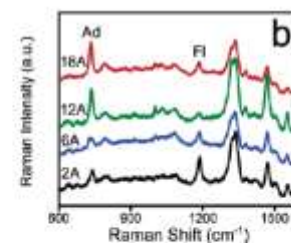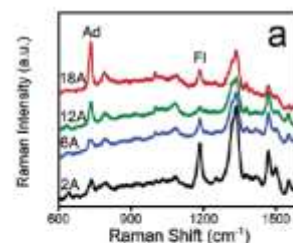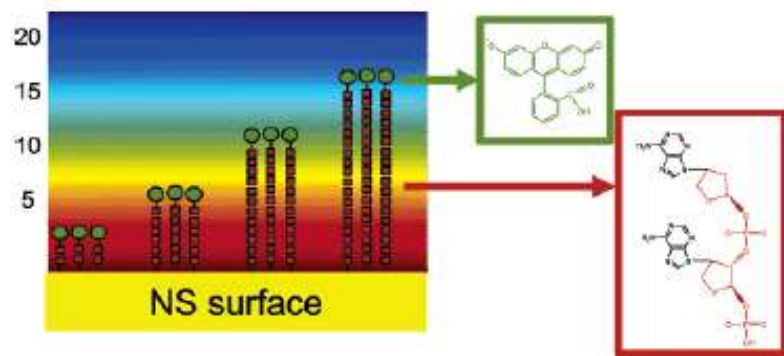
Spectroscopic Tags Using Dye-Embedded Nanoparticles and Surface-Enhanced Raman Scattering
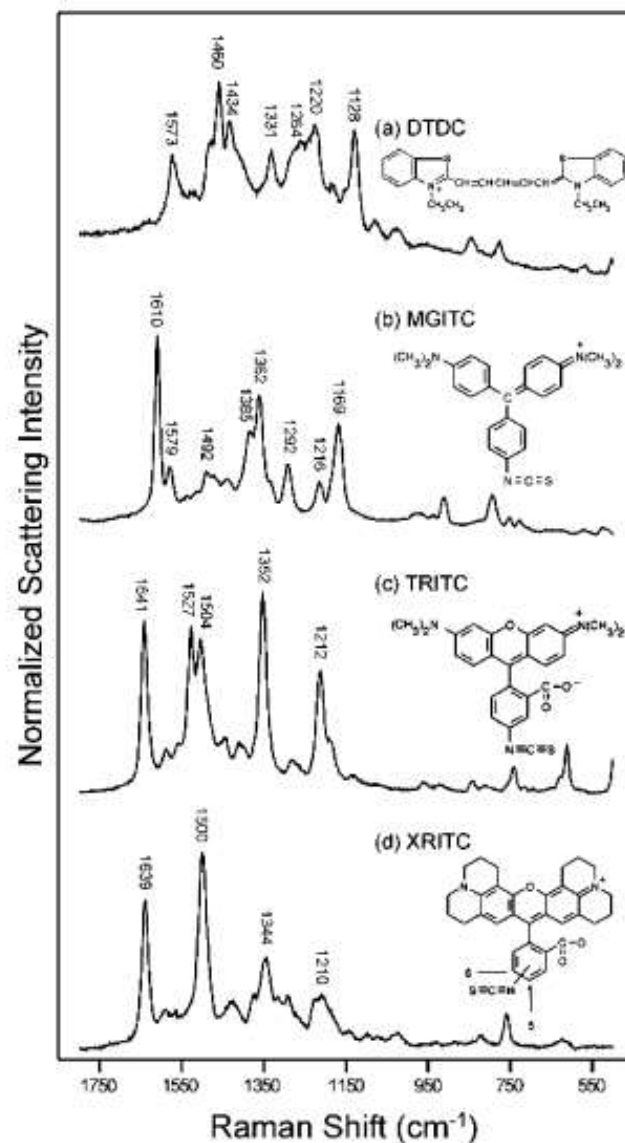
**Figure 4.** Chemical structures of four Raman reporters and their surface-enhanced resonance Raman spectra: (a) 3,3′-Diethylthiadicarbocyanine iodide (DTDC); (b) malachite green isothiocyanate (MGITC); (c) tetramethylrhodamine-5-isothiocyanate (TRITC); and (e) rhodamine-5-(and-6)-isothiocyanate (XRITC).

Nanoparticle Probes with Surface Enhanced Raman Spectroscopic Tags for Cellular Cancer Targeting
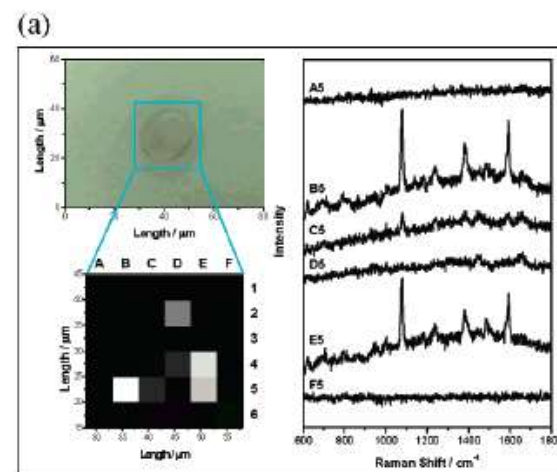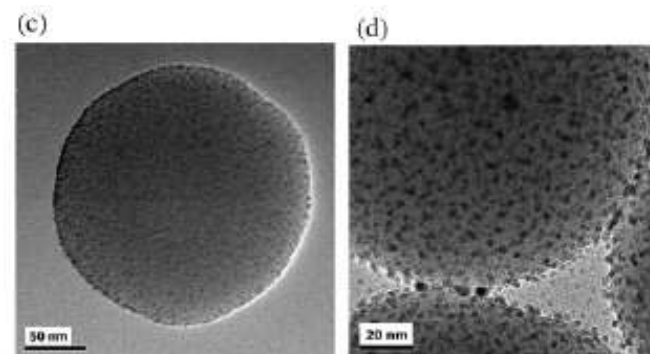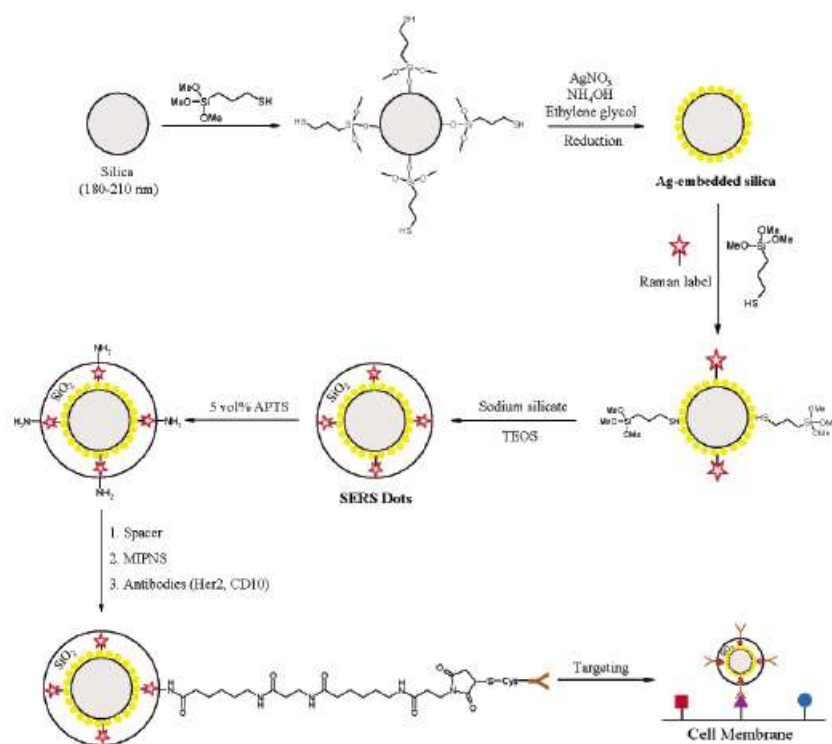
Biological Imaging of HEK293 Cells Expressing PLCγ1 Using Surface-Enhanced Raman Microscopy
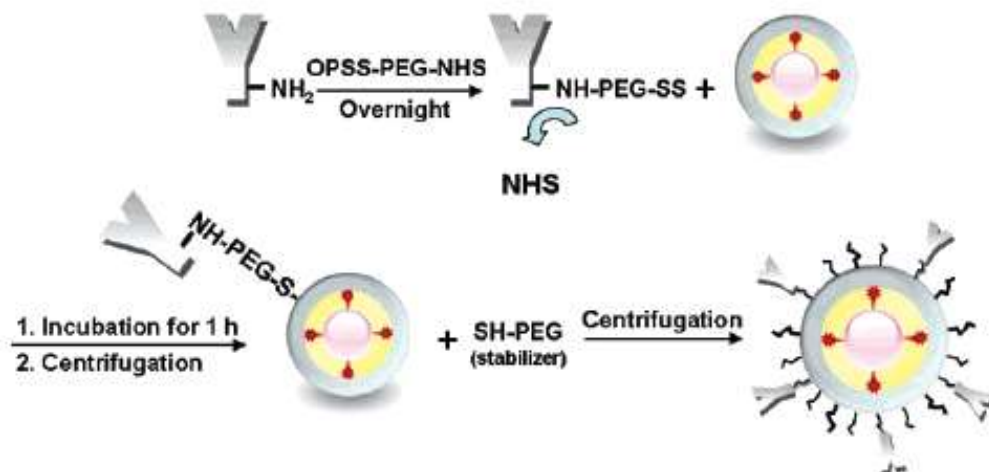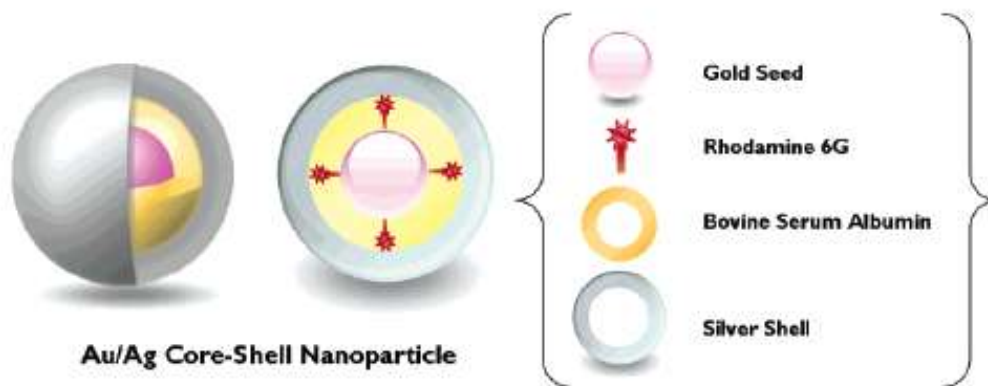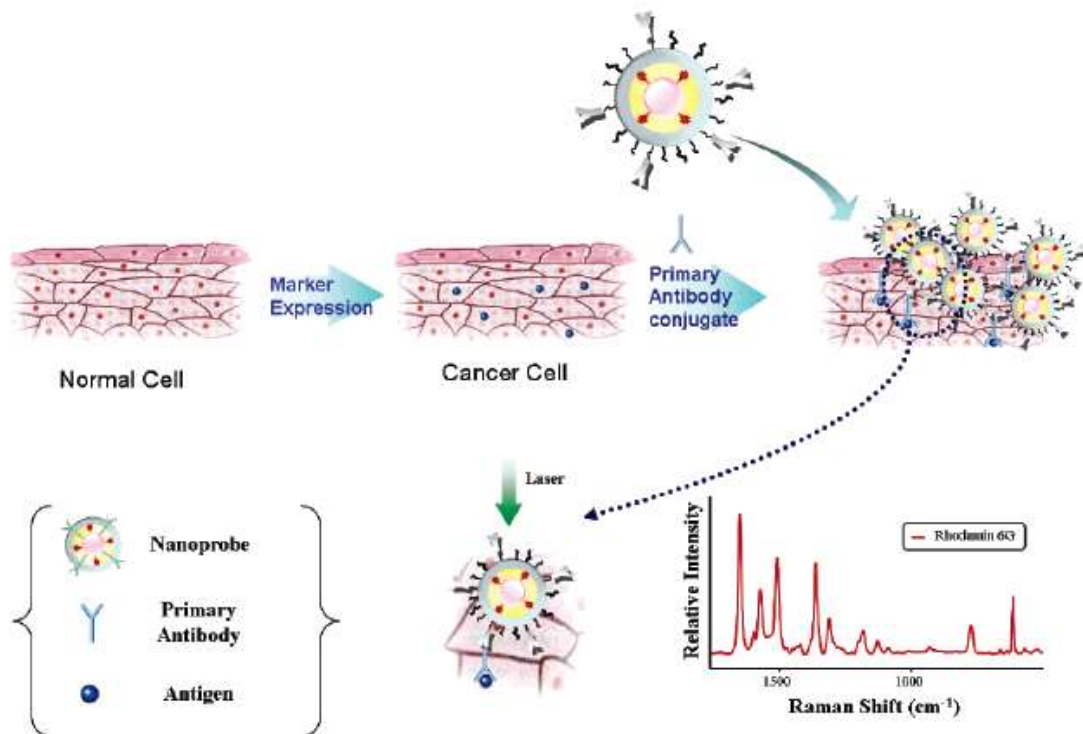
Figure 4. Schematic diagram depicting immobilization of Au/Ag core–shell nanoprobes on PLCγ1-expressing HEK293 cells and their SERS detection.
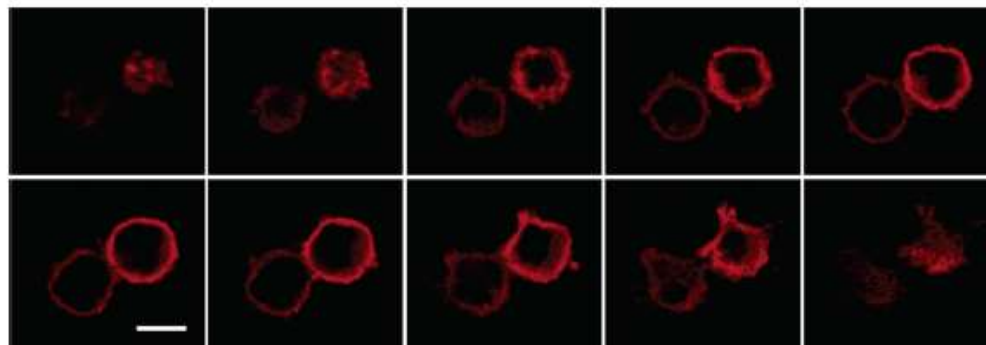

Figure 5. Serial fluorescence optical sections of PLCγ1-expressing HEK293 cells using red QDs. The z-axis interval of optical slices is 1.3 μm. Cells were incubated for 30 min in red QDs, after which the free QDs were washed away. These fluorescence images indicate that PLCγ1 markers are only expressed on the surface membranes. Scale bar, 10 μm.
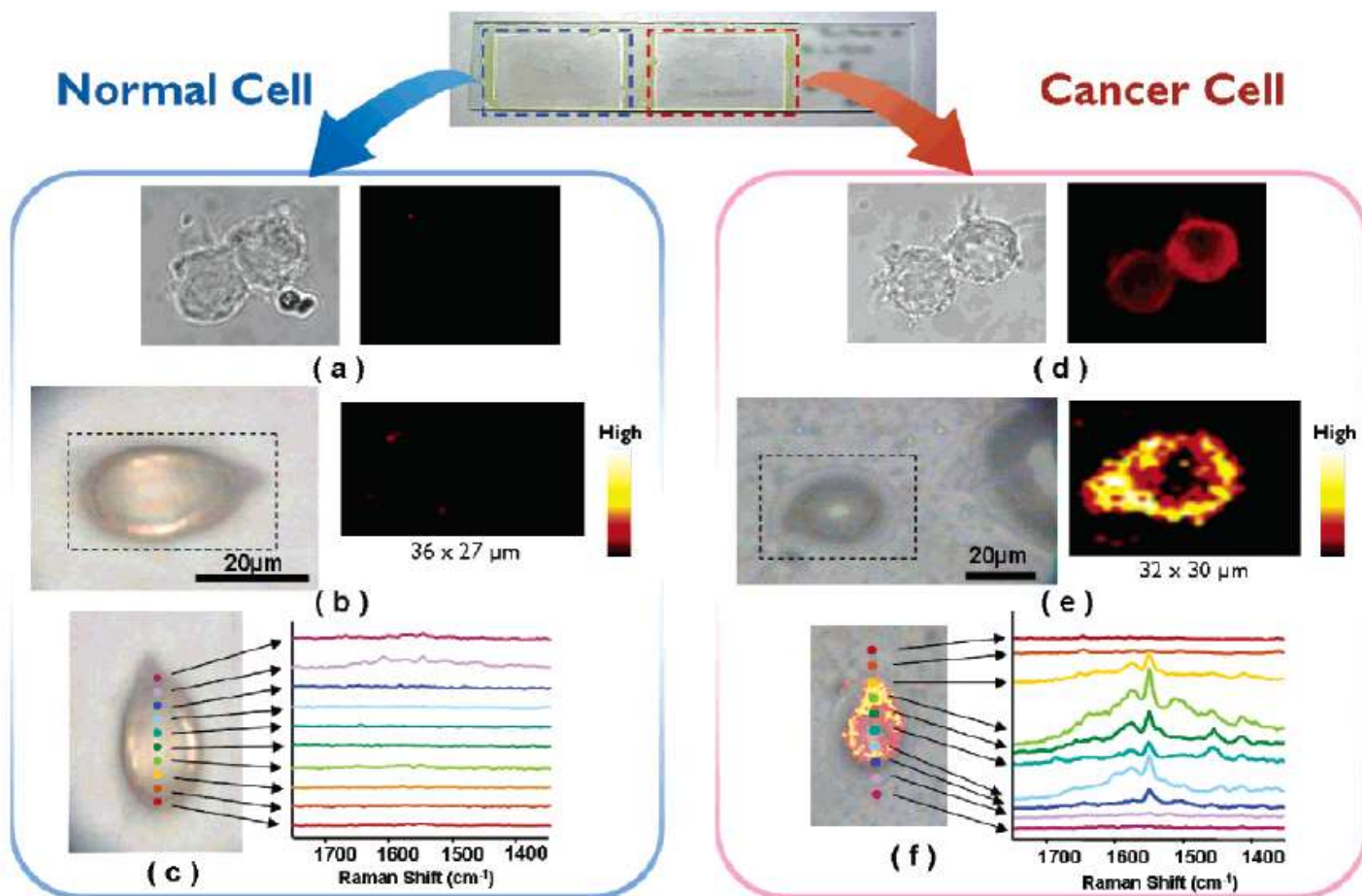
Figure 6. Fluorescence and SERS images of normal HEK293 cells and PLCγ1-expressing HEK293 cells. (a) QD-labeled fluorescence images of normal cells: (left) brightfield image, (right) fluorescence image. (b) SERS images of single normal cell: (left) brightfield image, (right) Raman mapping image of single normal cell based on the 1650-cm^{-1} R6G peak. The cell area was scanned with an interval of 1 μm. Intensities are scaled to the highest value in each area. (c) Overlay image of brightfield and Raman mapping for single normal cell. Colorful spots indicate the laser spots across the middle of the cell along the y axis. (d) QD-labeled fluorescence images of cancer cells: (left) brightfield image, (right) fluorescence image. (e) SERS images of single cancer cell: (left) brightfield image, (right) Raman mapping image of single cancer cell based on the 1650-cm^{-1} R6G peak. The cell area was scanned with an interval of 1 μm. Intensities are scaled to the highest value in each area. (f) Overlay image of brightfield and Raman mapping for single cancer cell. Colorful spots indicate the laser spots across the middle of the cell along the y axis.

Mammalian Cell Surface Imaging with Nitrile-Functionalized Nanoprobes: Biophysical Characterization of Aggregation and Polarization Anisotropy in SERS Imaging
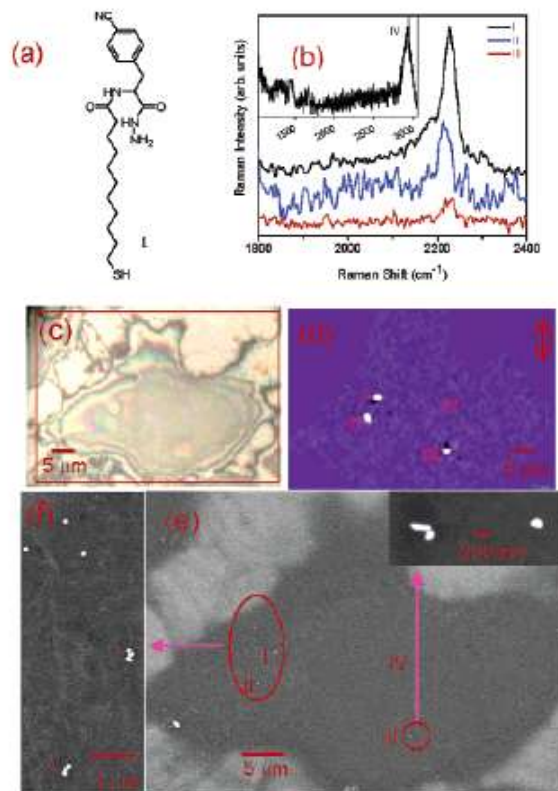

Figure 1. (a) The chemical structure of Raman reporter 1; (b) Raman spectra of the CN vibration mode extracted from positions I, II, and III of the cell shown in the optical image (c). Inset of (b) is a cellular Raman spectrum taken from spot IV of the same cell. (d) Raman intensity map of the C≡N band of the same cell, and (e) the corresponding SEM image. Inset in (e) showed the NPs in the lower right circle. (f) The group of NPs as shown in the large oval of (e).
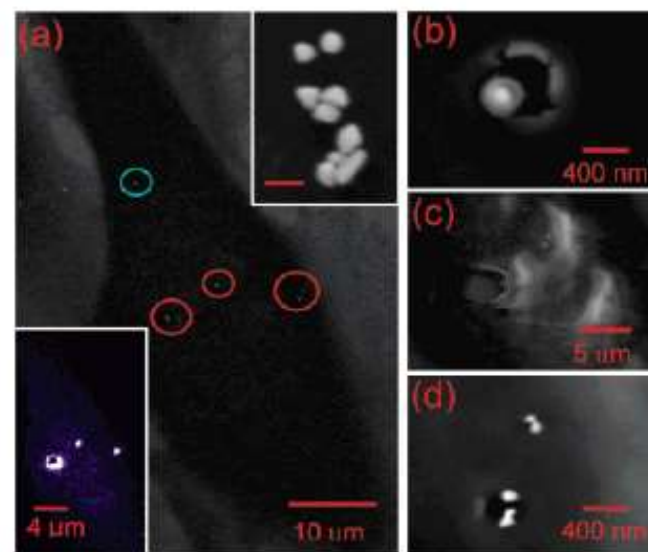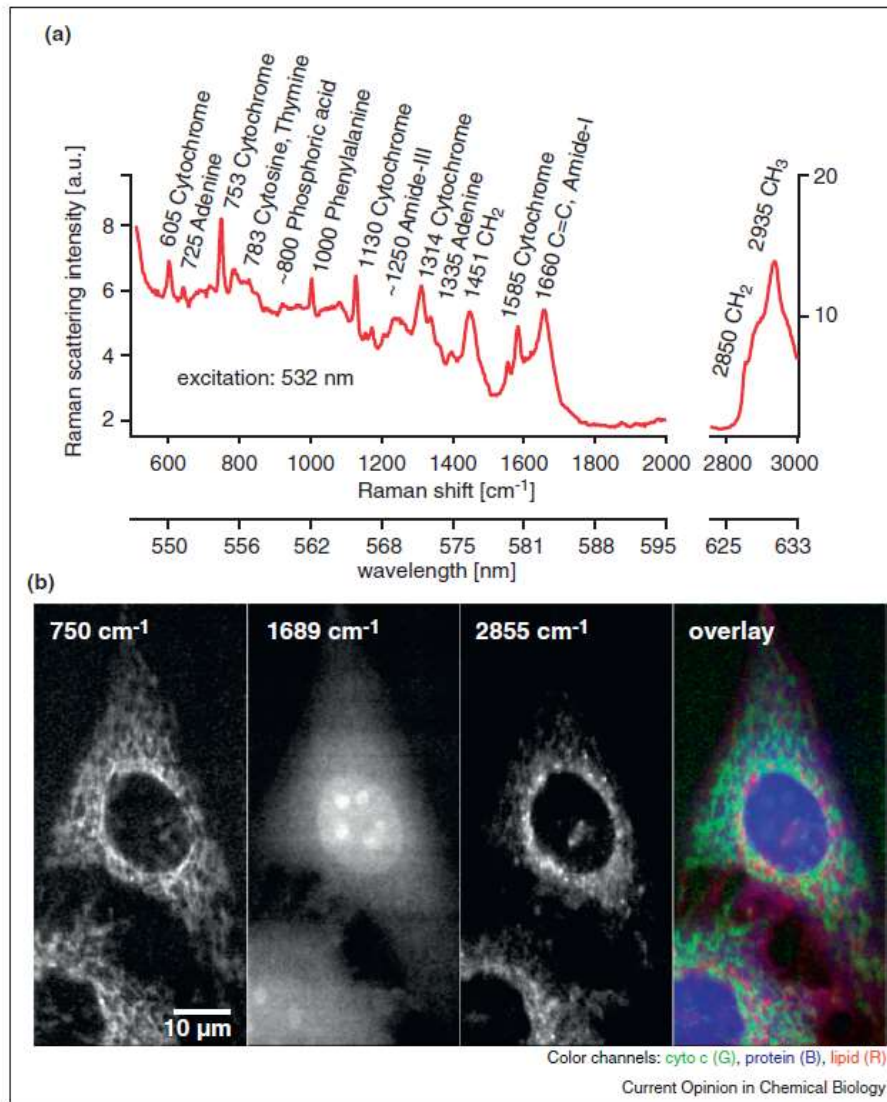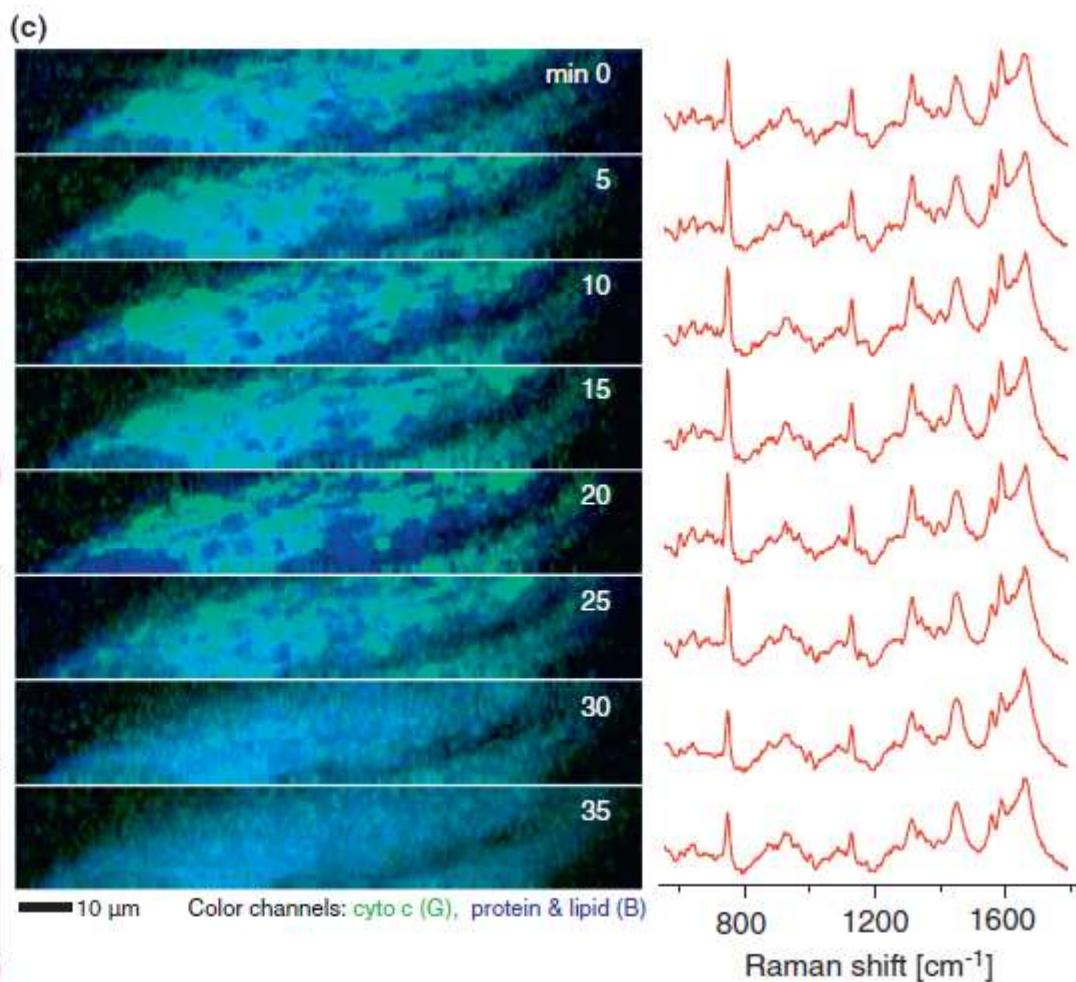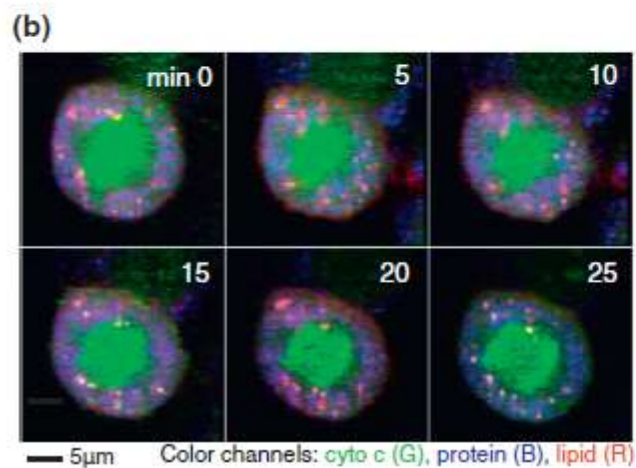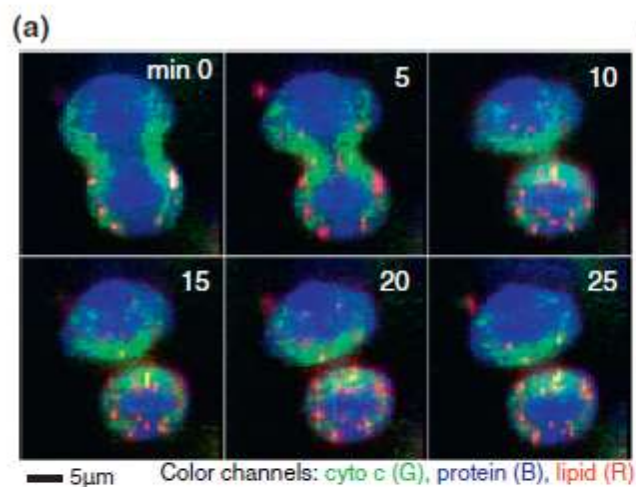

Figure 2. (a) SEM image of a cell. Upper right inset: magnification of a group of aggregated NPs. The scale bar is 200 nm. Lower left inset: the corresponding Raman intensity image of the same cell obtained with a power density of 10^5 W/cm^2. Laser-induced damage to the cell is shown in (b) the monomer (blue circle in a), (c) the aggregates, and (d) a pair of dimers.
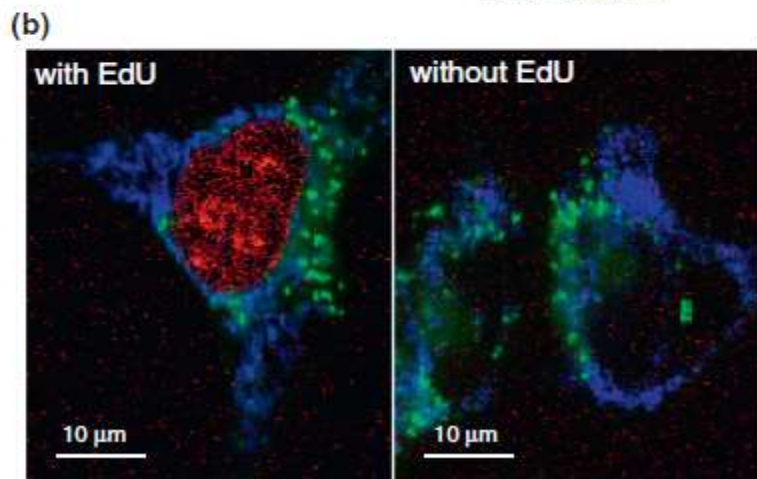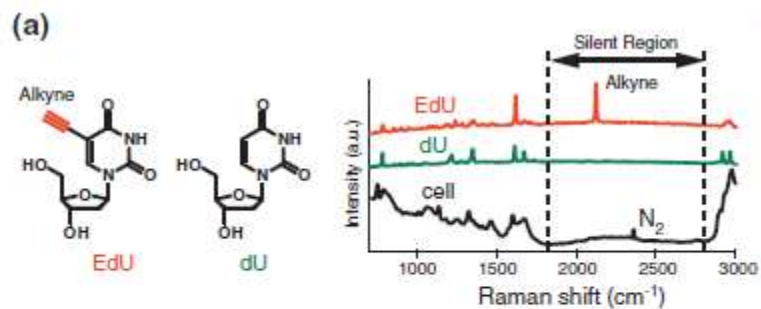
Molecular imaging of live cells by Raman microscopy

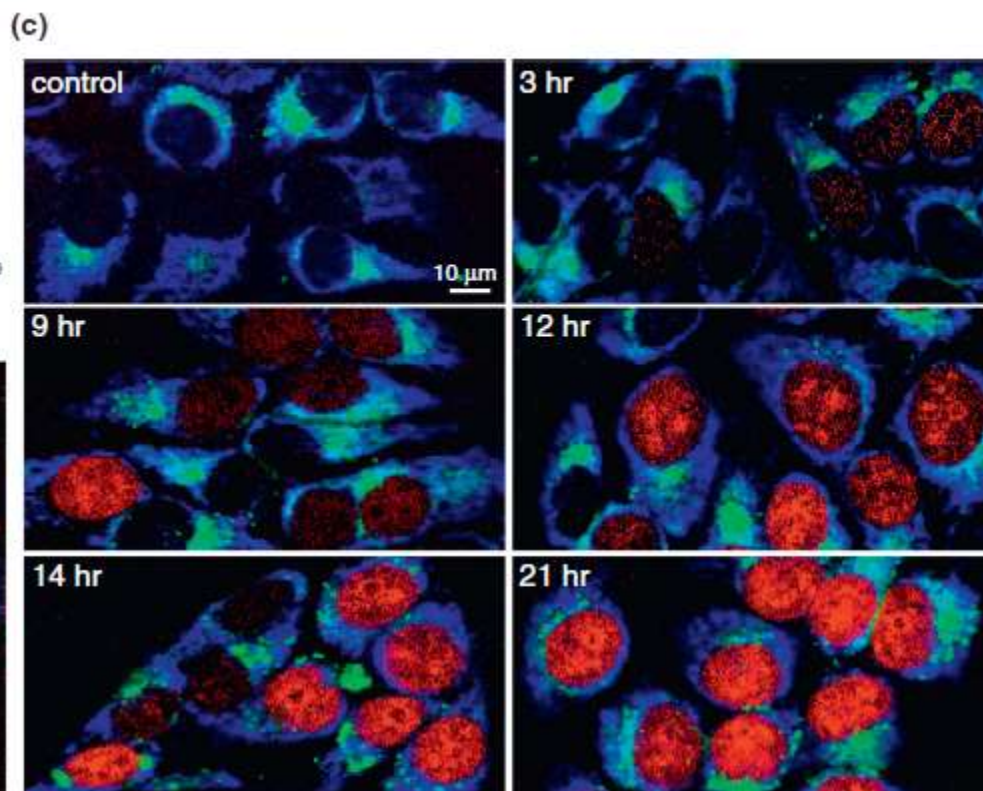Almar F Palonpon[1,2], Mikiko Sodeoka[2,3] and Katsumasa Fujita[1,2]

Color channels: cyto c (G), protein (B), lipid (R)

Current Opinion in Chemical Biology

(a)

min 0 5 10
15 20 25

5µm Color channels: cyto c (G), protein (B), lipid (R)

(b)

min 0 5 10
15 20 25

5µm Color channels: cyto c (G), protein (B), lipid (R)

(c)

min 0
5
10
15
20
25
30
35

10 µm Color channels: cyto c (G), protein & lipid (B)

Raman shift [cm⁻¹]

800 1200 1600

Current Opinion in Chemical Biology

(a)

Alkyne

EdU   dU

Silent Region
Alkyne
EdU
dU
cell
N₂

Intensity (a.u.)

Raman shift (cm⁻¹)

(b)

with EdU   without EdU
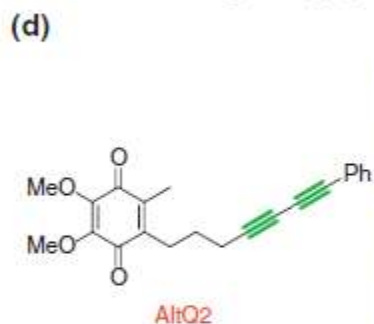
10 μm   10 μm

Color channels: cyto c (B), protein (G), EdU (R)

(c)

control   3 hr

10 μm

9 hr   12 hr

14 hr   21 hr

Color channels: cyto c (B), protein (G), EdU (R)

(d)

AltQ2

(e)

747 cm⁻¹   2122 cm⁻¹   2248 cm⁻¹   overlay

10 μm

Color channels: cyto c (B), EdU (R), AltQ2 (G)

Current Opinion in Chemical Biology

(a)

Alkyne vs Nitrile

CC
2110

CN
2242

2.34

1.00

Relative intensity

2000 2100 2200 2300
Raman shift (cm⁻¹)

Azide vs Nitrile

CN
2242

1.00

N₃
2096

0.38

Relative intensity

2000 2100 2200 2300
Raman shift (cm⁻¹)

Deuterium vs Nitrile

11xCD   CN
2124   2241

1.07
1.00

Relative intensity

2000 2100 2200 2300
Raman shift (cm⁻¹)

(b)

R: Alkyl, Alkenyl, Acyl, etc.
Ar: Aryl, X: SiMe₃, Br, or I

Raman Intensity versus EdU (RIE)

F Ar ≡ Ar

E3 Ar ≡ X Ar ≡ Ar *C*   *E2* Ar ≡ R

E1 Ar ≡ H

D3 R ≡ X   *D2* R ≡ R

B3 Ar ≡ X

EdU

B1 Ar ≡ H   *D1* R ≡ H Ar ≡ R *B2*

A3 R ≡ X

A1 R ≡ H   *A2* R ≡ R

10

1

0.1

2100   2150   2200   2250
Raman shift (cm⁻¹)

(c)

CHO ≡ (ortho)   OHC— ≡ (para)   Ph —≡— Br   Ph —≡— I

RIE: 0.73   1.3   0.85   2.8
Raman shift: 2100   2103   2194   2164

Current Opinion in Chemical Biology

A) General click chemistry

1 step

fixation

2 step

fluorescent imaging

N₃

Cu catalyst

click reaction

SM = small molecule
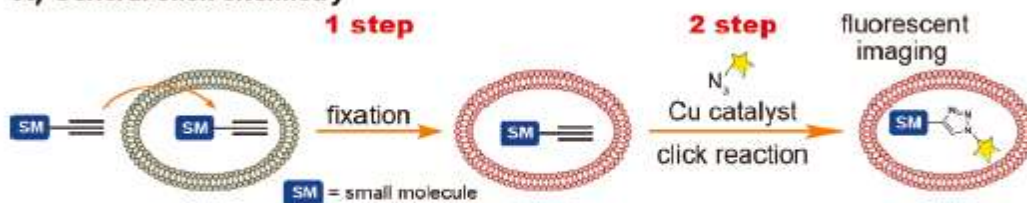
B) Cu-free click chemistry

1 step

fluorescent imaging

SM-N₃

Cu-free click reaction

C) This time (Click-free)

Raman Tag

Direct Raman imaging in living cells
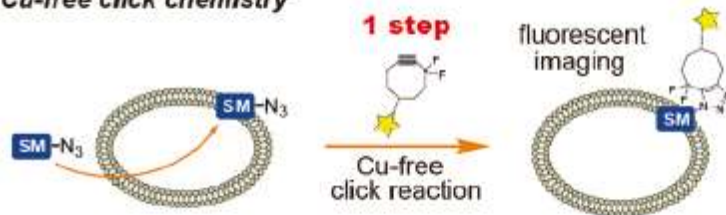
Figure 1. Concept of click-free imaging.

2122

Intensity (a.u.)

EdU

BrdU

dU

silent region

N₂

representative cellular signal

Raman shift (cm⁻¹)

alkyne tag

EdU

BrdU

dU
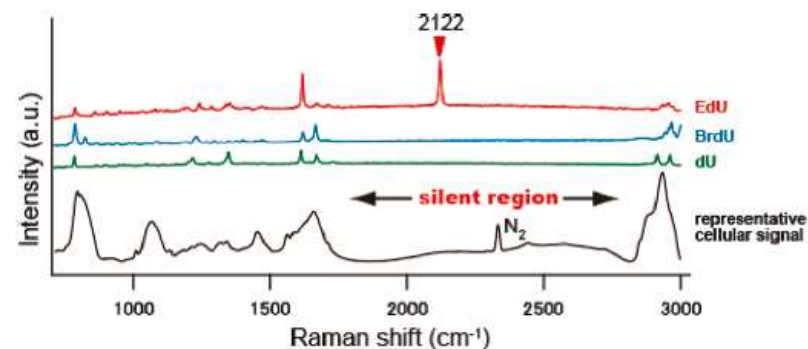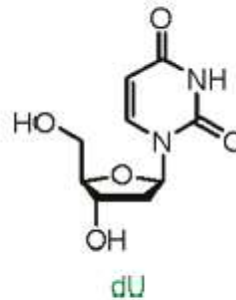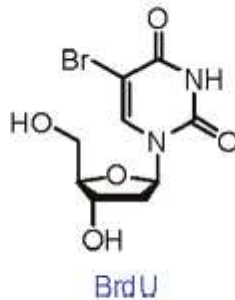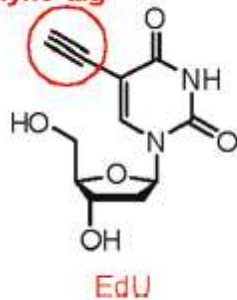
Figure 2. Structures of thymidine analogues.

a

Laser

Spectrometer

Halogen lamp

BP filter

Condenser lens/DF condenser

CCD

Slit

Sample

GLP

L4

Objective

Shutter

≈ To PC

Edge filter

L1

Raman excitation/detection

L2

Cylindrical lens

L3

BF/DF observation

Periscope

GM1 (x)

L5

L6

Dichroic mirror

Microscope tube lens

DF observation

IR

Filter

≈ From CCD

EM-CCD-1

L7

L8

— Line-shaped laser focus

PC

Video camera

BF observation

To PC

TV monitor

b

PC
Voltage output at V_n

Galvanometer mirror
Relocate laser focus at X_n

Cooled CCD camera
Camera exposure

Trigger

Shutter for laser
Shutter open

PC
Save nth frame of CCD image

$n = n + 1$

c

Bright-field image

y direction

Scan direction

$x_1 x_2 x_3 \cdots$ x_n
x direction

A cm^{-1} B cm^{-1} C cm^{-1}

y direction

CCD image
(400 × 1,340 pixel)

x direction

Wavenumber

Raman image at A cm^{-1}

B cm^{-1}

C cm^{-1}

y direction

x direction x direction x direction

Alkynyl sugar analogs for the labeling and visualization of glycoconjugates in cells

Scheme 1. Modified sugar analogs and probes used in this study.
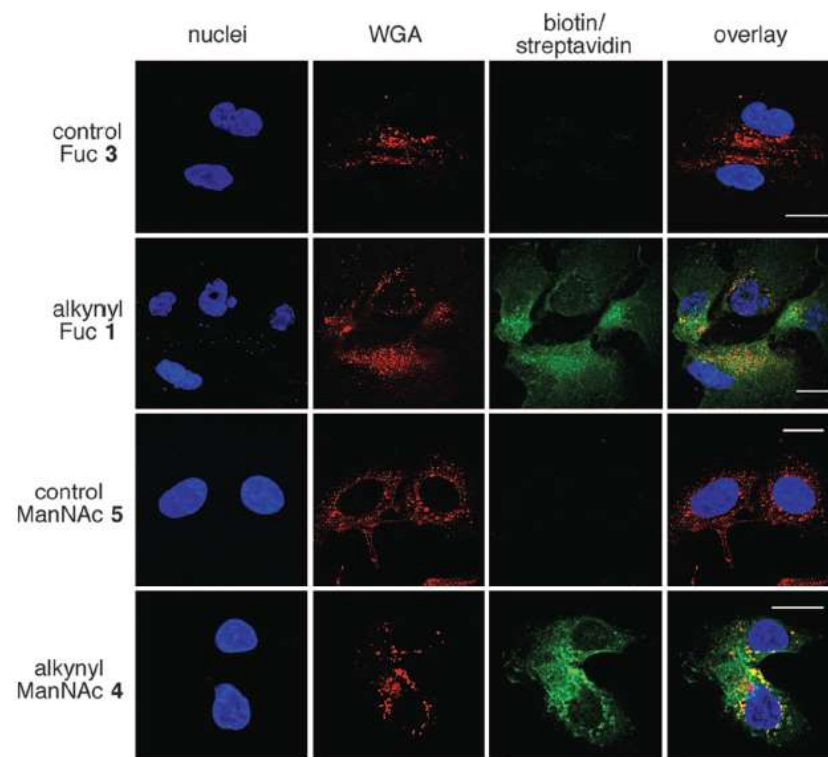
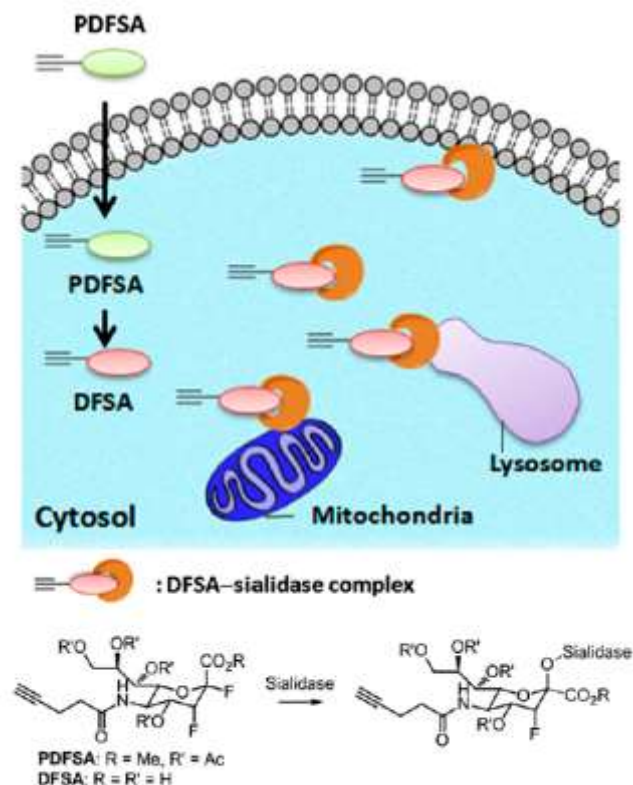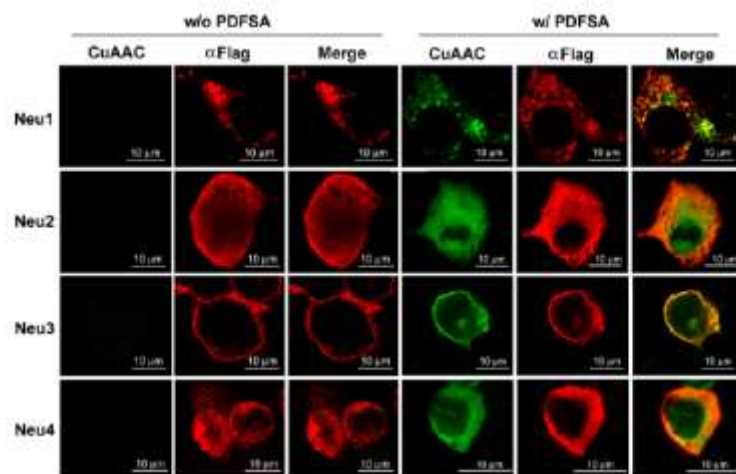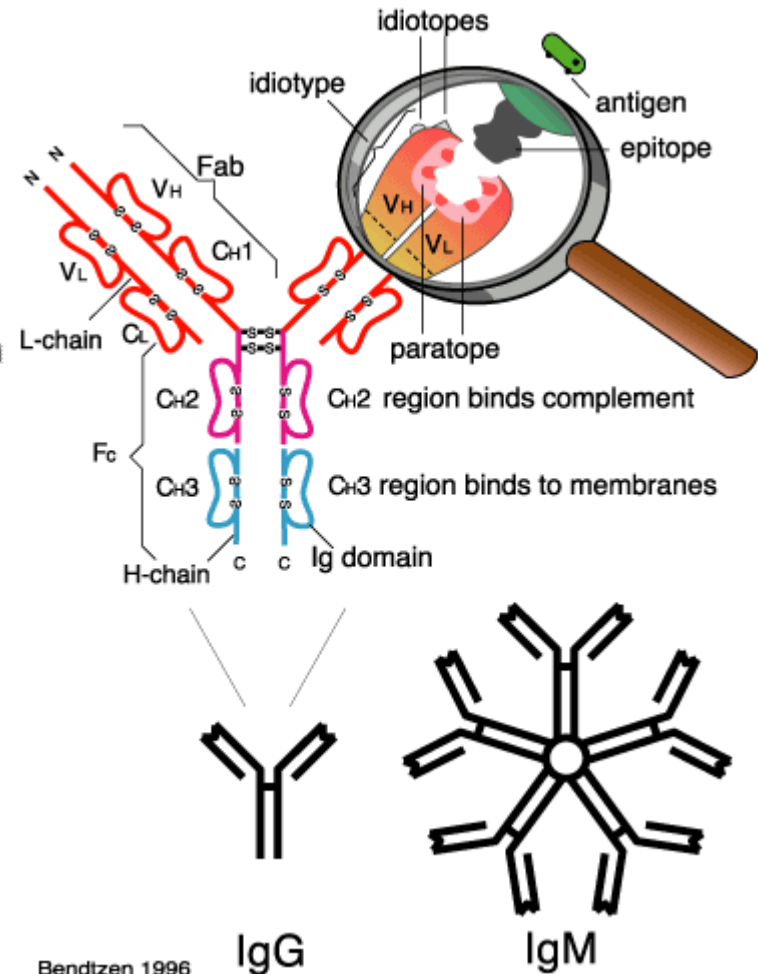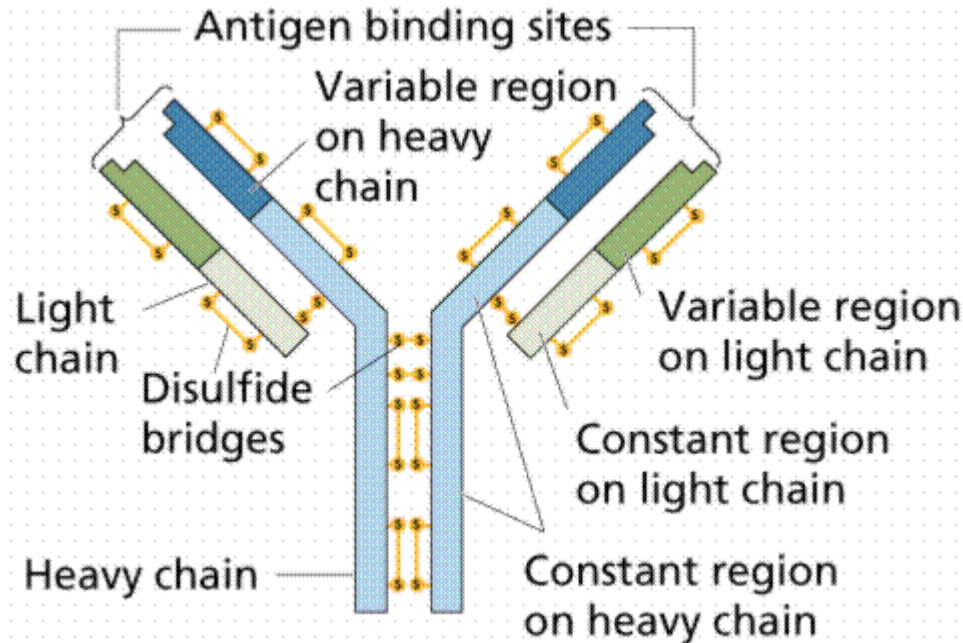# Cell-permeable probe for identification and imaging of sialidases

Fig. 1. Identification and imaging of sialidase with activity changes using these activity-based sialidase probes.
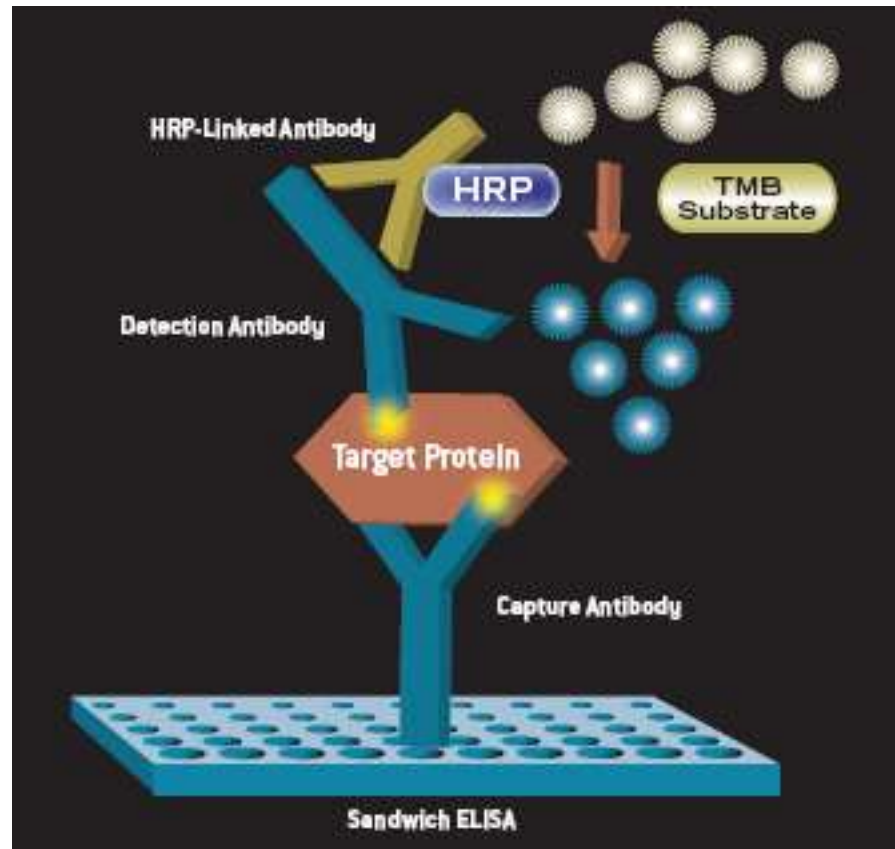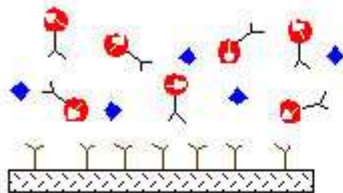
Antibody and Antigen

Bendtzen 1996

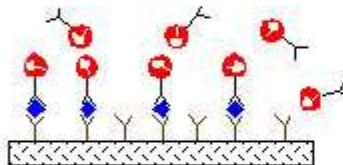# Enzyme-Linked ImmunoSorbent Assay (ELISA)

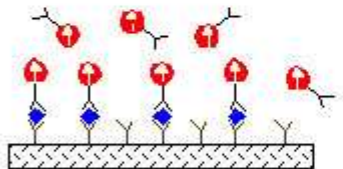

Labeling
BSA/PEG

Microarray

Biomolecules of interest

Capture antibody
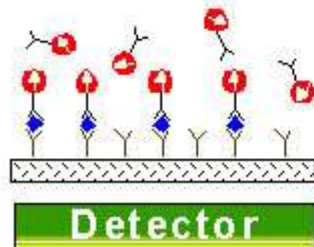
Solid support

Magnetically labeled antibody

Add biomolecules of interest and magnetically labeled detect antibodies to well coated with capture antibody.

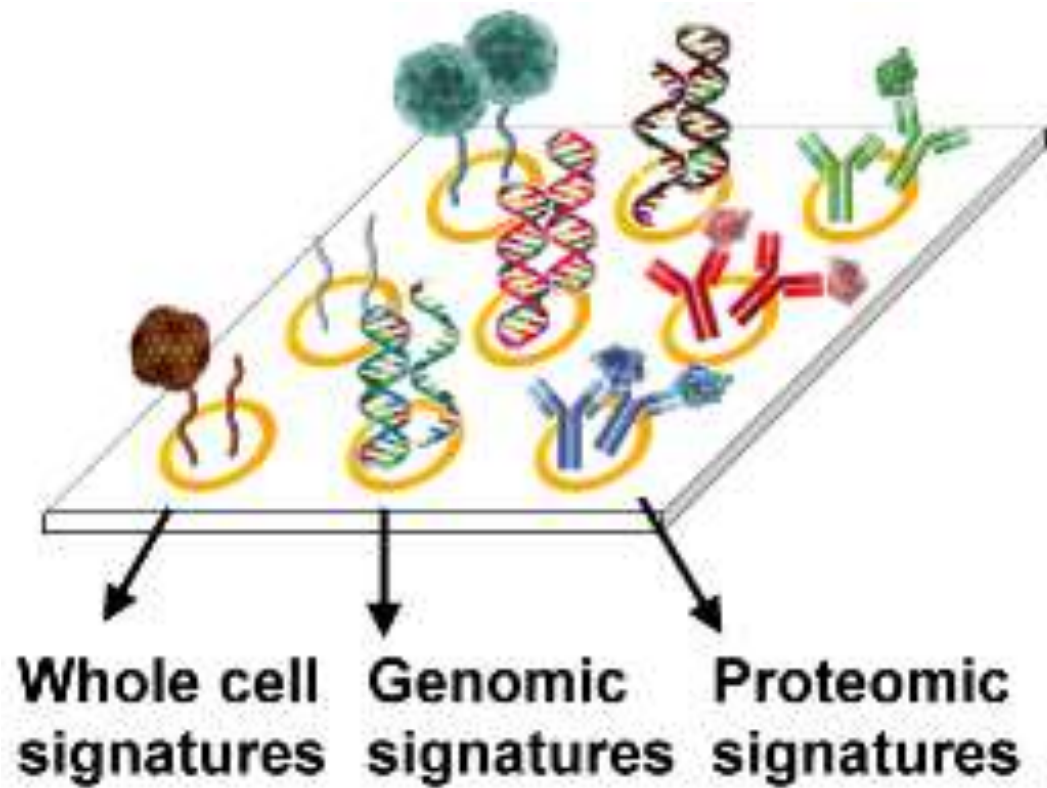Immobilized immune complexes form on solid support.

Apply external magnetic field, magnetic dipoles align.

Remove field, measure net magnetization due to bound antibody labels. Unbound labels randomize quickly and contribute no net signal.

Detector

Microarray

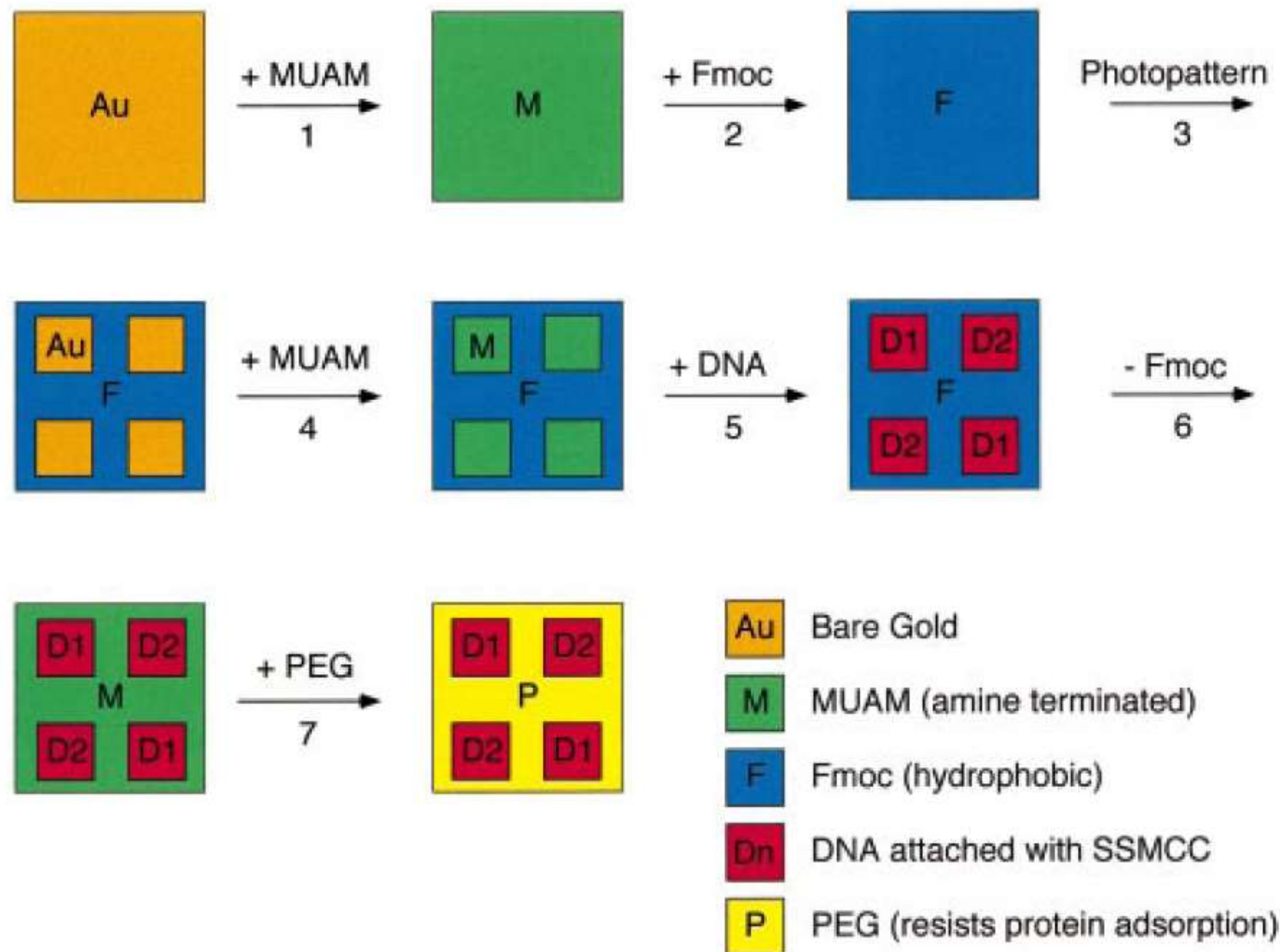Whole cell signatures   Genomic signatures   Proteomic signatures

Figure 1. Fabrication scheme for the construction of multi-element DNA arrays. A clean gold surface is reacted with the amine-terminated alkanethiol MUAM, and subsequently reacted with Fmoc-NHS to create a hydrophobic surface. This surface is then exposed to UV radiation through a quartz mask and rinsed with solvent to remove the MUAM+Fmoc from specific areas of the surface, leaving bare gold pads. These bare gold areas on the sample surface are filled in with MUAM, resulting in an array of MUAM pads surrounded by a hydrophobic Fmoc background. Solutions of DNA are then delivered by pipet onto the specific array locations and are covalently bound to the surface via the bifunctional linker SSMCC. In the final two steps, the Fmoc-terminal groups on the array background are removed and replaced by PEG groups which prohibit the nonspecific binding of analyte proteins to the background.
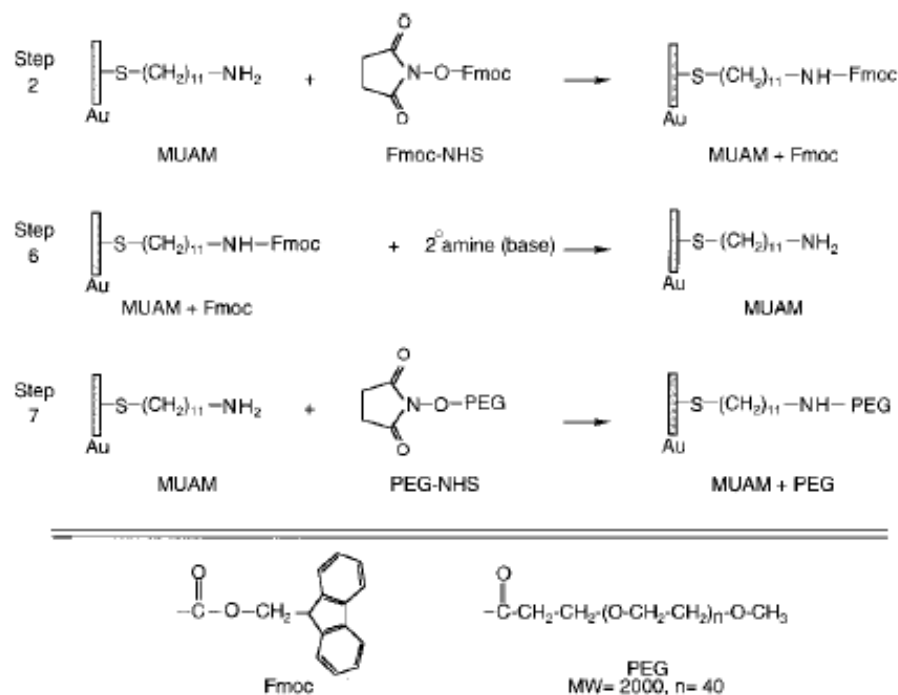
Figure 2. Surface reaction scheme showing the steps involved in the reversible modification of the array background. (Step 2) The starting amine-terminated alkanethiol surface (MUAM) is reacted with the Fmoc-NHS protecting group to form a carbamate linkage thus creating a hydrophobic Fmoc-terminated surface. (Step 6) After DNA immobilization (see Figure 3), the hydrophobic Fmoc group is removed from the surface with a basic secondary amine, resulting in the return of the original MUAM surface. (Step 7) In the final array fabrication step, the deprotected MUAM is reacted with PEG-NHS to form an amide bond that covalently attaches PEG to the array surface.
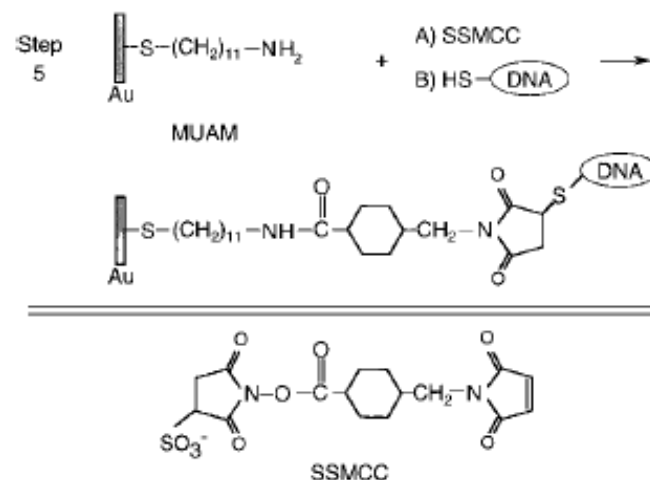

Figure 3. Surface reaction scheme showing the immobilization of thiol-terminated DNA to the array surface. In Step 5 of the DNA array fabrication, the heterobifunctional linker SSMCC is used to attach 5′-thiol modified oligonucleotide sequences to reactive pads of MUAM. This linker contains an NHSS ester functionality (reactive toward amines) and a maleimide functionality (reactive toward thiols). The surface is first exposed to a solution of the linker, whereby the NHSS ester end of the molecule reacts with the MUAM surface. Excess linker is rinsed away and the array surface is then spotted with 5′-thiol-modified DNA that reacts with the maleimide groups forming a covalent bond to the surface monolayer.

Glass Surface Modification
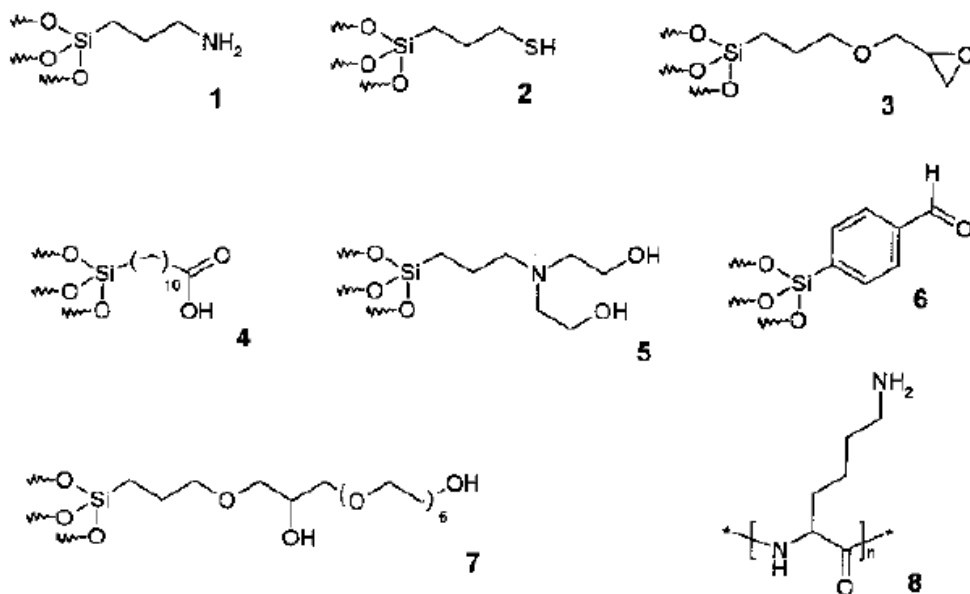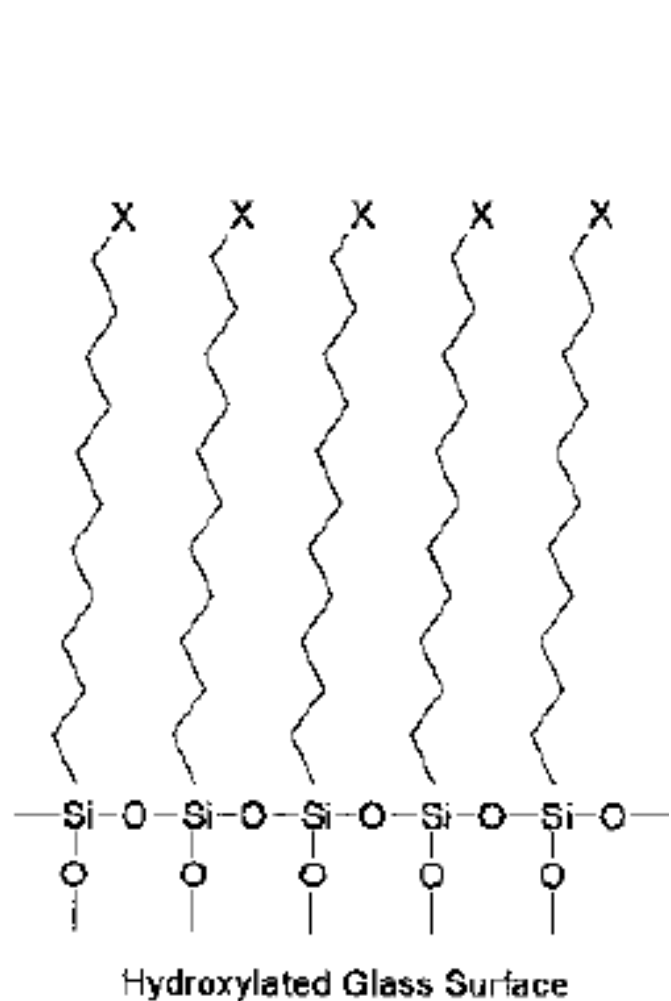
Scheme 2.2 Reagents for derivatization of glass surfaces. 1 APTES = aminopropyltriethoxysilane; 2 MPTS = 3-mercaptopropyltrimethoxysilane; 3 GPTS = glycidoxypropyltrimethoxysilane; 4 TETU = triethoxysilane undecanoic acid;

5 HE-APTS = bis(hydroxyethyl)aminopropyltriethoxysilane); 6 4-trimethoxysilylbenzaldehyde; 7 GPTS/HEG – glycidoxypropyltrimethoxysilane-hexaethylene glycol; 8 poly(lysine).

Hydroxylated Glass Surface

Scheme 2.1 2D schematic description of a polysiloxane monolayer on a glass surface (X = terminal functional

NHS-Biotin

EDA

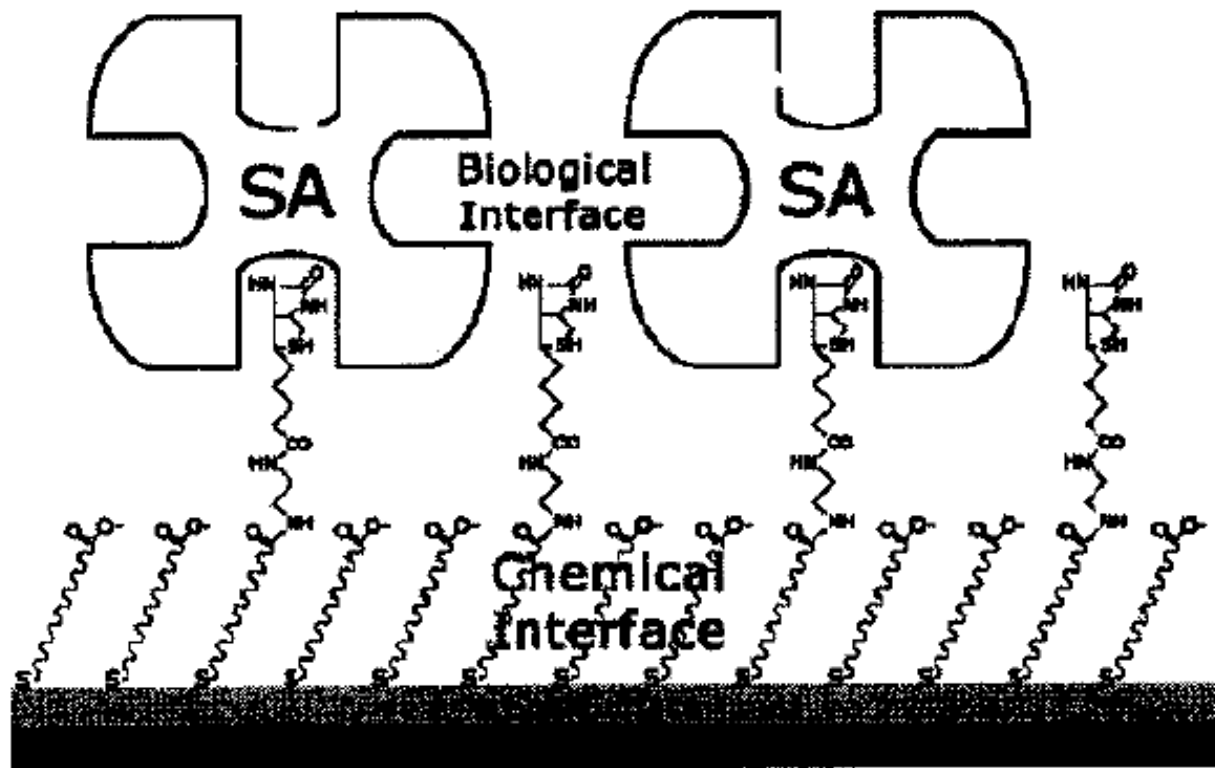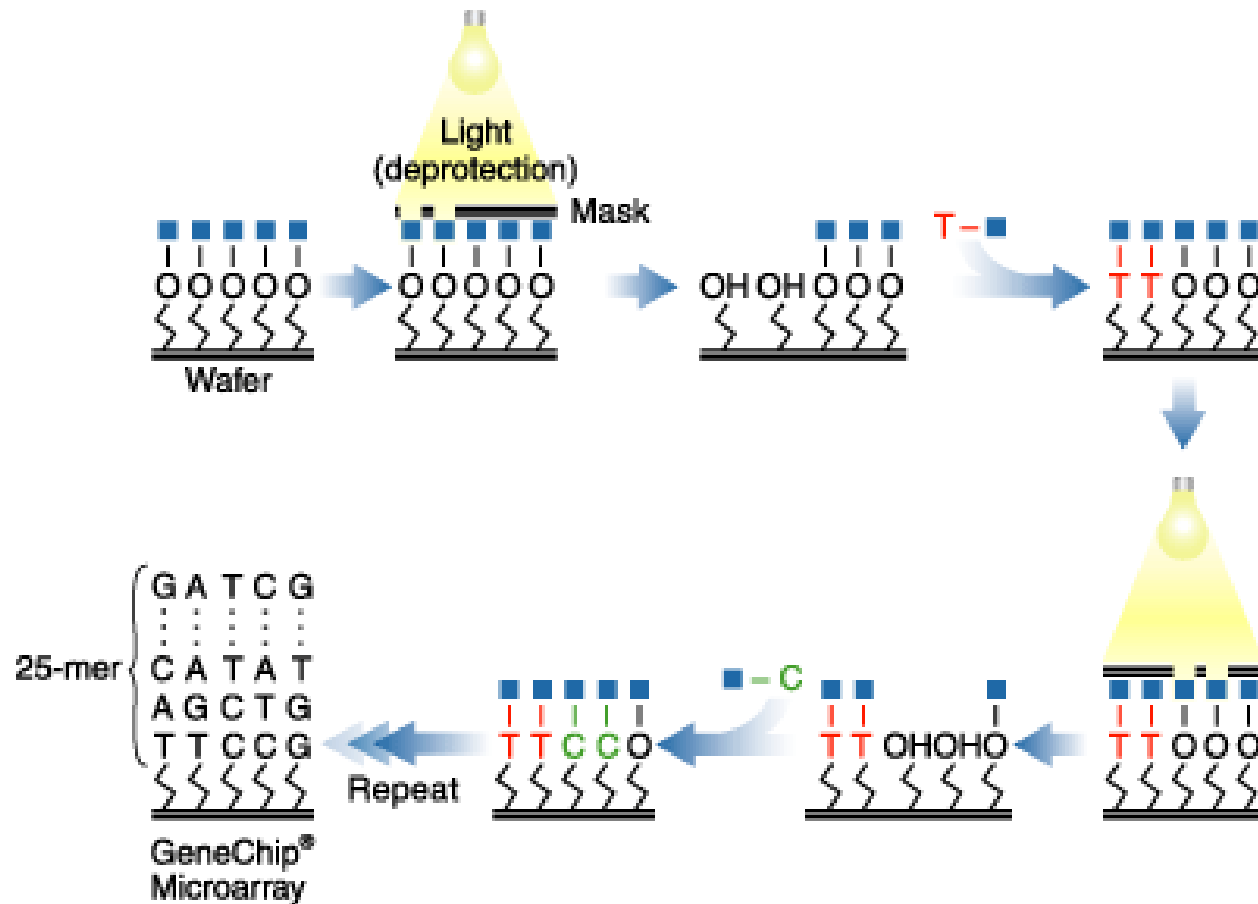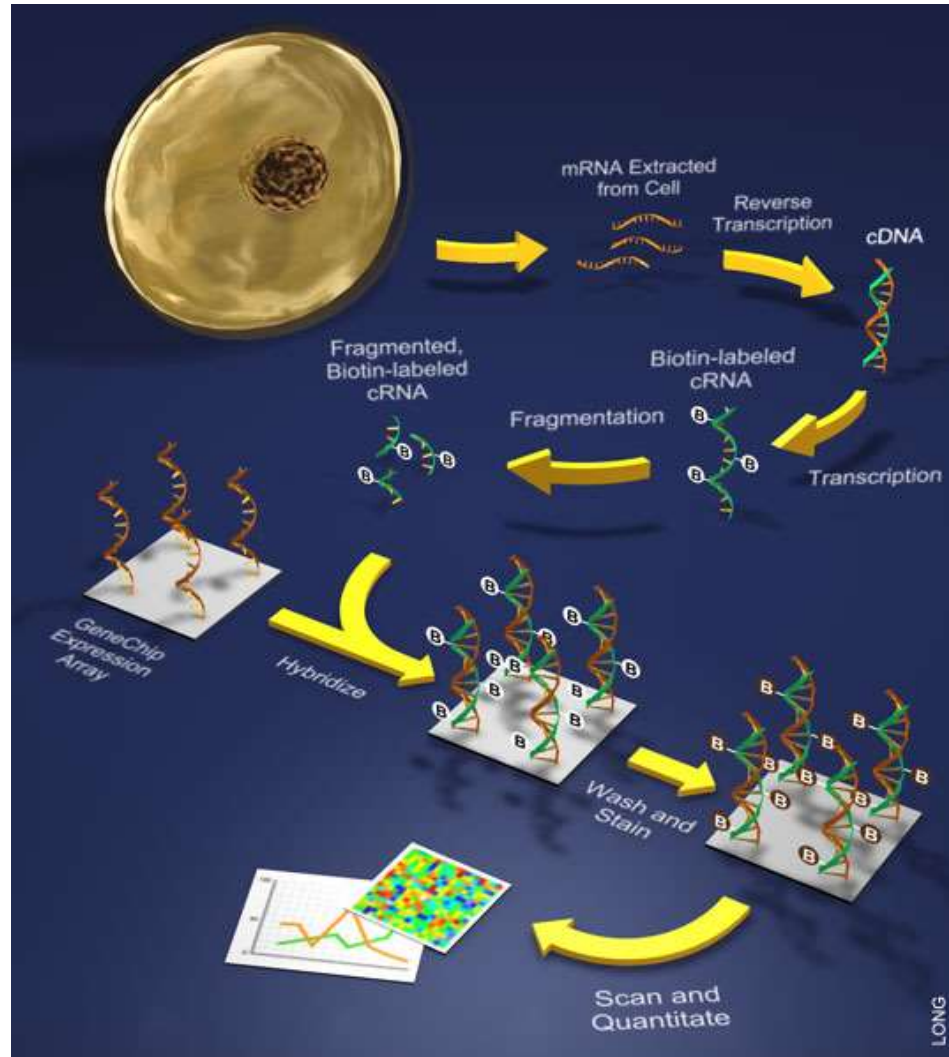Silicon substrate

A

B

C
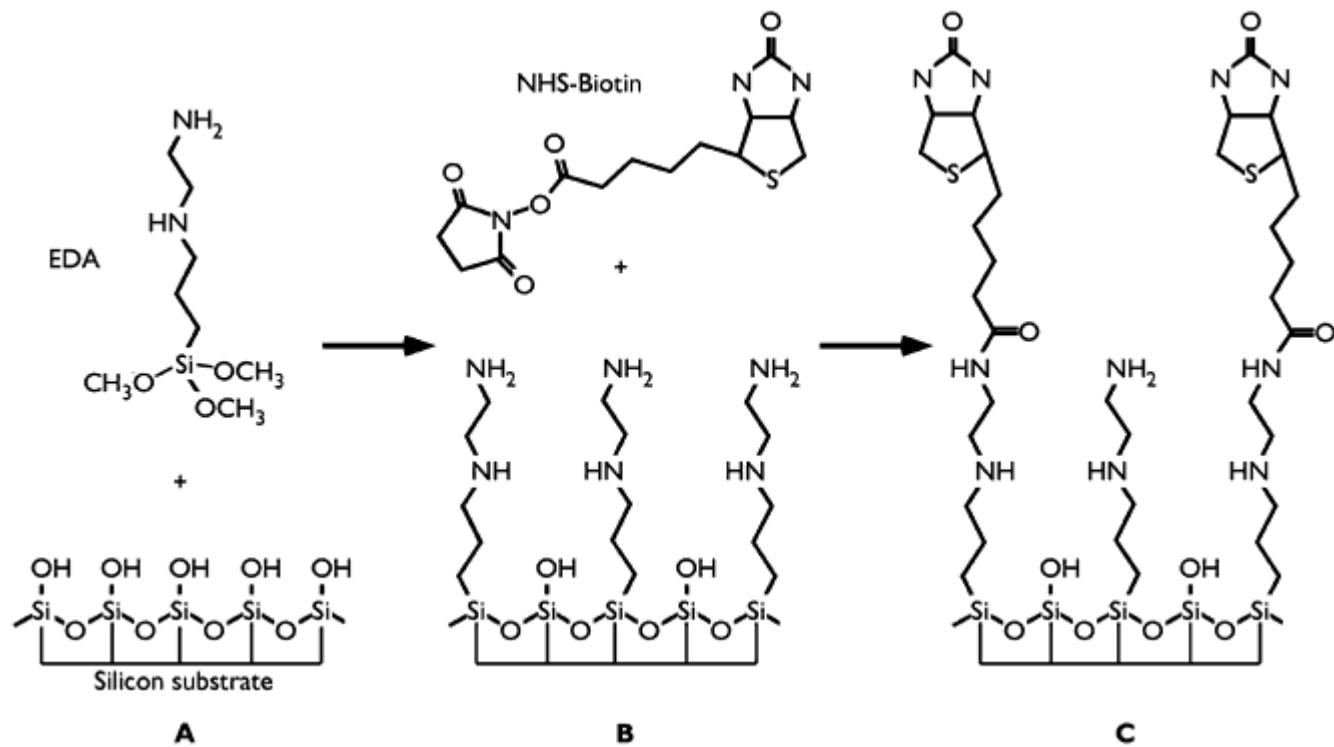
Biotin-Streptavidin

Figure 2.3 Schematic respresentation of a steptavidin sensor surface assembled on a reaction-controlled biotinylated SAM [28].
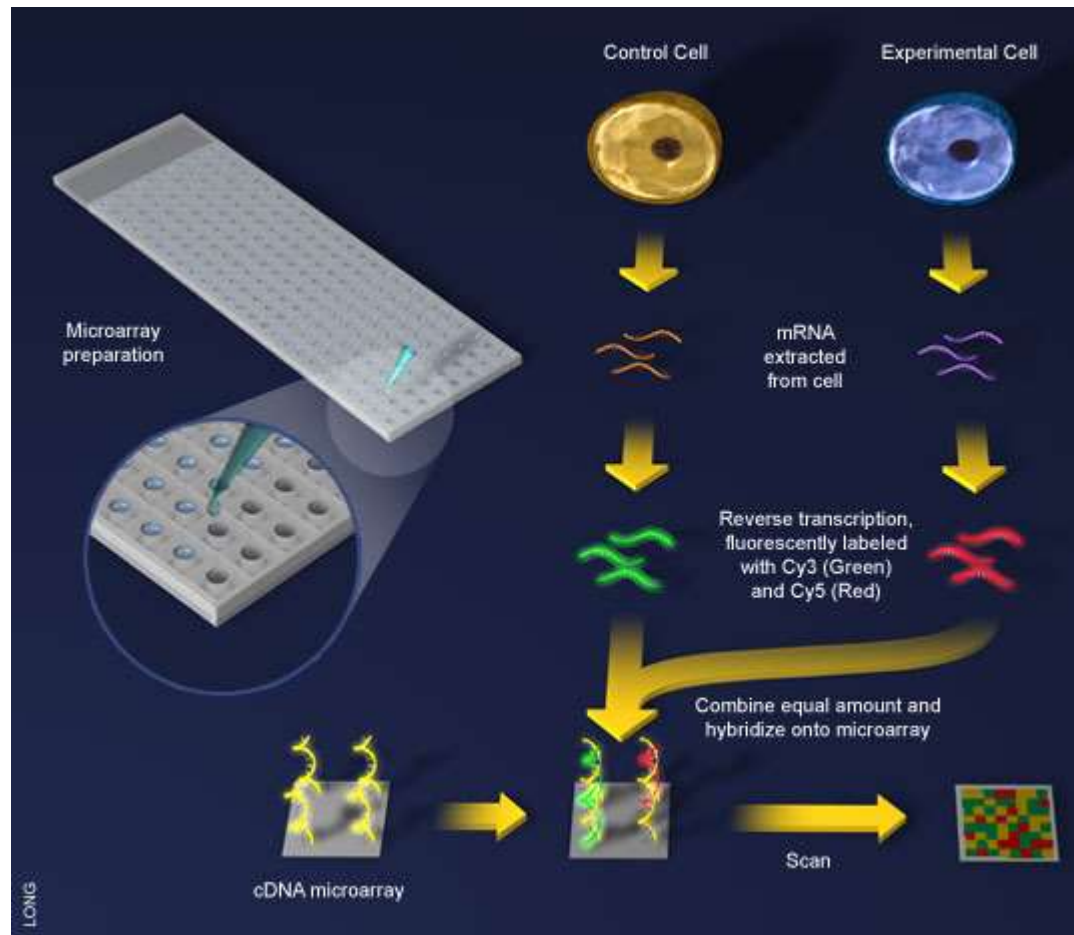
GeneChip

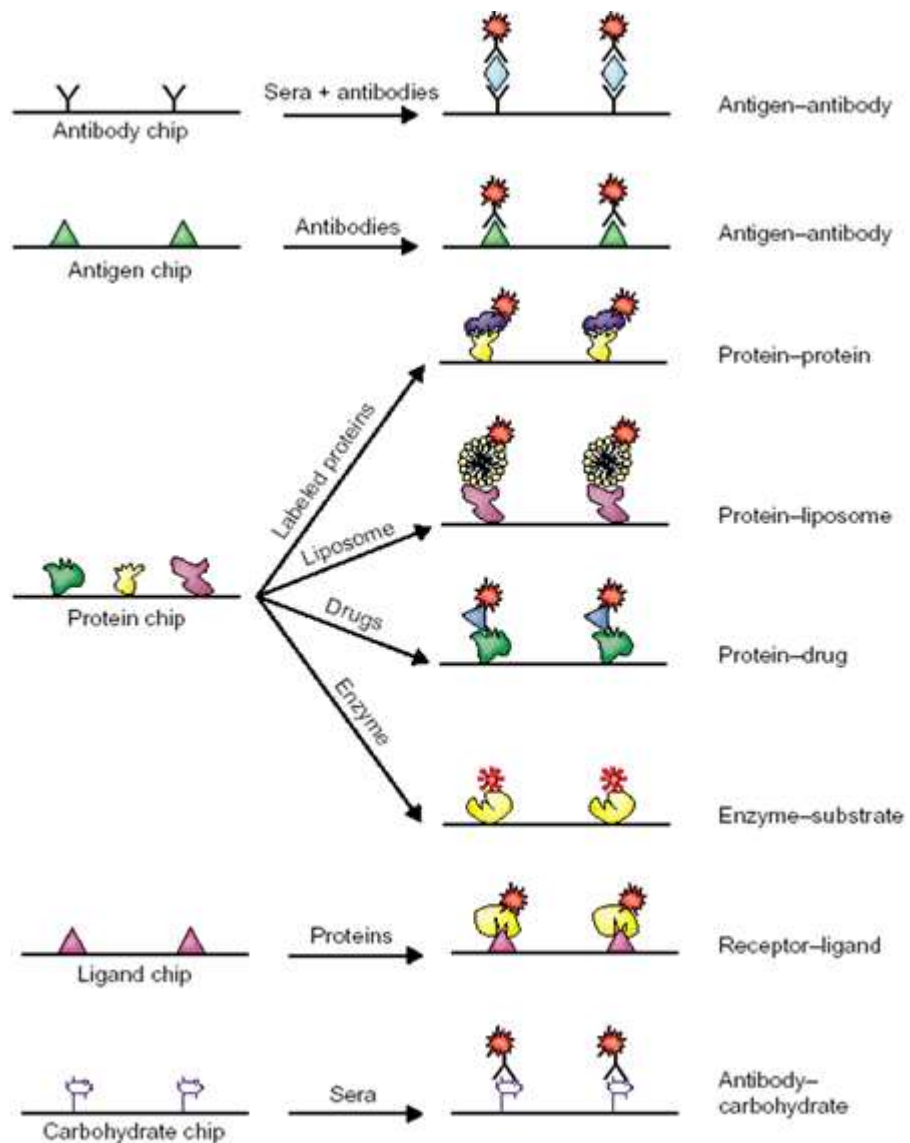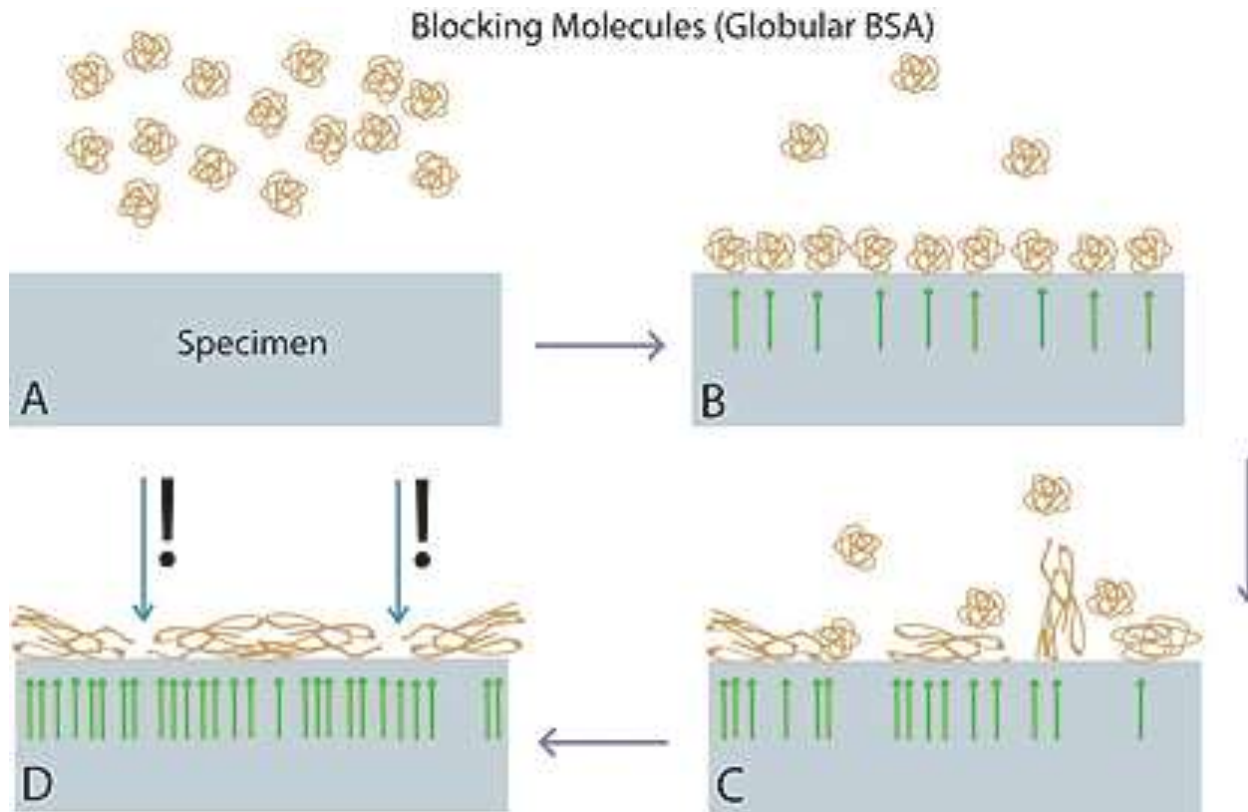# Scheme

cDNA Microarray

Protein Array

Antibody chip → Sera + antibodies → Antigen–antibody

Antigen chip → Antibodies → Antigen–antibody

Protein chip → Labeled proteins → Protein–protein

→ Liposome → Protein–liposome

→ Drugs → Protein–drug

→ Enzyme → Enzyme–substrate

Ligand chip → Proteins → Receptor–ligand

Carbohydrate chip → Sera → Antibody–carbohydrate

Current Opinion in Chemical Biology

BSA Blocking

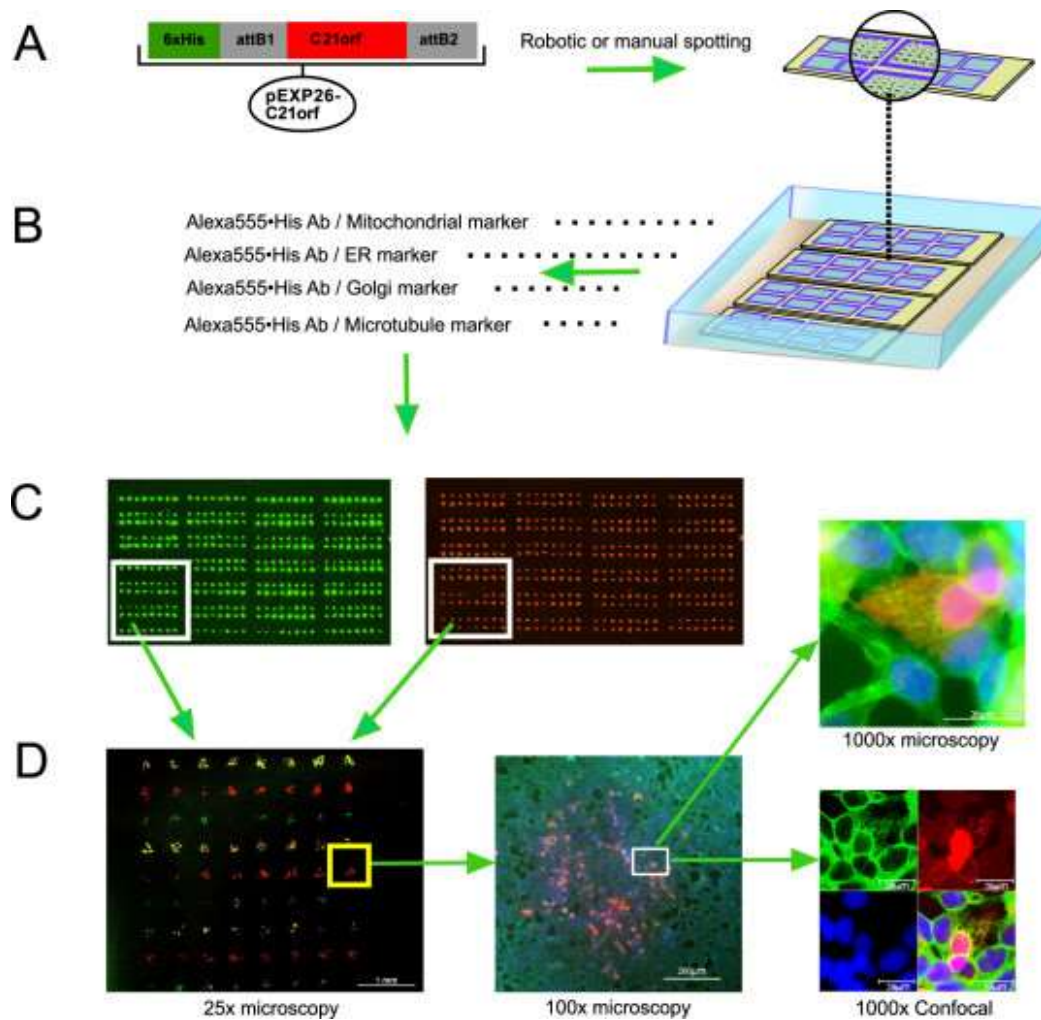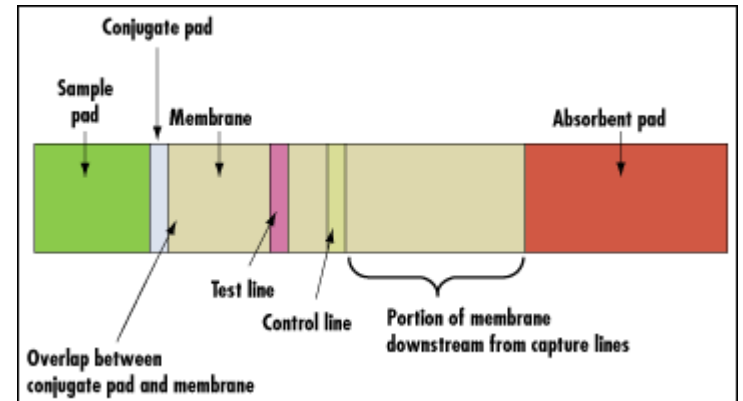# Cell Array

hCG immunoassay

human chorionic gonadotropin (hCG)

Nucleotide Sensor